Quantum measurement and feedback control of nano-mechanical systems and atomic spin-ensembles

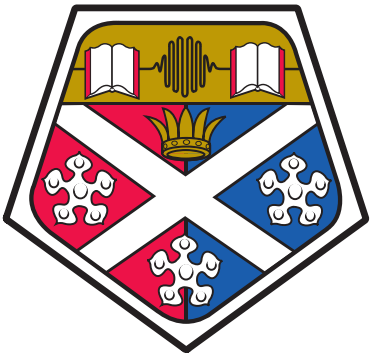

University of Strathclyde

Department of Physics and SUPA

Liam Walker

November, 2020

This thesis is the result of the author's original research. It has been composed by the author and has not been previously submitted for examination which has led to the award of a degree.

Signed:

Date:

Abstract

In recent years, considerable developments have been made in controlling quantum systems through a combination of measurement and feedback. All measurements naturally disturb the system in question, as they necessitate some level of interaction in order to extract information. However, if we can characterise the resulting disturbance and correctly interpret the information - especially in the case of weak measurements - then we can determine how to feed back the measurement in such a way as to drive desired evolution, preparing potentially highly non-classical states.

In this thesis, we investigate using feedback to prepare and manipulate quantum states of motion of levitated nano-particles, as well as for the preparation of many-body squeezed states in atomic ensembles. We first consider a possible route to ground state cooling with a levitated nanoparticle, magnetically trapped by a strong permanent magnet. The trap frequency of this system is much lower than those involving trapped ions or in many other nano-mechanical resonators. Minimisation of environmental heating is therefore challenging as it requires control of the system on a timescale comparable to the inverse of the trap frequency. We show that these traps are an excellent platform for performing optimal feedback control via real-time state estimation, and that they may also be an ideal testing ground for quantum collapse models when operating in the free particle limit. We go on to explore a separate system, considering applications of feedback for preparing collective pseudo-spin states in a dilute cloud of atoms. We model how information in typically discarded measurement channels can be used to stabilise noise in order to produce enhanced levels of spin squeezing.

In these projects we make use of quantum trajectory techniques alongside analytical models, to explore and simulate realistic parameter regimes for current or near-future experiments. Throughout, we develop ideas for creating non-classical states in a new generation of quantum technologies.

Contents

1 Introduction

Technologies that rely on the properties of quantum systems are becoming increasingly relevant in order to outperform more conventional tools. Perhaps the most cited example is the promise of quantum computers and simulators, which will be capable of computations far beyond the reach of classically designed machines[1, 2]. Quantum metrology is another highly active field of research which already impacts many aspects of day to day life. From atomic clocks[3] which make possible the global positioning system, to gravitational wave detectors[4] which provide a new lens through which to make astronomical observations. Several platforms exist where quantum technologies are being developed. Historically, optical systems have provided a remarkably controlled environment to study quantum effects. Today quantum states are readily prepared in cold atomic gases[5], cryogenically cooled superconducting circuits[6], and in the motion of microscopic oscillators[7]. It is of growing importance to understand how to measure and control quantum systems, in order to continue to advance these technologies and to probe the edges of quantum theory.

In measurement theory ideas such as conditional state distributions and stochastic processes, have long been necessary in the description of purely classical systems where quantum effects are not apparent. Outside of idealised models, the state of a classical system can be represented by a probability distribution over a configuration space, for example, the position and momentum of particles. This distribution should reflect the knowledge gained through measurement. Realistic observations are made indirectly through some apparatus and always contain a finite level of uncertainty. This is also true for quantum systems, but there is an additional fundamental level of uncertainty where non-commuting observables cannot both be known with arbitrary precision, regardless of how well measurements are made. Quantum measurement theory already plays an essential roll in metrology[8, 9], computing[10, 11], and in exploring the boundary between quantum and classical physics[12, 13]. Furthermore, measurements can be incorporated in feedback loops to provide stabilisation, and drive desired evolution. Feedback has many poten-

tial applications in quantum systems, including in fault tolerant quantum computing[14], for stabilising spin-squeezed states in atomic gases[15], and for damping mechanical motion[16]. In this thesis we explore methods of measurement and feedback for producing non-classical states in nano-mechanical systems and in atomic spin-ensembles.

In the following section a brief background of open quantum systems is presented. This leads onto a discussion of quantum states conditioned on measurements, known as quantum trajectories. The development of measurement theory is discussed, as well as the usefulness of the trajectory technique for numerical simulations. Lastly, methods of feedback are touched upon in the context of controlling the evolution of quantum systems, alongside a few examples. This chapter ends with an outline of the structure of the rest of this thesis.

1.1 Open quantum systems

To reach a working description of a quantum measurement it is first necessary to know how the system in question interacts with its surroundings. It will be through this interaction that information is ultimately transferred to a measuring device. Moreover, before considering measurement, treating a system in isolation is often not sufficient outside of special cases. In the energy structure of an atom for example, spectral lines are not sharply defined. The linewidth arises due to coupling with the infinitely many degrees of freedom in the electromagnetic field. This infinite complexity requires a statistical treatment in addition to the already intrinsic probabilistic nature of quantum mechanics. Coupling to even modestly large many-body reservoirs requires an exponentially growing number of degrees of freedom as the number of components in the reservoir increases, and again a statistical description is often necessary. Open quantum systems are those that interact with their surroundings, and in this sense all real systems are open to some extent. If a sub-system is simple enough and sufficiently isolated, it can still have a tractable solution whilst being allowed to dissipate energy and information into its much larger environ-

ment. For macroscopic objects the environmental coupling will usually quickly destroy the peculiar features associated with quantum physics such as superposition states and entanglement. Unlike a system described solely by the Schrödinger equation this process is irreversible and goes some way to explaining the emergence of classical physics.

In the field of quantum optics the coupling to the environment is well enough understood that it can be used to drive the system dynamics rather than just account for losses[17]. In particular, systems with a resonant optical frequency which is separated by several orders of magnitude from the frequency of the coupling induced dynamics, have very tractable theoretical descriptions. As such many methods used to describe open systems were developed for use in quantum optics but have since gone on to become widely applicable in other areas of physics. Advances in cold atom physics have lead to incredible levels of control over Bose-Einstein condensates[18, 19, 20] and Fermi gases suspended in optical lattices[21, 22]. This has provided a versatile setting in which to explore open many-body physics and provide insights into condensed matter theory[2]. There has also been significant progress in creating a range of nano-mechanical quantum systems, which naturally couple strongly to their environment[23, 24, 25, 26]. These systems largely rely on our excellent control of light which is then interfaced with matter. The initial sections of this thesis will focus on advances in preparing levitated nanoscopic and microscopic particles in motional quantum states.

1.2 Quantum trajectories

Much of early quantum theory did not require a description of the measurement process beyond von Neumann's projection postulate. In von Neumann's approach, the state transformation due to measurement happens distinctly from the time evolution described by Schrödinger's equation. This was generally good enough to describe experimental measurements which would effectively destroy the state of the system being observed anyway. However, projective measurements are not sufficient to describe a system that is contin-

uously monitored. In these cases, the evolution of a quantum state should be modified to reflect the information continuously being transferred to the environment. One of the first experiments to highlight this was the observation of photons emitted from a single trapped ion[27, 28, 29]. This drew attention to the fact that the measurement theory of the time was incomplete and would lead on to the development of a stochastic dynamical equations for quantum states.

To move beyond simple projective measurements, we can consider open quantum systems which are explicitly coupled to some measurement apparatus. However, if we then go on to make projective measurements of the apparatus, it initially feels like we have only shifted the problem. In a sense this is true, to move forward there must be some point where a definite result is drawn from the probabilistic quantum description. This point is termed Heisenberg's cut and one way of stating the so-called measurement problem in quantum mechanics is that there is no physical basis for when to do this. It is sometimes possible to find a subsystem for which the dynamics are effectively Markovian, where the environment has no memory of the system state. In some of these cases it is possible to define a point where we know that treating the measurement apparatus classically will not influence the dynamics of the system. This is due to decoherence, which roughly amounts to the conversion of a quantum superposition into a classical mixture due to interactions with the environment. Detectors are designed to have certain classical observable properties that correlate with the state of the system we want to know about. If the apparatus is left in a classical mixture of these observable states, after decoherence we can make projective measurements of the apparatus without disregarding information contained in possible quantum correlations. This does not solve the measurement problem, there is still a discontinuity in the theory where the measurement is made, but it does alleviate the problem.

Considering again photo-detection from a single ion, each detection at a definite time can be associated with a sudden change of the ion state. In the formulation of continuous quantum measurement these "quantum jumps" are treated explicitly as part of the time

evolution of the system. The methodology is now widely known as the quantum trajectories approach[30]. The theory extends to measurements of more general observables such as the position of a particle and other observables of infinite-dimensional systems described by quantum diffusion equations. Even when measurements are intended to be instantaneous it can be helpful to understand the continuous effects of measuring the system. A single pulsed measurement will still take some finite time and if the dynamics of the measured system are fast enough continuous measurement theory can be useful. We later explore an example of this when considering repeated pulsed measurements of a free levitated particle.

Quantum trajectories are not only a useful predictive model but also a powerful computational tool. A practical algorithm was developed in the 1990s, in parallel by three independent groups[31, 32, 30], where quantum jumps are simulated and averaging over many stochastic trajectories yields measured quantities. Stochastic simulation methods offer advantages due to their scaling with system size. The deterministic evolution of an open quantum system described by a master equation is encoded in N^2 coupled differential equations where N is the dimension of the Hilbert space. Stochastic wavefunction simulations on the other hand scale as N. When simulating large system sizes this can provide a substantial speed up and more practical storage. The trade off is the need for stochastic sampling. Several trajectories are required to build up a picture of the ensemble average behaviour described by a master equation. Averaging n trajectories typically converges slowly as $1/\sqrt{n}$, and although these can be executed efficiently in parallel, this is only worthwhile if N is very large and small statistical errors are not an issue. Individual trajectories can be useful in their own right, given the correct circumstances they can be interpreted as realisations of what would be measured in an experiment.

1.3 Feedback and control

Feedback control generally involves making measurements and using the information gained to modify the system Hamiltonian in real time. For example, in optics, feedback can be used to stabilise the phase or intensity of a laser. Some systems can be designed so that they have intrinsic stabilisation mechanisms that function as a sort of naturally occurring feedback. The first optical systems that reached the noise constraints of Heisenberg's uncertainty principle were achieved using intrinsic non-linearities[33, 34], with techniques such as four wave mixing and parametric down conversion. It was Wiseman and Milburn who first developed a theory for using active feedback of a photo-current[35]. Feedback of this sort offers versatile control over quantum systems. In this thesis we look at a practical feedback scheme for cooling the motion of levitated nanoparticles as well a method for preparing squeezed spin states of an atomic ensemble.

Wiseman and Milburn derived a master equation which followed a diffusive measurement process. They initially considered monitoring a homodyne current, but the theory could be applied generally to any measurement that effectively sampled from a Gaussian distribution, such as continually measuring the position of a quantum object. These types of measurement introduce noise into the system dynamics, which is associated with the fundamental uncertainty inherent in quantum mechanics. This noise then propagates throughout the feedback process. The result is analogous to the fluctuation-dissipation theorem where the measurement causes diffusion and the feedback can have a damping effect. An example of this type of feedback procedure was demonstrated in damping the motion of a trapped ion [16, 36]. The slowly varying quadrature components of an ion's motion in a harmonic trap can be measured in a similar manner to measuring the phase quadratures of an optical field. A signal proportional to the momentum quadrature can then be fed back to damp the harmonic motion. Photon shot noise contributes to heating in these traps, but feedback using information from the scattered light can be used to cool below the standard Doppler limit. A similar procedure can be used to align the collective

spin of an atomic ensemble[15]. Measurement can be used to reduce the uncertainty in a given spin component but consequently causes stochastic drift in the mean spin direction. Feedback can be used to stabilise against this.

In theoretical models and some well controlled systems, feedback proportional to the instantaneous measurement record can be directly reintroduced to the system. However, often experiments instead have access to some integral of the measurement. For example, after the use of any kind of band-pass filter, the signal has effectively been averaged. This can of course still be used for feedback but it is much more difficult to model the resulting dynamics. This issue is not confined to quantum physics and there are cases where methods from classical control theory can be borrowed to make the problem more tractable[37]. In some cases, integrals of the measurement record can provide continuous estimates of certain dynamical variables. Feedback can then be applied based on the estimated state, altering the system evolution in the usual way to obtain some desired behaviour. In the approximate limit of instantaneous feedback, the integrated measurement signal can even still produce Markovian evolution.

Ultimately, with relatively straightforward implementation feedback offers the ability to turn on and off non-trivial terms in the system Hamiltonian, and the opportunity to make use of information that is otherwise lost to the environment, to obtain desired behaviour.

1.4 Thesis outline

This thesis is comprised of six chapters. Following this introduction which serves to provide context, the second chapter presents a technical overview of quantum measurement and feedback which is the foundation for the research presented. What comes after is split into two sections covering nano-mechanics and many-body spin systems respectively. Chapter 3 provides more specific background details of nano-mechanical systems as well as examples of early calculations. Chapters 4 covers the main results from this topic. In turn, chapter 5 contains an overview of measurement and dissipation in many-body systems, followed

by the results relating to preparing spin-squeezed states. Finally, in chapter six the key results from the previous chapters are summarised and concluding remarks are presented.

More specifically, in chapter 2 the conditions required for a Markovian master equation are investigated, followed by a detailed derivation of quantum jumps and diffusion measurement models. In doing so, decoherence and some of the quirks of stochastic calculus are discussed. The chapter ends with the details of Wiseman and Milburn's formulation of feedback alongside methods from classical control theory that map onto quantum systems.

In chapter 3 the discussion turns to nano-mechanical systems. A brief review of the background of the field is presented, followed by an overview of some recent developments achieved with levitated nanoparticles, for which new feedback cooling schemes are proposed and analysed in chapter 4. A general measurement model for a trapped particle is constructed and then used to explore in detail various specific methods of measuring levitated particles, in order to determine which are best suited when using magnetic confinement. This leads on to an evaluation of which feedback methods are most appropriate for these systems, and an analysis of how to overcome the challenges of working with relatively low-quality oscillators.

In chapter 4 an analysis for cooling magnetically confined particles is presented. A final model is shown alongside measurement simulations and the outcomes of a proposed feedback procedure. The chapter concludes with discussion of an ongoing project to look for diffusion of a free particle's position that is expected in a continuous spontaneous localisation model. Predictions are made using the same models from the feedback analysis, that are applicable to proposed future experiments.

In chapter 5 the focus shifts to many-body systems, opening with an overview of spin squeezing in atomic ensembles. The research in this chapter is motivated by a proposed experiment that would have access to typically discarded measurement channels, when probing an atomic cloud in free space. An analysis of how these measurements can be used to stabilise noise to produce enhanced levels of spin squeezing is presented. The

chapter ends with details of an ongoing investigation into techniques to produce a steady state of the feedback procedure that is useful for metrology.

Contributions during PhD

Publications

- L. S. Walker, G. R. M. Robb, & A. J. Daley, Measurement and feedback for cooling heavy levitated particles in low-frequency traps. Physical Review A, 100(6), 063819, 2019

The author of this thesis performed all of the analytical and numerical calculations, wrote the majority of the article, and produced all of the plots.

Conference presentations

- L. S. Walker, G. R. M. Robb, & A. J. Daley, Quantum measurement and control of levitated nano-particles, *European Quantum Technologies Conference* (Grenoble, France) 2019
- L.S. Walker, T. Bintener, S. Flannigan, G.R.M. Robb, & A.J. Daley, Measurement and feedback for state preparation of quantum systems, *SFB-FoQuS International Conference* (Innsbruck, Austria) 2019
- L.S. Walker, T. Bintener, S. Flannigan, G.R.M. Robb, & A.J. Daley, Measurement and feedback for state preparation of quantum systems, *PASQuanS Kickoff Meeting* (Munich, Germany) 2019
- L. S. Walker, G. R. M. Robb, & A. J. Daley, Measurement and feedback with levitated nano-particles, *PHOTON Conference* (Birmingham, UK) 2018

- L. S. Walker, G. R. M. Robb, & A. J. Daley, Quantum measurement and control of levitated nano-particles, *Q2C Conference* (Glasgow, UK) 2018
- L. S. Walker, Measurement and feedback in quantum systems, *YAO2018 Conference* (Glasgow, UK) 2018
- L. S. Walker, G. R. M. Robb, & A. J. Daley, Feedback cooling and continuous quantum measurement, *CCPQ Workshop* (Windsor, UK) 2017
- L. S. Walker, G. R. M. Robb, & A. J. Daley, Feedback control of levitated nano-particles, *QuAMP International Conference* (Glasgow, UK) 2017
- L. S. Walker, G. R. M. Robb, & A. J. Daley, Feedback Cooling and Quantum Measurement, *SU2P Conference* (Edinburgh, UK) 2017

2 Measurement and feedback

In this chapter the conditions required for a Markovian master equation are investigated, and a derivation is outlined. The resulting equation is used to give an example of decoherence and highlight its importance for understanding continuous measurement. This is followed by a detailed derivation of quantum jumps for a two level system, and then a derivation of more general diffusion measurement models. The rules of Ito calculus are touched upon, along with a discussion of how it will be used in the rest of this thesis. The chapter ends with the details of Wiseman and Milburn's formulation of feedback alongside a discussion of methods from classical control theory that map onto quantum systems.

2.1 Born-Markov master equation

The full dynamics of a quantum system coupled to its environment are contained in the Schrödinger equation,

$$\dot{\rho}_{tot} = -\frac{i}{\hbar}\big[H_s + H_E + V, \rho_{tot}\big], \tag{2.1}$$

where ρ_{tot} is the combined state of the system and the environment. H_s is the system Hamiltonian, H_E is the Hamiltonian of the environment and V describes the interaction between the two. We can derive a more tractable equation for the system dynamics alone if the coupling to the environment is weak, causing slow evolution on the uncoupled time scales of the system. A weak coupling ensures the environment is negligibly influenced by the system, which is the assumption made in the Born approximation. The Markovian approximation requires further restriction on the properties of the environment, assuming it to have no memory of the system.

If the coupling Hamiltonian V is weak it can be treated as a perturbation, and as in many cases, it is then useful to move to the interaction frame. In doing so we effectively split the relatively simple evolution due to $H_0 = H_s + H_E$ from the more complicated interaction

term. We do this via the transformations

$$\tilde{\rho}_{tot}(t) = e^{i(H_s+H_E)t/\hbar}\,\rho_{tot}(t)\,e^{-i(H_s+H_E)t/\hbar}, \tag{2.2}$$

$$\tilde{V}(t) = e^{i(H_s+H_E)t/\hbar}\,V\,e^{-i(H_s+H_E)t/\hbar}. \tag{2.3}$$

This in effect hides the evolution due to H_0 so as to focus on the slow dynamics induced by V. In the interaction frame the state evolution becomes

$$\dot{\tilde{\rho}}_{tot}(t) = -\frac{i}{\hbar}\big[\tilde{V}, \tilde{\rho}_{tot}(t)\big]. \tag{2.4}$$

The evolution of the original state can be recovered with the inverse of transformation (2.2). For the rest of this section we will drop the tilde and work exclusively in the interaction frame.

To proceed we can implicitly integrate from 0 to t,

$$\rho_{tot}(t) = \rho_{tot}(0) - i\int_0^t dt_1\big[V(t_1), \rho_{tot}(t_1)\big], \tag{2.5}$$

and we can begin an iterative expansion by substituting this solution back into (2.4),

$$\dot{\rho}_{tot}(t) = -\frac{i}{\hbar}\big[V(t), \rho_{tot}(0)\big] - \frac{1}{\hbar^2}\int_0^t dt_1\big[V(t), \big[V(t_1), \rho_{tot}(t_1)\big]\big]. \tag{2.6}$$

The reason for expanding to second order is that this leaves a non-vanishing contribution to the evolution after making the Born and Markov approximations. We are interested only in the evolution of the system so we can also trace over the environmental degrees of freedom,

$$\dot{\rho}(t) = -\frac{i}{\hbar}\,\mathrm{Tr}_E\big(\big[V(t), \rho_{tot}(0)\big]\big) - \frac{1}{\hbar^2}\int_0^t dt_1\,\mathrm{Tr}_E\big(\big[V(t), \big[V(t_1), \rho_{tot}(t_1)\big]\big]\big), \tag{2.7}$$

where we have defined the state of the system alone $\rho \equiv \mathrm{Tr}_E(\rho_{tot})$.

So far we still have an exact equation, our first assumption will be that the states of the system and environment approximately factorise,

$$\rho_{tot}(t) = \rho(t) \otimes \rho_E. \tag{2.8}$$

This is the Born approximation. It is justified by noting that with weak coupling, perturbations to the environment will be small and the induced correlations in the environment should die away quickly. We will show later that making a coarse graining approximation of the time evolution smooths out the fast induced dynamics in the environment and amounts to the same thing. Conversely however, the system is still heavily influenced by the interaction. It becomes entangled with the environment which leads to the production of mixed states after performing the trace. The approximation that they factorise is only good within the equation of motion.

It follows from this approximation that $Tr_E(V(t)\,\rho(0) \otimes \rho_E) = 0$. This can be interpreted as saying that the coupling consists of fluctuations about a zero mean, which can always be enforced by absorbing any diagonal terms in $V(t)$ into the choice of H_0. We can therefore eliminate the first term in (2.7).

The state equation is still non-local in time and difficult to solve. We can make some further simplifying assumptions to reach a Markovian, or local in time, equation. We first require $\rho(t_1) \approx \rho(t)$, which is a reasonable approximation if the integrand is small everywhere when $t_1 \neq t$. Secondly we need to extend the integral $\int_0^t dt_1 \rightarrow \int_{-\infty}^t dt_1$. Extending the integral assures the equation does not have time dependent coefficients. Again this is reasonable if the integrand is sharply peaked around t. For the integrand to have this behaviour relies on the properties of the environment, specifically we need the correlation functions for the environment to decay away quickly. This is often the case in the context of quantum optics. The free space electromagnetic field has a dense energy spectrum and the coupled system can always effectively interact with a new part of the environment where any correlations have quickly dissipated.

After making these changes we have arrived at the Born-Markov master equation,

$$\dot{\rho}(t) = -\int_{-\infty}^{t} dt_1 \, \mathrm{Tr}_E\big(\big[V(t), \big[V(t_1), \rho(t) \otimes \rho_E\big]\big]\big). \tag{2.9}$$

One of the most simple physical examples of this master equation is for a two-level atom coupled to the electromagnetic field. This allows us to see the Lindblad form of the master equation and illustrate the idea of decoherence. The system and environment Hamiltonian respectively are

$$H_{sys} = \omega_0 \sigma^\dagger \sigma, \qquad H_E = \sum_k \omega_k b_k^\dagger b_k, \tag{2.10}$$

where $\sigma = |e\rangle\langle g|$ is the atomic lowering operator and $|e\rangle$ and $|g\rangle$ are the two internal energy states. $b_k(b_k^\dagger)$ are the electromagnetic annihilation and creation operators for a given mode k. ω_0 is the frequency of the atomic transition and ω_k are the frequencies of the electromagnetic modes. The interaction can be described by the dipole coupling Hamiltonian,

$$V = -d.E = \sum_k \big(g_k b_k + g_k^* b_k^\dagger\big)\big(\sigma + \sigma^\dagger\big). \tag{2.11}$$

In the interaction frame following the transformation (2.3)

$$\begin{aligned} \tilde{V} &= \sum_k \big(g_k b_k e^{-i\omega_k t} + g_k^* b_k^\dagger e^{i\omega_k t}\big)\big(\sigma e^{-i\omega_0 t} + \sigma^\dagger e^{i\omega_0 t}\big) \\ &= \sum_k \big(g_k b_k \sigma^\dagger e^{-i(\omega_k - \omega_0)t} + g_k^* b_k^\dagger \sigma e^{i(\omega_k - \omega_0)t}\big), \end{aligned} \tag{2.12}$$

using the property of the phase-shifting operator $U = e^{-i\theta\hat{n}}$, $U^\dagger a U = a e^{-i\theta}$. In the last line we made the rotating wave approximation. This system has a large dominant frequency around the atomic transition where the light is also resonant. This allows us to eliminate any terms at frequencies $\omega_k + \omega_0$ since they will average to zero in the timescale of the other induced dynamics at $\omega_k - \omega_0$.

We can now substitute this interaction Hamiltonian into the exact state equation (2.7). If we specify the initial state of the environment ρ_E to be the electromagnetic vacuum, after

making the Born approximation we have,

$$\dot{\rho} = -\int_0^t dt_1\, \Gamma(t-t_1)\big(\sigma^\dagger\sigma\rho(t_1) - \sigma\rho(t_1)\sigma^\dagger\big) + \Gamma(t-t_1)^*\big(\rho(t_1)\sigma^\dagger\sigma - \sigma\rho(t_1)\sigma^\dagger\big), \quad (2.13)$$

where we have defined

$$\Gamma(t-t_1) = \sum_k |g_k|^2 e^{-i(\omega_k-\omega_a)(t-t_1)}. \quad (2.14)$$

In free space there are an infinite number of modes and the coupling coefficients g_k are infinitesimally small, so we can replace the sum over modes with an integral,

$$\Gamma(\tau) = \int_0^\infty d\omega\, D(\omega)g(\omega)^2 e^{-i(\omega-\omega_a)(\tau)}, \quad (2.15)$$

where we have introduced the density of states $D(\omega)$ and defined $\tau = t - t_1$. Putting in the proper form of the coupling coefficient in the free space limit, it turns out that $D(\omega)g(\omega)^2$ is a smoothly varying function in the vicinity of ω_0. The integral in (2.15) is effectively a Fourier transform and a smooth function will translate to a peaked function at $\tau = 0$. This can be seen with a toy model where $D(\omega)g(\omega)^2$ is a top-hat function from $0 \to 2\omega$, which produces a sinc() function after integrating.

The sharpness of the integrand means we can make the Markov approximation. It works out that the integral

$$\int_0^\infty d\tau\, \Gamma(\tau) = i\Delta\omega_0 + \frac{\gamma}{2}, \quad (2.16)$$

has a real and imaginary component. We have defined two new constants, the first term proportional to Δ is small and corresponds to a frequency shift in the system. This is known as the Lamb shift, the exact value of which can be calculated with a full relativistic treatment. The second term proportional to γ corresponds to radiative decay, and can be equated to the Einstein A coefficient for spontaneous emission. Substituting this solution

into the master equation gives

$$\begin{aligned}\dot{\rho} &= \big(-i\Delta\omega_0 - \frac{\gamma}{2}\big)\big(\sigma^\dagger\sigma\rho(t) - \sigma\rho(t)\sigma^\dagger\big) + \big(i\Delta\omega_0 - \frac{\gamma}{2}\big)\big(\rho(t)\sigma^\dagger\sigma - \sigma\rho(t)\sigma^\dagger\big) \\ &= -i\Delta\omega_0\Big[\sigma^\dagger\sigma, \rho\Big] + \gamma\mathcal{D}[\sigma]\rho.\end{aligned} \tag{2.17}$$

This is the Lindblad form of the master equation for spontaneous emission from a two level atom, where we have defined the Lindblad super-operator

$$\mathcal{D}[c]\rho = c\rho c^\dagger - \frac{1}{2}\big(c^\dagger c\rho + \rho c^\dagger c\big), \tag{2.18}$$

for any arbitrary operator c.

2.1.1 Decoherence

The coherence terms $\rho_{eg} = |e\rangle\langle g|\,, (\rho_{ge} = \rho_{ge}^\dagger)$ in the density matrix can be seen to decay following the evolution of the Lindblad master equation $\dot{\rho_{eg}} = -\gamma/2\,\rho_{eg}$. Over time they are damped to zero. Damping of the off diagonal elements in a reduced density matrix due to interaction with the environment is typical in many systems. This process is known as decoherence and has significance in alleviating the quantum measurement problem.

The measurement problem in quantum physics is that there is no known mechanism for translating between a probabilistic quantum description to a deterministic outcome. In classical physics it is assumed that a true state of the universe exists, where every particle has a well defined position and momentum. Newtonian mechanics is entirely deterministic, and probabilistic descriptions due to measurement imprecision are still in reference to a true underlying state. On the other hand, in quantum theory the state of a system is described by its wavefunction. Wavefunctions themselves evolve deterministically according to Schrödinger's equation, but they offer fundamentally probabilistic predictions of observing particular properties of the system. Experiments that show evidence of Bell's inequalities, correlations between entangled systems that cannot be explained by any

combination of local variables, suggest that there is no chance of locally-real underlying quantum state.

Born's rule tells us which classical observations we should expect to see from a quantum description, and although the mechanism that brings about the deterministic outcome is not understood, it provides remarkably accurate predictions. Early in quantum theory, making deterministic measurements would coincide with the end of the quantum evolution of the system, as the measurement effectively destroyed any quantum properties of the state. In certain Markovian systems, the process of decoherence allows for this description to be developed a step further. We can model the continuous measurement of some apparatus coupled to a quantum system. Since the apparatus will be strongly coupled to its environment it will decohere quickly and can be well approximated at all times to be in a classical mixture of states. This means we can sample deterministic measurement outcomes from the apparatus without throwing away any information contained in quantum correlations.

A minimal model that illustrates this process consists of the states of a system $|s\rangle$, an apparatus $|a\rangle$ and the environment $|e\rangle$. Part of the environment will usually be accessible as part of the measurement and this can be included in the compound of system and apparatus. If we imagine we want to measure an observable

$$X = \sum_n x_n \left|s_n\right\rangle\!\left\langle s_n\right|, \tag{2.19}$$

which we represent as a sum of projectors onto the state $|s_n\rangle$ with eigenvalue x_n. We can also expand the system in eigenstates of X, $|s\rangle = \sum c_n |s_n\rangle$.

A measurement should correlate the apparatus with the system such that

$$|\psi\rangle = \left(\sum_n c_n |s_n\rangle\right)|a_0\rangle \to \sum_n c_n |s_n\rangle |a_n\rangle . \tag{2.20}$$

Here we have sketched the idea of an the apparatus starting in some initial state $|a_0\rangle$,

transforming into a superposition state entangled with the system, where observing the state $|a_n\rangle$ would tell us the system was in state $|s_n\rangle$. Ideally an apparatus also would have states that are distinct $\langle a_n|a_m\rangle = \delta_{nm}$. The problem with this simple model is that since the outcome is a superposition of states, making a projective measurement onto a single state destroys quantum correlations that could have otherwise influenced the future evolution. We can see that this is not an issue if we include coupling to the environment in a modified setup,

$$|\psi\rangle = \left(\sum_n c_n |s_n\rangle\right)|a_0\rangle|e_0\rangle \to \sum_n c_n |s_n\rangle|a_n\rangle|e_n\rangle\,. \tag{2.21}$$

We have assumed that correlations build with the environment in the same way as with the apparatus, but in contrast the environment states do not form an orthonormal basis, $\langle e_n|e_m\rangle \neq \delta_{nm}$. We also assume that an observer will not have access to the environment states and so any correlations there are effectively lost. As with when deriving the master equation we can trace out the environment,

$$\begin{aligned}\rho_{SA} = \mathrm{Tr}_E\,|\psi\rangle\langle\psi| &= \sum_{n,m} c_n c_m^* |s_n\rangle|a_n\rangle\langle s_m|\langle a_n| \sum_k \langle e_k|e_n\rangle\langle e_m|e_k\rangle \\ &= \sum_{n,m} c_n c_m^* |s_n\rangle|a_n\rangle\langle s_m|\langle a_n|\ \langle e_n|e_m\rangle\,.\end{aligned} \tag{2.22}$$

In the last line we have used a resolution of identity to simplify the term $\sum_k \langle e_k|e_n\rangle\langle e_m|e_k\rangle = \langle e_n|e_m\rangle$. Now, if we work under the assumption that decoherence will drive the reduced density matrix so that is left with only diagonal elements,

$$\rho_{SA} = \sum_n |c_n|^2 |s_n\rangle\langle s_n| \otimes |a_n\rangle\langle a_n|\,. \tag{2.23}$$

We are left with a classical mixture of apparatus states correlated with the system. Finding the state $|a_n\rangle$ would correspond to measuring the eigenvalue x_n of the observable X. Any quantum coherence that existed has been shifted to the unobservable environment. We can then safely make projective measurements of the apparatus without destroying any

information that wasn't already lost. The decoherence in the joint system and apparatus is assumed to occur due to the strong coupling of the apparatus to the environment. The system will of course also interact with its surroundings (often necessarily so to couple to the apparatus in the first place), but will typically be better isolated and not decohere on the timescale of the measurement. In cases where there is a well defined separation between the system and apparatus, it is then possible to develop a model of continuous quantum measurement.

2.2 Quantum jumps

The evolution of a quantum system without dissipation can be fully described by the Schrödinger equation. On the other hand non-coherent processes, such as spontaneous emission or measurement collapse, can not be described by a unitary transformation of the state. Usually we turn to the density matrix formalism where a statistical ensemble of states is constructed to contain other probabilistic information beyond fundamental quantum uncertainty. A master equation like the one derived in the previous section is used to describe how on average the evolution will proceed.

However, it is also possible to model single quantum realisations for dissipative systems using a stochastic form of the Schrödinger equation[38, 39]. The methodology, coined by Howard Carmichael[30], is now widely known as the quantum trajectories approach. A quantum state of interest can be considered to undergo normal time evolution (under a carefully adjusted Hamiltonian) but with the chance of a stochastic jump occurring at any point along it's trajectory corresponding to say, absorption and emission events. The equation of motion is constructed in such way that averaging over several of these trajectories reproduces exactly the results of the density matrix approach. This can be both physically insightful and computationally very efficient as a wavefunction occupying a size N Hilbert space can be propagated with N equations, where as a density matrix will contain N^2. This avoids a bottleneck of computational power when the number of

trajectories required is small compared the growing complexity of a mixed system.

Here we will derive an illustrative quantum jump model for a two level dipole interacting with a classical optical driving field. The system and driving Hamiltonian are

$$H_{sys} = \hbar\omega_0 \left|e\right\rangle\!\left\langle e\right|, \tag{2.24}$$

$$H_D = \frac{\hbar\Omega}{2}\Big((e^{i\omega t} + e^{-i\omega t})\left|e\right\rangle\!\left\langle g\right| + (e^{i\omega t} + e^{-i\omega t})\left|g\right\rangle\!\left\langle e\right|\Big), \tag{2.25}$$

where ω_0 is the atomic transition frequency, ω is the optical driving frequency, Ω is the Rabi frequency and $|g\rangle$ and $|e\rangle$ are the atomic ground and excited states respectively. We move to the interaction frame via the unitary transform

$$U = e^{i\tilde{H}_{sys}t/\hbar} = \left|g\right\rangle\!\left\langle g\right| + e^{i\omega_0 t}\left|e\right\rangle\!\left\langle e\right|. \tag{2.26}$$

Such that

$$\tilde{H}_D = UH_DU^\dagger = \frac{\hbar\Omega}{2}\Big((e^{i\omega t} + e^{-i\omega t})e^{i\omega_0 t}\left|e\right\rangle\!\left\langle g\right| + (e^{i\omega t} + e^{-i\omega t})e^{-i\omega_0 t}\left|g\right\rangle\!\left\langle e\right|\Big). \tag{2.27}$$

We can apply the rotating wave equation, where terms oscillating at $\omega + \omega_0$ will rapidly average to zero and can be neglected leaving

$$\tilde{H}_D = \frac{\hbar\Omega}{2}\Big(e^{-i(\omega-\omega_0)t}\left|e\right\rangle\!\left\langle g\right| + e^{i(\omega-\omega_0)t}\left|g\right\rangle\!\left\langle e\right|\Big). \tag{2.28}$$

As in the previous section, the interaction Hamiltonian for coupling to the quantized electric field takes a similar form,

$$V = \hbar\int_{\omega_0-\theta}^{\omega_0+\theta} d\omega\,\sqrt{\frac{\gamma}{2\pi}}\Big(b^\dagger(\omega)e^{i(\omega-\omega_0)t}\sigma - \sigma^\dagger b(\omega)e^{-i(\omega-\omega_0)t}\Big). \tag{2.29}$$

Where $b(\omega)$ and $\sigma = |g\rangle\langle e|$ are ladder operators for the bath and system respectively. The bath operators create and annihilate photons of frequency ω over a range set by θ. We

justify this restricted range by arguing that the system will dominantly couple near the resonance frequency ω and note that we require $\theta \ll \omega_0$ so that terms $\omega + \omega_0$ can still be neglected in the rotating wave approximation. We have also started with the Markovian assumption that the coupling strength γ varies slowly enough to be considered constant over the bounded range of relevant frequencies. Finally, it will be helpful going forward to redefine the bath operators

$$b \equiv \frac{1}{\sqrt{2\pi}} \int_{\omega_0-\theta}^{\omega_0+\theta} d\omega \, b^\dagger(\omega) e^{i(\omega-\omega_0)t}, \tag{2.30}$$

so that we can write

$$V = \hbar\sqrt{\gamma}\,(b^\dagger\sigma - \sigma^\dagger b). \tag{2.31}$$

From here we will consider the evolution of the two-level system coupled to the electromagnetic vacuum $|\psi(0)\rangle = |s\rangle \otimes |e_{vac}\rangle$. The methodology we use can be generalised to consider couplings to other environments, but a vacuum state will make for a cleaner derivation. Straight away we do not need to consider the environment Hamiltonian as $H_E\,|e_{vac}\rangle = 0$. The Schrödinger equation for the coupled state in the interaction frame is then

$$\frac{d}{dt}\,|\psi\rangle = \left(-\frac{i}{\hbar}\tilde{H}_{sys} + \sqrt{\gamma} b^\dagger\sigma - \sqrt{\gamma}\sigma^\dagger b \right) |\psi(t)\rangle\,. \tag{2.32}$$

We have included the effects of optical driving and detuning in $\tilde{H}_{sys} = \tilde{H}_D$ which could in principle include any other slowly varying dynamics.

2.2.1 Perturbative expansion

In what follows we will make use of the commutation relation between the newly defined bath operators,

$$\left[b(t), b^\dagger(t')\right] = \frac{1}{2\pi} \int_{-\theta}^{\theta} d\omega \, e^{-i\omega(t-t')} \approx \delta(t-t'). \tag{2.33}$$

The commutator is a slowly varying delta function that can be approximated as a true delta function if the timescale $|t - t'| \gg 1/\theta$. This restricts us to considering dynamics on times much longer than $1/\theta$ whilst also making sure to keep $\theta \ll \omega_0$ for the rotating wave approximation. This resulting hierarchy of required timescales are happily well adhered to in many quantum optical settings,

$$\Omega, \Delta, \gamma \ll \theta \ll \omega_0. \tag{2.34}$$

It is possible here to pick a large enough cut off frequency θ, because the system and environment dynamical time scales are so small compared to that of the coupling dynamics. Models are often constructed so that the boundary between the system is a weak point of interaction, and enforcing the inequality amounts to us making the Born approximation in our derivation. We will now perform a coarse grained integration of the Schrödinger equation, considering incremental use of the time evolution operator. Using the delta function we just defined will allow us to neglect higher order terms arising from the interaction.

We choose to integrate in time steps Δt such that

$$\tau_{sys} \gg \Delta t \gg 1/\theta, \tag{2.35}$$

where τ_{sys} are the timescales of the induced system dynamics. These increments are chosen to be small on the scale of the interesting dynamics whilst long enough to allow many optical cycles to occur in each time step, maintaining the validity of our previous approximations. From here in order to perform perturbation theory we consider a Dyson series like approach to expanding the time evolution operator $U(t, t_0)$. In the interaction picture the operator itself evolves like

$$\frac{d}{dt}U(t, t_0) = -\frac{i}{\hbar}H(t)U(t, t_0), \tag{2.36}$$

which has the formal integral solution

$$U(t,t_0) - U(t_0,t_0) = -\frac{i}{\hbar}\int_{t_0}^{t} dt'\, H(t')U(t',t_0), \tag{2.37}$$

$$U(t,t_0) = 1 - \frac{i}{\hbar}\int_{t_0}^{t} dt'\, H(t')U(t',t_0). \tag{2.38}$$

From this solution we are able to perform an iterative expansion,

$$U(t,t_0) = 1 - \frac{i}{\hbar}\int_{t_0}^{t} dt_1\, H(t_1) + \left(-\frac{i}{\hbar}\right)^2 \int_{t_0}^{t} dt_2 \int_{t_0}^{t_2} dt_1\, H(t_2)H(t_1) + \dots . \tag{2.39}$$

So that the evolution of our initial wavefunction $|\psi(0)\rangle$ over the interval Δt, expanded to second order looks like

$$\begin{aligned} U(\Delta t,0)\,|\psi(0)\rangle =& |\psi(\Delta t)\rangle \\ \approx& \left[1 - \frac{i}{\hbar}\tilde{H}_{sys}\Delta t + \sqrt{\gamma}\sigma\int_0^{\Delta t} b^\dagger dt - \sqrt{\gamma}\sigma^\dagger \int_0^{\Delta t} b\, dt \right. \\ &\left. + \left(-\frac{i}{\hbar}\right)^2 \gamma\sigma^\dagger\sigma \int_0^{\Delta t} dt \int_0^{t_2} dt'\, b\, b^\dagger \right] |\psi(0)\rangle\,. \end{aligned} \tag{2.40}$$

Usually, if we only wanted to keep terms of first order in Δt we would not need to keep any of the second order expansion. However, due to the singular nature of the commutator between the bath operators (they produce a delta function), the specific seemingly second order term we have left works out to be of first order in Δt. To illustrate this it is helpful to examine the integral

$$\begin{aligned} \int_0^{\Delta t} dt \int_0^{t} dt'\, b(t)\, b^\dagger(t')\,|e_{vac}\rangle &= \int_0^{\Delta t} dt \int_0^{t} dt'\, [b(t), b^\dagger(t')]\,|e_{vac}\rangle \\ &= \int_0^{\Delta t} dt \int_0^{t} dt'\, \delta(t-t')\,|e_{vac}\rangle \\ &= \frac{1}{2}\Delta t\,|e_{vac}\rangle\,. \end{aligned} \tag{2.41}$$

where in the first line we have used the fact that an additional term $b^\dagger b$ required to make use of the commutation relation, amounts to adding zero when acting on the vacuum state. The factor of a half appears in the last line because the range of our integral technically only covers half of the defined delta function. All other terms involving these operators in different configurations evaluate to zero; it is this single second order term that gives rise to an effective Hamiltonian in our system evolution,

$$H_{\text{eff}} = \tilde{H}_{sys} - \frac{i}{2}\hbar\gamma\sigma^\dagger\sigma. \tag{2.42}$$

With this expansion, we can write our resulting wavefunction after a single time step,

$$\begin{aligned} |\psi(\Delta t)\rangle =& U(\Delta t, 0)\,|\psi(0)\rangle \\ =& \left[1 - \frac{i}{\hbar}H_{\text{eff}}\Delta t + \sqrt{\gamma}\sigma\Delta B^\dagger(0) + \sqrt{\gamma}\sigma^\dagger\Delta B(0)\right]|\psi(0)\rangle\,. \end{aligned} \tag{2.43}$$

where we have defined the incremental operator

$$\Delta B = \int_t^{t+\Delta t} b(s)ds. \tag{2.44}$$

In our case the annihilation term acting on the vacuum state $\Delta B\,|e_{vac}\rangle = 0$ can immediately be dropped. These new operators represent creating excitations in the environment within a specific time interval. We can also now see the manifestation of the second half of the Markov approximation. The bath dynamics always quickly return to equilibrium (on timescales $\approx 1/\omega_0$) so excitations in different time intervals should be independent. This is reflected in the commutation between these operators,

$$\begin{aligned} \left[\Delta B(t), \Delta B^\dagger(t')\right] &= \int_t^{t+\Delta t}\int_{t'}^{t'+\Delta t}\left[b(s), b^\dagger(s')\right]ds\,ds' \\ &= \int_t^{t+\Delta t}\int_{t'}^{t'+\Delta t}\delta(s-s')ds\,ds' \\ &= \begin{cases}\Delta t & t = t' \\ 0 & t \neq t'.\end{cases} \end{aligned} \tag{2.45}$$

Where the final integral is only non-zero when the two time intervals overlap (eg. $t = t'$), implying independent excitations in separate intervals.

We can also use these operators to construct a coarse grained number operator that would physically correspond to photo-detection in the increments Δt,

$$N(t) = \frac{\Delta B^\dagger(t)}{\sqrt{\Delta t}} \frac{\Delta B(t)}{\sqrt{\Delta t}}. \tag{2.46}$$

The counting operator defined this way is normalised, in-keeping with the dimensional analysis of the commutation relation (2.45) such that

$$N\,|0\rangle = 0 \quad \text{and} \quad N\,|1\rangle = 1\,|1\rangle\,. \tag{2.47}$$

A normalised single wave packet can be written as

$$\frac{\Delta B^\dagger}{\sqrt{\Delta t}}\,|e_{vac}\rangle = |1\rangle\,. \tag{2.48}$$

2.2.2 Stochastic Schrödinger equation

Returning to the evolution equation (2.43), we can reason that all time steps in our description progress the same way since the operators $\Delta B(t_n)$ for each time interval commute. Our general wavefunction evolution looks like

$$\begin{aligned} |\psi(t+\Delta t)\rangle =& \left[1 - \frac{i}{\hbar} H_{\text{eff}} \Delta t + \sqrt{\gamma}\,\sigma \Delta B^\dagger(t)\right] |s(t)\rangle \\ =& |e_{vac}\rangle \otimes (1 - \frac{i}{\hbar} H_{\text{eff}} \Delta t)\,|\psi(t)\rangle + |1\rangle \otimes \sqrt{\gamma \Delta t}\,\sigma\,|s(t)\rangle\,. \end{aligned} \tag{2.49}$$

The full coupled system could be considered to evolve this way, branching into a growing superposition of states at each interval. Alternatively we could consider a conditional evolution where we assume that a particular outcome of the entangled state was realised at every step [40]. If we were to measure the environment state in each increment we would

know which way the system evolved. Either under the effective Hamiltonian if there was no photo-detection, or under the influence of the annihilation operator if there was. This type of evolution could even be considered without any real detection process, simulating the evolution based on a hypothetical stochastic record of the environment state. The resulting system evolutions are quantum trajectories. Simulating quantum jumps (instantaneous collapse of the system state) based on the number state of the environment is an example of one of many possible stochastic unravellings, where the simulated wavefunction evolution is conditioned on the environment.

In order to develop this technique further we will write down a stochastic Schrödinger equation that can be used to generate trajectories computationally. We will re-label the system state alone as $|\psi\rangle \equiv |s\rangle$ and replace the annihilation operator σ with a general jump operator c, which could represent a different coupling to the environment. The system state will undergo evolution under the influence of the effective Hamiltonian but with the chance of a randomly occurring jump at any time interval. If we had assumed the environment to be in a thermal state the resulting stochastic master equation would have contained a second stochastic term accounting for absorption events. In this case though, in each time interval Δt there is the possibility of either;
time evolution under H_{eff},

$$|\psi(t+\Delta t)\rangle = \exp\left(-\frac{i}{\hbar}H_{\text{eff}}\,\Delta t\right)|\psi(t)\rangle\,, \tag{2.50}$$

$$d\,|\psi\rangle \approx -\frac{i}{\hbar}\tilde{H}_{sys}\,|\psi(t)\rangle\;dt - \frac{\gamma}{2}c^{\dagger}c\,|\psi(t)\rangle\;dt. \tag{2.51}$$

or a stochastic jump to a lower state,

$$d\,|\psi\rangle = -\,|\psi\rangle + \frac{c\,|\psi\rangle}{\sqrt{\langle c^{\dagger}c\rangle}}. \tag{2.52}$$

Where the current state is replaced with an altered version of itself after the application of the jump operator c. This non-unitary transformation requires the addition of the present

re-normalisation factor.

The probability of a jump occurring can be found by taking the trace of the system acted on by the jump operators,

$$\begin{aligned} P_{jump} &= \mathrm{Tr}\big(\sqrt{\gamma\Delta t}\, c\,|\psi\rangle\langle\psi|\,\sqrt{\gamma\Delta t}\, c^\dagger\big) \\ &= \gamma\Delta t\,\mathrm{Tr}\big(c^\dagger c\rho\big) \\ &= \gamma\,\Delta t\langle c^\dagger c\rangle. \end{aligned} \tag{2.53}$$

During intervals where the state is regularly evolving, explicit re-normalisation is also required after the influence of the non-Hermitian effective Hamiltonian. If we consider the state evolution after time Δt,

$$\begin{aligned} \langle\psi(t+\Delta t)|\psi(t+\Delta t)\rangle &\approx \langle\psi(t)|\,(1+\frac{i}{\hbar}H_{\text{eff}}^\dagger\,\Delta t)(1-\frac{i}{\hbar}H_{\text{eff}}\,\Delta t)\,|\psi(t)\rangle \\ &= \langle\psi(t)|\psi(t)\rangle - \frac{i}{\hbar}\Delta t\,\langle\psi(t)|\,H_{\text{eff}} - H_{\text{eff}}^\dagger\,|\psi(t)\rangle + \mathcal{O}(\Delta t) \\ &\approx 1 - \Delta t\,\langle\psi(t)|\,\gamma\,c^\dagger c\,|\psi(t)\rangle \\ &= 1 - \Delta t\,\gamma\langle c^\dagger c\rangle \\ &= 1 - \Delta p. \end{aligned} \tag{2.54}$$

In order to re-normalise the state after letting it evolve for a small amount of time, we can include an additional factor of Δp in the wavefunction. Adding a factor like this, proportional to the current state vector, uniformly re-scales the wavefunction so that it remains normalised. The effective Hamiltonian captures the idea that even when not detecting any signal in the environment we are gaining information from the system which in turn alters its evolution. For example, when measuring emission events no signal implies that the system is more likely to be in the ground state.

The last step is to introduce the stochastic variable,

$$dN = \begin{cases} 0 & \text{probability of no jump} \quad (1-\Delta p) \\ 1 & \text{probability of jump} \qquad \Delta p \end{cases}. \tag{2.55}$$

Combining all of these elements we can write,

$$d\left|\psi\right\rangle = -\frac{i}{\hbar}\tilde{H}_{sys}\left|\psi\right\rangle dt + \frac{\gamma}{2}(\langle c^\dagger c\rangle - c^\dagger c)\left|\psi(t)\right\rangle dt + (\frac{c\left|\psi\right\rangle}{\sqrt{\langle c^\dagger c\rangle}} - 1)\left|\psi\right\rangle dN \tag{2.56}$$

This is a general form of a stochastic Schrödinger equation with quantum jumps. The wavefunction described by this equation by design remains normalised as it evolves. (It was not necessary to include a pre-factor of $(1-dN)$ with the terms describing the regular evolution without jumps, since contributions of order $dN\,dt$ are negligibly small).

The Lindblad equation (2.18) we arrived at in the previous section turns out to be a very general description of dissipative quantum systems, and in fact we can see exact equivalence with the stochastic Schrödinger equation we have written. We must first note that when using the product rule here a higher order correction must be included. Whilst usually neglected in normal calculus, the second order derivative makes first order contributions since terms $dN^2 = dN$. So we have

$$\begin{aligned}\frac{d\rho}{dt} &= \left((\frac{d}{dt}\left|\psi\right\rangle)\left\langle\psi\right| + \left|\psi\right\rangle(\frac{d}{dt}\left\langle\psi\right|) + (\frac{d}{dt}\left|\psi\right\rangle)(\frac{d}{dt}\left\langle\psi\right|)\right) \\ &= -\frac{i}{\hbar}\Big[\tilde{H}_{sys},\rho\Big]\,dt - \frac{\gamma}{2}\Big\{c^\dagger c,\rho\Big\}\,dt + \gamma\langle c^\dagger c\rangle\rho dt + (\frac{c\,\rho\,c^\dagger}{\sqrt{\langle c^\dagger c\rangle}} - \rho)dN.\end{aligned} \tag{2.57}$$

This is a conditional master equation which when averaged (using the fact that $\langle dN\rangle = \gamma\langle c^\dagger c\rangle dt$) returns the usual Lindblad form,

$$\frac{d\langle\!\langle\rho\rangle\!\rangle}{dt} = -i\big[\tilde{H}_{sys},\langle\!\langle\rho\rangle\!\rangle\big] + \frac{\gamma}{2}(2c\langle\!\langle\rho\rangle\!\rangle c^\dagger - c^\dagger c\langle\!\langle\rho\rangle\!\rangle - \langle\!\langle\rho\rangle\!\rangle c^\dagger c). \tag{2.58}$$

Here we use double angled brackets to denote the ensemble average over many trajectories, as opposed to the expectation value of an observable associated with a given state or ensemble of states.

We can again consider our specific example case, the driven two level atom provides a good demonstration of implementing quantum jumps. Figure 2.1 shows the numerical

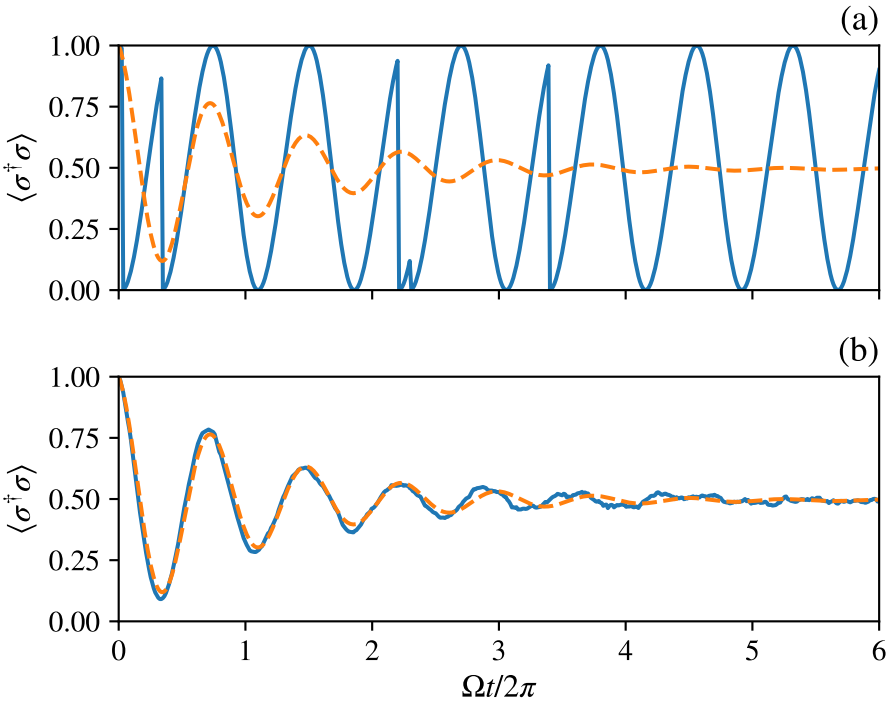

Figure 2.1: Results of a numerical quantum jumps simulation for a driven two level atom. Figure a) shows the excited state occupancy in a single trajectory, in the absence of emission there are distorted oscillations due to the effective Hamiltonian, at the Rabi frequency Ω. Figure b) shows an average of 1000 trajectories. The dashed line in both plots shows the solution to the Lindblad master equation with the same parameters.

simulation of a single trajectory alongside an average of 1000 of these trajectories. The averaged result is plotted in comparison with the results of numerically integrating the Lindblad master equation describing the same system.

2.3 Quantum diffusion

The form of the stochastic Schrödinger equation we arrived at is quite versatile, but it is not a unique unravelling of the master equation. It is possible to write diffusive equations with white noise, rather than stochastic jumps, to reproduce the same statistical dynamics.

These equations in turn can be related to a different conditional measurement theory, for example based on balanced homodyne detection.

The stochastic jump equation can be associated with photo-detection, in a sense measuring the field intensity $b^\dagger b$ (in this section we relabel the annihilation operator associated with a given time $b(t) \equiv \Delta B(t)$). Although the complex field amplitude b is not directly measurable the quadrature components of the light field are,

$$b = \frac{1}{\sqrt{2}}(q + ip), \tag{2.59}$$

where we have defined the quadrature components

$$q = \frac{1}{\sqrt{2}}(b^\dagger + b) \quad \text{and} \quad p = \frac{i}{\sqrt{2}}(b^\dagger - b). \tag{2.60}$$

The quadrature operators q and p behave like the position and momentum counterparts for a trapped particle in a harmonic well. Their construction means they share a similar commutation rule,

$$[q, p] = i. \tag{2.61}$$

The quadrature states can also be used to represent wavefunctions of a light field in phase space $\psi(q) = \langle q|\psi\rangle$, although q does not actually have any relation to the 'position' of any part of the light field, and neither does p have any relation the the momentum of the field. In order to derive a stochastic diffusion equation we will consider balanced homodyne detection of the light quadratures, as sketched in Fig. 2.2.

If we first imagine that all of the light radiated from an atom is somehow collimated into a directed beam, instead of using direct photo-detection, the light could first be interfered with another coherent light source. Perfectly collecting all the light is not actually necessary but will simplify the derivation, for simplicity we will also assume that the interference occurs at a perfect 50/50 beam splitter. The extra input field $\alpha = |\alpha|e^{i\phi}$, known as a local oscillator, will usually be intense enough to be treated classically and

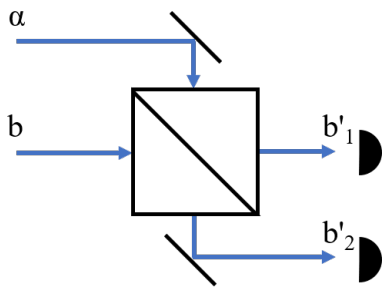

Figure 2.2: Simplified diagram of balanced homodyne detection. A quantum signal b to be measured, passes through a 50/50 beam splitter mixed with a reference source α. The reference beam serves to amplify the quantum signal so that the output beams (b_1', b_2') can more easily be measured by photo-detectors.

is there to serve as a phase reference. The goal is through interference to amplify the signal from the quantum light mode we are interested in [41]. From an experimental point of view, this has the advantage of being able to bring a weak quantum signal above the noise floor of photo-detectors. For homodyne detection both light beams must have a fixed phase relationship, which is often the case when the quantum system of interest is being illuminated by the same common laser source that generates the local oscillator. The signals at the two outputs of the beam splitter will be in a superposition of both the signal and the reference field,

$$b_1' = \frac{1}{\sqrt{2}}(b - \alpha) \quad \text{and} \quad b_2' = \frac{1}{\sqrt{2}}(b + \alpha). \tag{2.62}$$

Photo-detectors measuring these signals would then produce currents proportional to the photon counts

$$\begin{aligned} N_1 &= b_1'^{\dagger} b_1' = \frac{1}{2}(b^\dagger b - b^\dagger \alpha - b\alpha^* + |\alpha|^2) \\ N_2 &= b_2'^{\dagger} b_2' = \frac{1}{2}(b^\dagger b + b^\dagger \alpha + b\alpha^* + |\alpha|^2). \end{aligned} \tag{2.63}$$

The two generated currents can then be filtered and subtracted from each other, leaving

a photo difference current proportional to a combination of the quadrature states,

$$I_{21} \propto (N_2 - N_1) = |\alpha|\big(e^{-i\phi}b + e^{i\phi}b^\dagger\big). \tag{2.64}$$

The phase reference of the local oscillator can be varied to measure the full range of both quadratures q and p. We can again associate measuring the state of the field with the conditional evolution of the atomic system.

Previously we modelled discontinuous jumps in the system evolution whenever radiated light was measured in the field. In a homodyne measurement the detected count rate needs to be modified to include a contribution from the local oscillator,

$$\begin{aligned} \text{Previous count rate:} \quad & \langle dN\rangle = \gamma\langle c^\dagger c\rangle dt = \mathrm{Tr}\big[\gamma\, c^\dagger c\,\rho\big]dt \\ \text{Homodyne count rate :} \quad & \langle dN\rangle = \mathrm{Tr}\big[(\sqrt{\gamma}\, c^\dagger + \alpha^*)(\sqrt{\gamma}\, c + \alpha)\rho\big]dt. \end{aligned} \tag{2.65}$$

We can transform the jump operators to reflect this extra contribution to the count rate. We know that regardless of how the field is measured we should still see the same average evolution of the atomic system, since the coupling Hamiltonian is unchanged. This would be the evolution expected if we discarded all the information in the environment. The master equation for the statistical ensemble (2.18) is invariant to a displacement of the jump operators c, as long as we also add a term to the Hamiltonian. Displacement equal to the amplitude of the local oscillator produces the desired count rate,

$$\begin{aligned} &\sqrt{\gamma}\, c \to \sqrt{\gamma}\, c + \alpha, \\ &\tilde{H}_{sys} \to \tilde{H}_{sys} - \frac{i}{2}\hbar\alpha\sqrt{\gamma}\,(c - c^\dagger), \end{aligned} \tag{2.66}$$

Since these changes cancel each other out in the master equation, we can safely make the same transformation in the stochastic Schrödinger equation (2.56) without changing the statistical dynamics (ie. averaging over the trajectories of the transformed equation will

still reproduce the same Lindblad equation),

$$\begin{aligned} d\,|\psi\rangle = &\left(-\frac{i}{\hbar}H - \frac{1}{2}(\gamma c^\dagger c + 2\alpha\sqrt{\gamma}c - \gamma\langle c^\dagger c\rangle - |\alpha|\sqrt{\gamma}\langle\tilde{q}\rangle)\right)|\psi\rangle\, dt \\ &+ \left(\frac{\sqrt{\gamma}c+\alpha}{\sqrt{\langle(\sqrt{\gamma}c^\dagger+\alpha)(\sqrt{\gamma}c+\alpha)\rangle}} - 1\right)|\psi\rangle\, dN, \end{aligned} \tag{2.67}$$

where we have defined the system quadrature

$$\tilde{q} = (e^{-i\phi}c^\dagger + e^{i\phi}c). \tag{2.68}$$

This updated equation has been normalised in the same manner as (2.56). Now, photo-detection events correspond to applying the operator $C = \sqrt{\gamma}\,c + \alpha$ to the system. There are more frequent jumps than before but the collapse operator c is weighted less as α increases. More of the old wavefunction state after each jump is kept due to the extra local oscillator factor.

In a homodyne measurement the local oscillator amplitude will be very large compared to the quantum signal, and we can consider the limit where $\alpha \to \infty$. In doing so we can re-write the count rate

$$\begin{aligned} dN &= (\sqrt{\gamma}c^\dagger + \alpha^*)(\sqrt{\gamma}c+\alpha)dt \\ &= (|\alpha|^2 + |\alpha|\sqrt{\gamma}\tilde{q} + \gamma c^\dagger c)dt \\ &\approx (|\alpha|^2 + |\alpha|\sqrt{\gamma}\tilde{q})dt \\ &\equiv |\alpha|^2 dt + |\alpha|\, dQ(t). \end{aligned} \tag{2.69}$$

In the third line we have dropped the term not proportional to the large oscillator strength α. In the final line we have defined the stochastic operator $dQ(t)$, similar to the increment operators dN we defined for direct photo-detection. We can see that as $\alpha \to \infty$, $Q(t)$ takes on Gaussian properties. From our definition we can easily see the mean value

$$\langle dQ\rangle = \sqrt{\gamma}\langle\tilde{q}\rangle dt \tag{2.70}$$

and by rearranging (2.69), and using the fact that $dN^2 = dN$,

$$\begin{aligned} dQ^2 = \frac{(dN - \alpha^2 dt)^2}{\alpha^2} = \frac{dN}{\alpha^2} = dt + \frac{dQ}{\alpha} \\ \lim_{\alpha\to\infty} dQ^2 \to dt. \end{aligned} \tag{2.71}$$

And lastly we note that $dQ(t)dt = 0$, since it is of order dt^2.

If we only measure dN over time intervals $\Delta t \gg 1/\alpha$, by the central limit theorem, we may approximate the Poisson jump process (2.69) with a mean drift plus white noise. Effectively regarding dQ as a Gaussian random variable of mean $\sqrt{\gamma}\langle\tilde{q}\rangle dt$ and variance dt,

$$dQ = \langle dQ\rangle + dW = \sqrt{\gamma}\langle\tilde{q}\rangle dt + dW. \tag{2.72}$$

Where dW is a Wiener increment with the properties $dW^2 = dt$, and $\langle dW\rangle = 0$. In the same way that we associated dN with a physical count rate in direct photo-detection, we can relate dQ to a stochastic homodyne current. The current from an idealised photo-detector can be written in terms of the count rate,

$$I(t) = e\frac{dN}{dt}, \tag{2.73}$$

where e is the total charge conducted at each detection event. For direct photo-detection $dN/dt = \sum_i \delta(t - t_i)$, so the current is made up of a sum of delta functions at different times. In the case of a homodyne measurement we want to subtract the large constant photo-current due to the local oscillator field from (2.69),

$$\begin{aligned} I(t) &= \frac{1}{\alpha}\left(\frac{dN}{dt} - |\alpha|^2\right) = \frac{dQ}{dt} \\ &= \sqrt{\gamma}\langle\tilde{q}\rangle + \xi(t), \end{aligned} \tag{2.74}$$

where we have normalised the current by dividing through by $e|\alpha|$. We also introduced $\xi(t) = dW/dt$, which is a Gaussian white noise function.

Taking the strong oscillator limit in (2.67) and re-writing the increment dN in terms of the white noise increment $dQ(t)$ finally gives us a diffusive stochastic Schrödinger equation,

$$d\left|\psi\right\rangle = \left(-\frac{i}{\hbar}\tilde{H}_{sys}\left|\psi\right\rangle dt - \frac{\gamma}{2}(c^{\dagger}c - \langle\tilde{q}\rangle c + \frac{1}{4}\langle\tilde{q}\rangle^{2})dt + \sqrt{\gamma}(c - \frac{1}{2}\langle\tilde{q}\rangle)dW \right)\left|\psi(t)\right\rangle . \quad (2.75)$$

Where in order to normalise this wavefunction we made use of the Ito rule $dW^2 = dt$. Writing

$$d\left|\psi\right\rangle = (\alpha dt + \beta dW)\left|\psi\right\rangle , \quad (2.76)$$

the square amplitude was calculated including higher order terms and then forced to equal one,

$$\begin{aligned}\langle\psi(t+\Delta t)|\psi(t+\Delta t)\rangle &= \langle\psi|\,(1+\alpha^{\dagger}dt+\beta^{\dagger}dW)(1+\alpha dt+\beta dW)\,|\psi\rangle \\ &= \langle\psi|\psi\rangle + dt\,\langle\psi|\,\alpha+\alpha^{\dagger}\,|\psi\rangle + dW\,\langle\psi|\,\beta+\beta^{\dagger}\,|\psi\rangle + dt\,\langle\psi|\,\beta^{\dagger}\beta\,|\psi\rangle \\ &\equiv 1.\end{aligned} \quad (2.77)$$

An equation written in terms of these increments dW will have a diffusive evolution. That is to say the paths of a Wiener process $W(t)$ follow highly erratic trajectories with probability distributions that diffuse outward from their origins as time increases. The width of the distribution grows like $\sqrt{t}$ and slowly tends to infinity. These are the same paths that are used to describe the motion of Brownian particles [42]. In differential equations the increments dW can be simulated by generating random numbers selected from a Gaussian distribution of width dt.

Figure 2.3 shows an example of stochastic trajectory generated with equation (2.75). Again, a driven two level system is considered and the evolution was solved using a Euler-Maruyama style integrator for Ito stochastic equations. The conditional evolutions are of notably different from those generated with quantum jumps but an average of 100 trajectories approximates the same statistical evolution of the Lindblad master equation. This

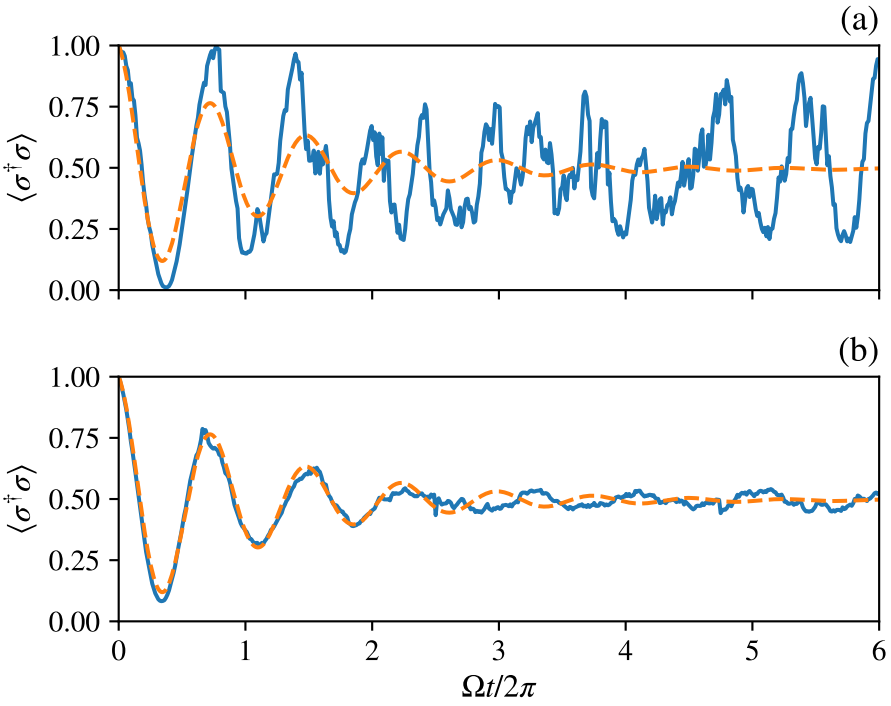

Figure 2.3: Results of a quantum diffusion simulation of a driven two-level atom with Rabi frequency Ω. Figure a) shows a single trajectory which appears to be highly erratic as the system quadrature is continuously measured forcing random wavefunction collapse. Although seemingly very different from the jump model, figure b) shows that an average over 100 of these trajectories converges to the same ensemble dynamics predicted by the Lindblad equation, which is overlaid as a dashed line.

is ten times fewer trajectories than we averaged over when simulating quantum jumps but produces a similar degree of accuracy. This is often the case when simulating a diffusive master equation, however, there is a trade off in that integrating an equation with white noise is more computationally intensive. As such simulating 100 diffusive trajectories was only around twice as fast as simulating 1000 jump trajectories.

We have explored two quantum trajectory techniques that can be used to describe the conditional evolution of open quantum systems under continuous measurement. Both techniques provide insights into understanding quantum measurement whilst also provid-

ing a tool to simulate statistical ensembles with computational efficiency. The apparent ambiguity how the conditional evolution progresses for individual trajectories is mathematically rooted in the fact that the Lindblad equation can be transformed and written with an array of different jump operators to describe the same dynamical system. The physical interpretation of this comes back to how we measure the environment, ultimately dictating which is the appropriate method to use, beyond pure computational efficiency.

2.3.1 White noise

In this section we will briefly discuss some of the properties of white noise in more detail, and the consequences of its use in differential calculus. Previously we defined white noise as the derivative of a Wiener noise process $W(t)$. This is the path followed by idealised Brownian particles, it is a Markovian process and can be described by a Fokker Planck equation (the time evolution of the path probability distribution),

$$P(W,t) = \frac{1}{\sqrt{2\pi t}} \exp\left(-\frac{W^2}{2t}\right). \tag{2.78}$$

Although the mean value of this process is zero, individual sample paths are highly irregular, the variance growing as the square root of time and becoming infinite as $t \to \infty$. Each path is also fractal in nature, continuous but also nowhere differentiable.

A realistic portrayal of a physical pseudo-stochastic process would usually have some finite correlation function,

$$\langle \xi(t)\xi(t')\rangle = \frac{D}{2k}\, e^{-k|t-t'|}\ . \tag{2.79}$$

However, it is mathematically convenient to consider idealised white noise in the limit where $k \to \infty$ and $\xi(t)$ becomes delta correlated. This is a reasonable approximation to make when the system dynamics occur on time-scales much larger than the correlation time, as was the case in deriving the quantum diffusion equation. This function has a flat power spectrum across all frequencies, and has sample paths $\int \xi(t)dt$ which exactly share

the properties of $W(t)$. This implies a worrying definition of white noise as the derivative of the non-differentiable function $W(t)$. It is therefore good mathematical practice to express differential equations involving white noise as integral equations,

$$\begin{aligned} dx &= \int a(x,t)\,dt + \int b(x,t)\xi(t)\,dt, \\ &= \int a(x,t)\,dt + \int b(x,t)\,dW. \end{aligned} \tag{2.80}$$

Equations of this form are examples of Langevin equations.

The issue now lies in considering how to evaluate integrals of a stochastic process. Formally an integral is defined as the limit of the Riemann sum,

$$\int_{t_0}^{t} f(t')\,dt' = \lim_{n\to\infty} \sum_{k=0}^{n-1} f(\tilde{t_k})(t_{k+1} - t_k). \tag{2.81}$$

Usually the position of $\tilde{t_k}$ within the interval $[t_k, t_{k+1}]$ does not matter when taking the limit for smooth functions as the sum always converges to the same value. White noise never becomes smooth and as such choosing a different position for $\tilde{t_k}$ gives rise to different results. There are two main fields of thought as to the best way to define this integral.

The Stratonovich approach considers $\tilde{t_k} = (t_{k+1} + t_k)/2$. This integral definition initially seems appealing as it preserves all the rules of normal calculus. If you want to manipulate the Langevin equation defined this way you can safely use the usual product and chain rules. This is a reassuring result when trying to write down a model for physical continuous processes that should have no reason for straying from the rules of standard calculus. This choice attempts to capture the physics of a noise process that has truly finite time correlations that are short enough to be approximated as zero. However in this calculus multiplicative processes with the noise term do not average to zero, $\langle b(t)W(t)\rangle \neq 0$. This is a result of the fact that evaluating the Stratonovich integral amounts to averaging over different instances of the noise. The way the integral was defined leads any function of time multiplying the noise to be correlated with it in some way, with no easy analytic

method for handling these terms. This does seem to reflect the idea of attempting to model physical processes that would in fact have some non-zero correlation over short time scales.

Ito's interpretation of the integral is the other most widely used. This calculus embraces idealised white noise describing truly random, independent events. The position of $\tilde{t_k}$ is chosen (usually at the far left of the interval $\tilde{t_k} = t_k$) such that $\langle b(t)W(t)\rangle = 0$, preserving the Martingale property that the future of the two functions are not linked in any way. This is often considered appropriate for statistical modelling, financial models for example are often not the limit of some differential equation but constructed as a sequence of distinct steps. A truly independent increment dW also makes it easier to better mathematically define Ito calculus. It can be shown in this framework that terms $dW^2 = dt$, at least loosely. A surprising result that means there now appear non-vanishing second order terms that would have other wise been discarded under normal circumstances.

Both approaches have their advantages although Langevin equations that are meant to be approximately describing continuous processes are usually considered to be of Stratonovich form. It is helpfully possible to switch between the two calculi; if an equation written in Stratonovich form is considered to be the correct physical representation of some process it can be re-expressed in Ito form. The multiplicative function $b(t)$ is thought of as being adapted to some completely non-anticipating function of the noise (such that $\langle b(t)W(t)\rangle = 0$) and with this occurs an extra term in the integral. Generally a Stratonovich (S) SDE,

$$dx = a(x,t)\,dt + b(x,t)\xi(t)\,dt, \tag{2.82}$$

is equivalent to an Ito (I) SDE,

$$dx = a(x,t)\,dt + \frac{1}{2}\,b(x,t)\,\partial x\,b(x,t)\,dt + b(x,t)\xi(t)\,dt. \tag{2.83}$$

This is a very useful transformation when wanting to use the often more adaptable Ito calculus for performing analysis or numerical simulations. It also illustrates that the in

the case of only additive noise, when b(x,t) is constant, both integral forms are identical. The diffusion equation we derived followed from the discretized evolution of a quantum state, where each time interval was approximated to be truly independent. We should therefore treat it as an Ito equation even though it describes a physical process which would certainly have finite time correlations. In fact the corrective term that appears in switching from a Stratonovich equation is the same as the effective Hamiltonian term we already included from the time-dependent perturbation theory.

2.3.2 General Gaussian measurements

A measurement that projects a system onto a single eigenstate is known as a von Neumann measurement $P_n = |n\rangle\langle n|$. More generally though, and perhaps more naturally, a measurement will reduce the uncertainty regarding the state of an observable but not define it completely. For example the measurement operator

$$\Omega_\alpha = \sum_n \exp\big(-\kappa(x_n-\alpha)^2/4\big)\,|x_n\rangle\langle x_n| \tag{2.84}$$

is a Gaussian weighted sum of projector operators onto single states. Acting on a state that is initially completely mixed, these generalised measurements leave the system with a peaked probability of having eigenvalue α, but this is not its definite value. The certainty of this depends on the strength of the measurement, here characterised by κ. A weak measurement with a small κ will proved less certainty and also cause less disturbance to the system.

A continuous measurement can be defined as a sequence of weak measurements taken in intervals Δt,

$$A(\alpha) = \left(\frac{4\kappa\Delta t}{\pi}\right)^{\frac{1}{4}} \int_{-\infty}^{\infty} \exp\big(-2\kappa\Delta t(x-\alpha)^2\big)\,|x\rangle\langle x|\,dx. \tag{2.85}$$

This set of operators has the same form as (2.84) but we are now looking at a continuous

set of eigenstates $|x\rangle$ of some operator X, and a continuum of measurement results labelled by α. We have also written $A(\alpha)$ such that it is normalised $\int A^\dagger(\alpha)A(\alpha)\,\mathrm{d}\alpha = I$. The probability of obtaining a measurement result from some initial state is then $P(\alpha) = \mathrm{Tr}\big(A(\alpha)^\dagger A(\alpha)\rho\big)$, and for small Δt the probability density for α is approximately Gaussian and centred about $\langle X\rangle$.

It can be useful to treat α as a stochastic quantity, representing one possible realisation of the measurement record,

$$\alpha = \langle X\rangle + \frac{\Delta W}{\sqrt{8\kappa}\Delta t}. \tag{2.86}$$

Here ΔW is a Gaussian random variable with variance Δt, which is a proper Wiener increment in the limit $\Delta t \to 0$. Working with this stochastic representation, we can expand $A(\alpha)$ to first order in dt

$$A(\alpha) \propto \exp\big(-2\kappa\,dt(X-\alpha)^2\big) \approx 1 - \big(\kappa X^2 - 4\kappa X\langle X\rangle\big)dt + \sqrt{2\kappa}X\,dW. \tag{2.87}$$

This operator describes the incremental evolution of the system when making a measurement in each time step dt, given that the observer obtains the measurement result α. We can now use the form of (2.87) to derive a stochastic master equation with the physical interpretation of a system that is being continuously measured. In order to consider the most general possible evolution due to a stochastic operator, we can first re-write

$$A = 1 - i\frac{H}{\hbar}dt + b\,dt + c\,dW, \tag{2.88}$$

where we have explicitly included the unitary evolution of the Schrödinger equation, and introduced the freely defined operators b and c. Under the constraint of preserving the positive eigenvalues of ρ, the most general transformation of the density matrix is

$$\rho \to \sum_n A_n \rho A_n^\dagger. \tag{2.89}$$

For $A = 1 - i\frac{H}{\hbar}dt$, we get the usual Hamiltonian evolution. Putting (2.88) into the

transformation we find

$$d\rho = -\frac{i}{\hbar}[H,\rho]dt + \{b,\rho\}dt + c\rho c^\dagger dt + (c\rho + \rho c^\dagger)dW. \tag{2.90}$$

This equation already has features reminiscent of the Lindblad equation (2.18). We can put some constraints on the operators b and c by considering the trace of ρ. Since we are modelling the discretised evolution of the state - where we assume the noise to be independent in each increment - we can treat this as an Ito equation. Therefore, in the ensemble average $\langle\!\langle \rho\, dW \rangle\!\rangle = 0$, and so

$$d\langle\!\langle\rho\rangle\!\rangle = -\frac{i}{\hbar}[H,\langle\!\langle\rho\rangle\!\rangle]dt + \{b,\langle\!\langle\rho\rangle\!\rangle\}dt + c\langle\!\langle\rho\rangle\!\rangle c^\dagger dt. \tag{2.91}$$

Since the trace $\mathrm{Tr}\left(\rho\right) = 1$, the derivative $\mathrm{Tr}\left(d\rho\right) = 0$, which gives the constraint

$$\mathrm{Tr}\left(\langle\!\langle\rho\rangle\!\rangle(2b + c^\dagger c)\right) \equiv 0 \quad \rightarrow \quad b = -\frac{c^\dagger c}{2}. \tag{2.92}$$

The same argument for the conditional evolution implies

$$\mathrm{Tr}\left(\rho(c + c^\dagger)dW\right) \equiv 0. \tag{2.93}$$

We can enforce normalisation by subtracting a term proportional to (2.93) from (2.90). This results in the final form of this stochastic master equation (SME),

$$d\rho = -\frac{i}{\hbar}\big[H,\rho\big]dt + \mathcal{D}[c]\rho\, dt + \mathcal{H}[c]\rho\, dW. \tag{2.94}$$

where $\mathcal{D}[c]$ is the Lindblad super-operator and $\mathcal{H}[c]$ is the measurement super-operator,

$$\mathcal{D}[c]\rho = c\rho c^\dagger - \frac{1}{2}(c^\dagger c\rho + \rho c^\dagger c), \tag{2.95}$$

$$\mathcal{H}[c]\rho = c\rho + \rho c^\dagger - \langle c + c^\dagger\rangle\rho. \tag{2.96}$$

The first term in the master equation describes the usual evolution due to reversible dynamics, and the Lindblad term describes the back-action or disturbance to a system due to measurement. The final term represents the information gain due to the measurement process and the induced fundamental noise due to the quantum state collapsing. We can relate this stochastic state evolution back to the original measurement operator we considered (2.87) by identifying $c = \sqrt{2\kappa}X$. From (2.86), this implies a measurement record

$$dI(t) = \frac{\langle c + c^\dagger \rangle}{2} dt + \frac{dW}{2}. \tag{2.97}$$

This measurement record and the master equation (2.94) exactly maps onto the diffusive stochastic Schrödinger equation we derived for homodyne measurement if we calculate $d(|\psi\rangle\langle\psi|)$.

To consider multiple possible measurements we can introduce a sum over many of these collective terms whilst also introducing an efficiency η for each channel,

$$d\rho = -\frac{i}{\hbar}\big[H, \rho\big]\, dt + \sum_n \left(\mathcal{D}[c_n]\rho\, dt + \sqrt{\eta_n}\mathcal{H}[c_n]\rho\, dW \right). \tag{2.98}$$

This stochastic master equation is suitable for describing most measurement processes that result in Wiener noise.

2.4 Feedback

We end this chapter with the details of Wiseman and Milburn's formulation of feedback alongside methods from classical control theory that map onto quantum systems. Feedback control in a general sense involves measuring a system and using the information gained to influence the future dynamics. Wiseman and Milburn developed the first theory for feeding back a photo-current obtained from a continuous quantum measurement. They considered how the fundamental noise associated with measuring quantum systems would correlate with the system dynamics when reintroduced in the form of feedback. The theory

was implemented experimentally and accurately predicted how to reduce laser shot-noise to its quantum limit.

Wiseman and Milburn derived a master equation which followed a diffusive measurement process. They initially considered monitoring a homodyne current, but the theory can be applied generally to any measurement that effectively samples from a Gaussian distribution. The measurement noise propagates throughout the feedback process which results in analogous behaviour to the fluctuation-dissipation theorem, where the measurement causes diffusion and the feedback can be designed to have a damping effect.

2.4.1 Direct feedback

Here we will derive a feedback master equation using the results and notation we built up in the previous sections. We start with a diffusive measurement record of the form

$$I(t) = \langle x \rangle + \frac{\xi(t)}{\sqrt{8\,\eta\,\kappa}}. \tag{2.99}$$

In order to derive a Markovian master equation we will consider instantaneous feedback, which is often reasonable when the operating speed of the electronics and optics used to implement the feedback is much faster than the system dynamics. Idealised direct feedback introduces a term proportional to the measurement record to the state evolution,

$$\textbf{(S)} \quad d\rho_{\mathrm{fb}} = I(t)\mathcal{K}\rho\,dt = \langle x \rangle \mathcal{K}\rho\,dt + \frac{1}{\sqrt{8\,\eta\,\kappa}}\mathcal{K}\rho\,dW. \tag{2.100}$$

Where the super-operator $\mathcal{K}$ describes the effect of some action on the system proportional to the strength of the feedback current. We have introduced the annotation **(S)** to mark this as a Stratonovich equation. In order to derive an evolution of the system that remains physical, it will be important to keep track of when it is appropriate to be using Stratonovich or Ito **(I)** forms. The measurement record (2.99) we have written only approximately contains white noise. Over the timescales we are interested this will still

be reasonable. However, since we are introducing (2.100) which will truly have some finite time correlations, to the continuous evolution of the system, the induced dynamics from should be approximated in Stratonovich form[35].

The subtleties of the noise come into play when combining the evolution due to feedback with the measurement master equation (2.94). Since the master equation was constructed as an Ito equation, we need to covert (2.100) to Ito form following the procedure (2.83)

$$\textbf{(I)} \quad d\rho_{\text{fb}} = \langle x \rangle \mathcal{K}\rho\, dt + \frac{1}{\sqrt{8\,\eta\,\kappa}}\mathcal{K}\rho\, dW + \frac{1}{16\,\eta\,\kappa}\mathcal{K}^2\rho\, dt. \tag{2.101}$$

Even after this conversion however, if we include the feedback as an additive term we will still find that the resulting master equation is not trace preserving. In fact if we tried instead to convert our original master equation to Stratonovich form in order to correctly combine the two terms, then a clear problem emerges where the feedback super-operator sometimes acts before the measurement super-operator. We must take particular care to ensure we write our equation so that it corresponds to the physical process of measurement first and feedback second, rather than the two entering on an equal footing. To do this it helps to consider that in essence we want to write

$$d\rho \to d\rho + d\rho_{\text{fb}} \equiv dA\rho + dB\rho, \tag{2.102}$$

where we define the operator dA to describe the state evolution due to measurement, and the evolution due to feedback with the operator dB. With these newly defined operators, we can alternatively write

$$\rho + d\rho + d\rho_{\text{fb}} = (1 + dB)(1 + dA)\rho. \tag{2.103}$$

This construction ensures the measurement acts before the feedback, and is exactly equivalent to (2.102) if the measurement and feedback noise are not correlated. However, we have just approximated the noise from instantaneous feedback as being identical to the

system noise. In this case $dB\,dA$ is of order dW^2 and can not be neglected,

$$dB\,dA\,\rho = \mathcal{K}\,\mathcal{H}[x]\rho\,dt = \mathcal{K}(x\rho + \rho x)\,dt - \mathcal{K}\langle x\rangle\rho\,dt. \tag{2.104}$$

Therefore with feedback, our master equation takes the form

$$d\rho = \mathcal{L}_0\rho\,dt + \sqrt{2\,\eta\,\kappa}(\mathcal{H}[x] + (4\,\eta\,\kappa)^{-1}\mathcal{K})\rho\,dW + \frac{1}{2}\mathcal{K}(x\rho + \rho x)\,dt + \frac{1}{16\,\eta\,\kappa}\mathcal{K}^2\rho\,dt. \tag{2.105}$$

where we have defined the Livoullian $\mathcal{L}_0$ which accounts for all of the Hamiltonian and dissipative dynamics.

Equation (2.105) accurately describes a systems evolution whilst undergoing measurement and feedback, and preserves all the physical properties of the density matrix. We can further interpret the resulting dynamics if we make explicit the form of $\mathcal{K}$,

$$\mathcal{K}\rho = -i\lambda\big[F, \rho\big], \tag{2.106}$$

where F can be any arbitrary operator that corresponds to making some physical shift to the system. We have also included λ as a scaling constant for the feedback strength that could be controlled independently of the measurement record. It will be useful, and easier to work with analytically, an equation that describes the average effects of this cooling procedure. Being able to predict the average result of the feedback is usually more helpful than generating individual trajectories based on a particular measurement realisations. With the explicit form of $\mathcal{K}$, the ensemble averaged evolution

$$\langle\!\langle\dot{\rho}\rangle\!\rangle = \mathcal{L}_0\langle\!\langle\rho\rangle\!\rangle - i\,\frac{\lambda}{2}\big[F, x\langle\!\langle\rho\rangle\!\rangle + \langle\!\langle\rho\rangle\!\rangle x\big] + \frac{\lambda^2}{8\,\eta\,\kappa}\mathcal{D}[F]\langle\!\langle\rho\rangle\!\rangle. \tag{2.107}$$

The term proportional to λ describes the desired effect of the feedback, where as the term proportional to λ^2 corresponds to additional heating due to reintroducing noise from the measurement. We can see from this equation that feedback offers the ability to turn on and off non-trivial terms in the system Hamiltonian by making use of information that

would otherwise be lost to the environment.

2.4.2 State estimation

The method discussed above considers feedback proportional to the instantaneous measurement record being directly reintroduced to the system. However, often experiments instead have access to some integral of the measurement, or may first need to filter the measurement signal before using it for feedback. In this case it is usually much more difficult to make an analytic model of the resulting dynamics, and if the signal processing has significant delay this leads to non-Markovian evolution.

This issue is not confined to quantum physics and there are cases where methods from classical control theory can be borrowed to make the problem more tractable. For example, in some cases, integrals of the measurement record provide continuous estimates of certain dynamical variables. If we consider a continuous position measurement of a Gaussian state, the measurement signal can be integrated to provide estimates of the mean position and momentum. We can then express the feedback Hamiltonian as a linear function of the momentum and position operators scaled by functions of their estimates,

$$H_f = f(\langle x\rangle, \langle p\rangle)x + g(\langle x\rangle, \langle p\rangle)p. \tag{2.108}$$

Where f and g are functions of the estimated variables, and x and p are the position and momentum operators respectively. In the limit of instantaneous feedback, the optimal feedback strategy can be determined using classical control theory. We can define a cost function for a parameter we want to minimise, for example the energy, $C(x, p, f, g)$. The cost function should depend on the system state and the feedback functions. Minimising C then provides the optimal form of f and g, and the integral equations of the measurement continue to provide an estimate of the state variables. There are many classical examples of how to choose an appropriate cost function and how to minimise it.

In classical systems noise is not fundamentally linked to the measurement strength, as is the case with quantum measurement. Noise can however be artificially enforced, and in some cases, classical models can be made to map exactly onto quantum systems. We found that well developed control methods for cooling [43, 44, 45] were highly applicable to the nano-mechanical systems we go on to discuss in the following chapter.

3 Nano-mechanical systems

In this chapter the discussion turns to nano-mechanical systems, and a brief review of the background of the field is presented. This is followed by an overview of some recent developments achieved with levitated nanoparticles. Some key features of nano-mechanical systems are presented, in both classical and quantum noise models. The research in this and the following chapter, was inspired by advances in magnetically confined particles[46], and which methods are best suited for measuring these systems is explored in detail. This leads to an in depth evaluation of which feedback methods are most appropriate for magnetically levitated particles, and how to overcome the challenges of working with relatively low-quality oscillators.

3.1 Background

Quantum theory was first conceived to describe the behaviour of light, and the smallest constituents of matter, namely atoms and molecules. However, no part of the theory prohibited it from being applied to larger systems. As we discussed in chapter 2, the transition from quantum to classical mechanics seems to manifest due to the interaction between a system and its environment. Although large systems typically couple strongly to their surroundings, there is no fundamental reason that they cannot be well isolated to observe quantum behaviour. It is still a huge technical challenge, but over the last two decades there have been many advances in our ability to engineer macroscopic quantum systems.

To derive a quantum model of a macroscopic system it is common to start with a classical description, and then to quantise the collective degrees of freedom. Solving the Schrödinger equation for each of the individual constituents would be unfeasible, so we rely on the internal degrees of freedom being largely uncoupled from the macroscopic ones. One of the first major successes of this approach was quantising classical current and flux to provide a

theory of superconducting circuits[47]. The methodology can be applied generally to any classical system with a continuum of modes. Quantum features have long been studied in the collective excitations of superfluid helium[48], and more recently ground state cooling has been achieved in the elastic deformation of silicon nanostructures[49] and in the mechanical motion of breathing modes in optical microcavities[50]. Ground state cooling of the vibrational modes of trapped nanoparticles is also being pursued and the field is quickly progressing [51].

Advances in engineering these systems have relied heavily on the mechanical influence of light. The effect of optical gradient forces was first demonstrated with microscopic particles in 1970[52]. Optical control led to many breakthroughs including the realisation of a Bose-Einstein condensates, and the ability to trap and manipulate individual ions[53]. Today the opto-mechanical control of trapped ions allows for ground state cooling[54], the preparation of highly non-classical states[55, 56], and strings of interacting ions are used at the forefront of quantum simulation[57]. Some of the same control techniques can be applied to nanoscopic and macroscopic levitated particles, and there is an on-going push to achieve ground state cooling in these systems. If realised they hold the promise of new technologies, and would be a platform for many novel experiments.

3.1.1 Levitated particles

Levitated supra-atomic particles are of interest for metrology and for tests of fundamental quantum physics[58]. Sufficiently large systems offer the exciting possibility to probe the effects of gravity in a quantum mechanical setting. If interactions are strong enough there are proposals to explore quantum gravitational phenomena[59, 60]. Once ground state cooling has be achieved, experiments will be operating in a regime where incredibly sensitive quantum states could be prepared to explore non-Newtonian gravitational effects[61], and for gravitational wave detection[62]. Squeezed states of motion via back-action evading measurements can already be engineered in other opto-mechanical systems and can

be used to overcome quantum limits on measurement precision. For sensing, quantum interference effects can also be exploited to gain sensitivity to external forces and fields.

Nano-mechanical systems, such as optical microresonators[50] and photonic-crystals[49], have been prepared in quantum states of motion. Control over these systems is excellent, and state-of-the-art experiments have mechanical quality factors currently for exceeding that of levitated systems[51]. Advances in levitated particles are being made quickly however, with the goal of catching or even surpassing tethered systems. One exciting feature of levitated particles is that they are comparatively low mass, and therefore have the potential to make superior force sensors. Alongside tethered systems, levitated particles offer exciting new avenues to probe macroscopic quantum physics.

Optical and magnetic fields are the most commonly used for the confinement of large levitated particles, although there is a growing interest in all-electric levitation[63, 64]. Arguably the most progress towards reaching ground state cooling with a nanoscopic particle has been made in optical traps. Current experiments are capable of detecting, and are limited by, photon shot-noise[65]. They have already been used to investigate highly sensitive classical dynamics, and as detectors for ultra-weak forces[66, 67]. The main obstacle to cooling further is due to intrinsic noise associated with the optical gradient trapping fore. Scattered light causes diffusion of the particle's motion, equivalent to the measurement back-action described by the master equation (2.94). This can be interpreted as photon recoil heating analogous to that which limits Doppler cooling of atoms. The recoil energy scales inversely with a particle's mass making it a negligibly weak effect at high temperatures, but it becomes a significant source of heating after reaching a relatively low phonon occupancy. The large laser intensities required to trap particles has posed a substantial limit on these methods. A cavity surrounding the levitated particle can help minimise the lost scattered light and in this context there are proposed methods for ground state cooling[68].

Optically trapped particles have excellent quality factors, and there are proposed methods

for overcoming their heating issues, however, there are alternatives which circumvent their current limitations. Static magnetic traps are free from heating intrinsic to the confinement of the particle, and have recently been demonstrated as suitable for trapping and cooling nano-diamonds[46, 69]. Most materials are diamagnetic, and although much weaker than ferromagnets, with an applied field they will have an induced magnetic moment. This magnetic moment opposes the applied field, and causes a force towards the field strength minima. With strong rare earth magnets it is possible to create a stable potential well for particles weighing a few pico-grams. Nano-diamonds are of particular interest because of the potential to couple their external motion with the internal state of a nitrogen-vacancy (NV) centre. Magnetic traps are well suited for these experiments, as in high vacuums impurities in diamonds burn due the laser intensities used in optical traps[70].

Magnetic traps are typically around three orders of magnitude larger than their optical counterparts, spanning hundreds of micrometers across. Consequently they operate at much lower frequencies, of around 100Hz as opposed to 100kHz for an optical trap. This comes with the advantage of being able to hold and manipulate larger particles, but also makes it unfeasible to cool on timescales much longer than the oscillation period because of their relatively low quality factor. Although the oscillation frequency is significantly lower than in an optical trap, magnetic confinement is subject to similar environmental heating. Recent experiments[46, 65] have estimated the phonon reheating rate for these systems in high vacuum (10^{-8} mbar) to be $\Gamma_{\text{th}} \approx 100\text{Hz}$ and it is expected that this will be significantly reduced at lower pressures. In current experiments the motion of magnetically confined particles has been cooled from room temperature to sub-Kelvin temperatures axially and to only a few Kelvin vertically[71].

In the following sections we consider a possible route to ground state cooling of a levitated nano-particle, magnetically trapped, using a combination of measurement and feedback. One of the major considerations will be that the trap frequency in these systems is much lower than those involving optically trapped particles or other nano-mechanical resonators. Managing environmental heating in this regime currently requires control of the system on

a timescale comparable to the inverse of the trap frequency. We find that these traps are an excellent platform for performing optimal feedback control via real-time state estimation, for the preparation of motional states with measurable quantum properties.

3.2 General model

We are not yet able to prepare quantum states of motion with levitated particles, however, shot noise is a visible quantum feature in current experiments. This is different from classical heating sources, such as due to collisions with energetic air molecules, in that quantum noise is a fundamental consequence of the interaction between the particle and light. In the case of a probe light used for measurement, the corresponding noisy disturbance is called back-action. Although the source of the noise is intrinsically non-classical, the motion of the particles can still be described by classical equations. As such, it will be helpful to briefly consider a classical description of a mechanical oscillator coupled to its environment. This classical model will later map onto a fully quantum description and works as an illustrative example of stochastic differential equations.

3.2.1 Classical case

Initially we consider classical heating effects. When preparing a particle with a very low velocity it becomes important to consider collisions with surrounding air molecules. Even in a near vacuum these collisions are frequent over the timescale of an oscillation and induce significant fluctuations. To describe this motion, it is common to use a Langevin equation. As we discussed in the previous chapter, we can use a white noise process to approximate the quasi-random force due to the collisions. The so called Brownian motion of a free particle can be described by the stochastic differential equation

$$\frac{\partial v}{\partial t} = -2\gamma v + \sqrt{f}\,\xi(t)\ . \tag{3.1}$$

Where $v = dx/dt$ is the particle velocity, and γ is a drag coefficient which depends on the viscosity of the air and the particle size. The term $\sqrt{f}\,\xi(t)$ represents the force arising from the impacts with molecules, where f scales the size of the fluctuations and $\xi(t)$ is a noise process. The fluctuations in the particles motion are realistically expected to have some finite temporal correlations, and can be approximated with an auto-correlation function with the general form of a decaying exponential,

$$\langle \xi(t)\xi(t') \rangle = \frac{D}{2k}\, e^{-k|t-t'|} \ . \tag{3.2}$$

It is mathematically convenient to consider the idealised white noise limit where $k \to \infty$ and $\xi(t)$ becomes delta correlated. This is a reasonable approximation to make when the system dynamics occur on timescales much larger than the correlation time. As the limit of some physical process, (3.1) should be interpreted as a Stratonovich equation, but since there is only an additive noise term, there is no correction to add if we want to treat it as an Ito equation. This means we are free to use the Ito rules of calculus.

We can use the fluctuation-dissipation theorem to quantify the strength of the driving noise. We first note that the formal solution to our Langevin equation is

$$v(t) = v(0)\, e^{-2\gamma t} + \sqrt{f} \int_0^t dt'\, e^{-2\gamma(t-t')} \xi(t) \ . \tag{3.3}$$

Since the expectation value of a white noise process is zero, $\langle \xi(t) \rangle = 0$, we can see that the mean velocity

$$\langle v(t) \rangle = v(0)\, e^{-2\gamma t} \ . \tag{3.4}$$

The variance of the velocity can be found under the assumption that $\langle \xi(t)\xi(t') \rangle = \delta(t-t')$,

$$\begin{aligned}\langle v^2(t)\rangle - \langle v(t)\rangle^2 &= f\int_0^t dt' \int_0^t dt''\, e^{-2\gamma(t-t')} e^{-2\gamma(t-t'')} \langle \xi(t')\xi(t'')\rangle \\ &= f\int_0^t dt' \int_0^t dt''\, e^{-2\gamma(2t-t'-t'')}\delta(t'-t'') \\ &= \frac{f}{4\gamma}(1-e^{-4\gamma t}).\end{aligned} \tag{3.5}$$

The fluctuation dissipation theorem argues that the driving collisions and viscous drag will compete and in thermal equilibrium the two forces should balance. We can see in the long time limit that $\langle v^2(t)\rangle = f/4\gamma$, does reach a steady state. The equipartition theorem then allows us to equate the particle's energy to the environment's temperature, which gives us an expression for f in terms of measurable parameters,

$$\langle \frac{1}{2} m\, v^2\rangle = \frac{1}{2} k_B\, T \quad \rightarrow \quad f = \frac{4\gamma\, k_B\, T}{m}. \tag{3.6}$$

In early experiments with magnetic confinement, they operated in a room temperature vacuum, and measured the time for a trapped particle to come to equilibrium to be of the order of 100 seconds [46], corresponding to a damping coefficient of roughly $\gamma \approx 10^{-2} s^{-1}$.

If we add a harmonic potential to (3.1) we can derive equations of motion for a trapped brownian particle,

$$\frac{\partial v}{\partial t} = -\omega^2 x - 2\gamma v + \sqrt{f}\,\xi(t)\ . \tag{3.7}$$

It will be simpler to make a change of variables and solve for the mean square velocity. A variable change usually relies on the standard form of the chain rule, but since this a Stochastic equation we should use Ito's lemma. If we have a stochastic process, such as $v(t)$, which can be expressed as the solution to an equation of the form

$$dX = a\, dt + b\, dW, \tag{3.8}$$

then the derivative of a function $f(X(t))$ will have the form

$$\begin{aligned} \mathrm{d}f &= \frac{\mathrm{d}f}{\mathrm{d}X}\,\mathrm{d}X + \frac{\mathrm{d}^2 f}{\mathrm{d}X^2}\frac{dX^2}{2} + ... \\ &\approx a\frac{\mathrm{d}f}{\mathrm{d}X}\,\mathrm{d}t + b\frac{\mathrm{d}f}{\mathrm{d}X}\,\mathrm{d}W + \frac{b^2}{2}\frac{\mathrm{d}^2 f}{\mathrm{d}X^2}\,\mathrm{d}t\,. \end{aligned} \tag{3.9}$$

The first line here is a Taylor expansion of df, and in the second line we have truncated the expansion to first order in dt. The unusual extra term in the expansion remains since it was proportional to $dW^2 = dt$, and the expression is made exact in the limit $dt \to 0$. This is Ito's lemma, and if we identify $dX = dv$ and $f(v) = v^2$, we can transform (3.7),

$$d(v^2) = \big(-2v(\omega^2 x + 2\gamma v) + f\big)\,\mathrm{d}t - \big(2v\sqrt{f}\big)\,\mathrm{d}W\,. \tag{3.10}$$

If we then take the ensemble average,

$$d\langle v^2\rangle = (-2(\omega^2\langle xv\rangle + 2\gamma\langle v^2\rangle) + f)dt. \tag{3.11}$$

And following the same procedure for the position equation,

$$d\langle x^2\rangle = \big(2(\langle xv\rangle\big)\,\mathrm{d}t\,. \tag{3.12}$$

In steady state we have two simultaneous equations, immediately $\langle xv\rangle = 0$ and consequently we see $\langle v^2\rangle = f/4\gamma$, as was the case for a free particle. As a final step, we can write equations for the position and momentum variance of the particle. These will be useful equations that later directly map onto the quantum model,

$$\begin{aligned} dV_x &= \mathrm{d}\langle x^2\rangle - 2\langle x\rangle\,\mathrm{d}\langle x\rangle \\ &= 2\big(\langle xv\rangle - \langle x\rangle\langle v\rangle\big) = \frac{2}{m}C_{xp}, \end{aligned} \tag{3.13}$$

$$dV_p = -2m\omega^2 C_{xp} - 4\gamma\big(V_p + mk_bT\big), \tag{3.14}$$

where we have defined the position and momentum covariance $C_{xp} = \langle xv\rangle - \langle x\rangle\langle v\rangle$. We

can see in the momentum variance a balance of damping and diffusion proportional to the coupling strength to the environment.

3.2.2 Quantum case

We can quantise the harmonic oscillator by promoting the position and momentum to operators in the system Hamiltonian,

$$H_{\text{sys}} = \frac{p^2}{2m} + \frac{m\omega^2 x^2}{2}, \tag{3.15}$$

where m is the particle mass, and ω is the trap frequency. It will be sufficient to continue to model the motion of the particle in 1D, as although cooling is often applied along each trap axis, the frequencies of each motional degree of freedom can be well separated and safely decoupled.

The harmonic oscillator can also be naturally described by ladder operators $\left[a, a^\dagger\right] = 1$, which act to add or subtract phonons from the system. For a state with n phonons

$$a\left|n\right\rangle = \sqrt{n}\left|n-1\right\rangle \qquad a^\dagger\left|n\right\rangle = \sqrt{n+1}\left|n+1\right\rangle, \tag{3.16}$$

with the special case $a\left|0\right\rangle = 0$ when acting on the ground state. The ladder operators naturally define the number operator

$$a^\dagger a\left|n\right\rangle = n\left|n\right\rangle \quad \rightarrow \quad n = a^\dagger a, \tag{3.17}$$

and can be used to express the position and momentum operators,

$$x = x_0(a^\dagger + a), \qquad p = ip_0(a^\dagger - a), \tag{3.18}$$

where $x_0 = (\hbar/2m\omega)^{\frac{1}{2}}$ and $p_0 = (\hbar m\omega/2)^{\frac{1}{2}}$ are the zero point position and momentum respectively.

As in chapter 2 we can consider coupling our system to a continuum of harmonic oscillators that represents the environment,

$$V = \sum_k \left(g_k b_k + g_k^* b_k^\dagger\right)\left(a + a^\dagger\right). \tag{3.19}$$

If the oscillator frequency is sufficiently large compared to the rate of dissipation due to the coupling, then we can work under the rotating wave approximation. As with the two level atom, the system evolution is then described by a Lindblad master equation,

$$\dot{\rho} = -i[H_{sys}, \rho] + \gamma_{th}(1+\bar{n})\mathcal{D}[a]\rho + \gamma_{th}\,\bar{n}\mathcal{D}[a^\dagger]\rho, \tag{3.20}$$

where γ_{th} is the system-bath coupling strength. We have transformed out of the interaction frame here so as to directly observe the effects of H_{sys}, using the fact that $U^\dagger\,\mathcal{D}[a]\tilde{\rho}\,U = \mathcal{D}[a]\rho$, when U is a phase-shifting operator. The average phonon occupancy $\bar{n}$ is determined by the Bose-Einstein distribution function, and relates the rates of the spontaneous emission and absorption to the reservoir temperature. Since the ladder operators follow the bosonic commutation relation, Bose-Einstein statistics determine the phonon occupancy probability at each energy level in thermal equilibrium,

$$p(n) = \exp\left(-\frac{\hbar\omega n}{k_B T}\right)\left[1 - \exp\left(-\frac{\hbar\omega}{k_B T}\right)\right], \tag{3.21}$$

$$\bar{n} = \sum_n^\infty n\,p(n) = \left[\exp\left(\frac{\hbar\omega}{k_B T}\right) - 1\right]^{-1} \approx k_B T/\hbar\omega \tag{3.22}$$

In the last line we consider the limit of high temperatures, $\hbar\omega \ll k_B T$, and as expected the average phonon occupancy is equal to the thermal energy of the environment divided by the energy of a single phonon excitation. The last term in (3.20) accounts for spontaneous absorption, and arises when treating the environment as if it has some finite temperature, as opposed to a vacuum, when deriving the master equation.

Equation (3.20) describes dissipation and heating due to interactions with the environ-

ment, just as in the classical model. We can compare the quantum system evolution with the classical equations of motion, by considering the position and momentum observables. In the density matrix formalism we can use the trace to find the equations of motion for any observable $\langle A\rangle = Tr[\rho A]$. Using the fact that only ρ has time dependence in the Schrödinger picture,

$$\begin{aligned}\frac{\mathrm{d}\langle A\rangle}{\mathrm{d}t} = -i\langle\big[A,H\big]\rangle + \gamma_{th}(1+\bar{n})\langle 2a^\dagger A a - aa^\dagger A - Aaa^\dagger\rangle \\ + \gamma_{th}\,\bar{n}\langle 2aAa^\dagger - a^\dagger aA - Aa^\dagger a\rangle.\end{aligned} \tag{3.23}$$

The first order position and momentum work out to be

$$d\langle x\rangle = \frac{1}{m}\langle p\rangle dt - 2\gamma_{th}\langle x\rangle dt, \tag{3.24}$$

$$d\langle p\rangle = -m\omega^2\langle x\rangle dt - 2\gamma_{th}\langle p\rangle dt, \tag{3.25}$$

and decoupling these two differential equations gives

$$dt^2\langle X\rangle + 2\gamma_{th}\langle X\rangle dt + (\omega^2+\gamma_{th}^2)\langle X\rangle = 0, \tag{3.26}$$

which has the same form as the mean of (3.7), but with a shifted oscillation frequency $\omega_\gamma^2 = \omega^2 + \gamma_{th}^2$. Likewise, the second order moments work out to be

$$\frac{\mathrm{d}V_x}{\mathrm{d}t} = \frac{2}{m}C_{xp} - 4\gamma_{th}\bigg(V_x - \big(\bar{n}+\frac{1}{2}\big)\frac{\hbar}{m\omega}\bigg), \tag{3.27}$$

$$\frac{\mathrm{d}V_p}{\mathrm{d}t} = -2m\omega^2 C_{xp} - 4\gamma_{th}\bigg(V_p - \big(\bar{n}+\frac{1}{2}\big)\hbar m\omega\bigg), \tag{3.28}$$

$$\frac{\mathrm{d}C_{xp}}{\mathrm{d}t} = -\frac{2}{m}V_p + 2m\omega^2 V_x - 2\gamma_{th}C_{xp}, \tag{3.29}$$

where C_{xp} is symmetrised covariance. These equations almost perfectly map onto their classical counterparts (3.13,3.14) at high temperatures, as $\bar{n} \to k_B T/\hbar\omega$. However, in these equations there is an explicit damping term for the position variance, which is a consequence of having made the rotating wave approximation. In the equation for the expected phonon occupancy

$$d\langle n\rangle = -\gamma_{th}\langle n\rangle \,\mathrm{d}t + \gamma_{th}\bar{n}\,\mathrm{d}t\,, \tag{3.30}$$

we can see that the system energy decays smoothly, where as for a typical damping force we would expect the energy to be removed at a rate proportional to the current velocity. The oscillations in the decay rate have been smoothed out by assuming the RWA, but this is a reasonable approximation if the decay rate is slow compared to the oscillation period. The second difference from the classical case is apparent at low temperatures, where in the quantum case the variances never fall below the zero point limits. At room temperature the average phonon occupancy for a $\omega = 2\pi \times 100 s^{-1}$ oscillator would be $\bar{n} \approx 10^{11}$, which is safely described by the classical equations of motion. To reach the quantum ground state $\bar{n} = 0$ equates to cooling to a temperature of the order of a few nano-Kelvin.

We will build on these equations in the following sections. For the particular case of a quantum oscillator, the Gaussian position and momentum moments can describe the full state. These are much easier equations to solve both analytically and numerically than the full master equation. Thermal states are initially Gaussian and we will find that they stay that way when undergoing linear measurements of x and p. Furthermore, the Gaussian state equations later provide a useful approach for parameter estimation and feedback.

3.2.3 Measurement and resolution

We next want to include the effect of measuring the quantum oscillator. We can consider a general Gaussian measurement of the form discussed in chapter 2,

$$A(\alpha) = \left(\frac{4\kappa\Delta t}{\pi}\right)^{\frac{1}{4}} \int_{-\infty}^{\infty} \exp\big(-2\kappa\Delta t(x-\alpha)^2\big)\,|x\rangle\langle x|\,dx, \tag{3.31}$$

and we can consider making a continuous string of measurements by applying this operator in each time step Δt, where the observer obtains the measurement result α. If we identify x as the position operator, and if there is a measurement in each interval, as $\Delta t \to 0$, the system is described by the measurement master equation

$$d\rho = -\frac{i}{\hbar}\big[H_{sys},\rho\big]dt + 2\kappa\mathcal{D}[x]\rho\,dt + \sqrt{2\eta\kappa}\mathcal{H}[x]\rho\,dW. \tag{3.32}$$

Where we have let $c = \sqrt{2\kappa}\,x$ in (2.94). Since we have considered specifically a position measurement we can be more quantitative about the nature of the measurement strength κ. From (3.31) we can see that an individual measurement in a single time step will project an initially delocalised particle onto a state with width of order

$$\delta\alpha = \frac{1}{\sqrt{2\kappa\Delta t}}. \tag{3.33}$$

From classical optics we know that light from a point dipole would have a profile width of about an optical wavelength λ. For a single projective measurement then we might expect $\delta\alpha \approx \lambda$. If we assume the measurements are coming from scattered light at a rate $\gamma = 1/\Delta t$, we can estimate that the measurement strength $\kappa \approx \gamma/\lambda^2$.

Following the same procedure as before, we can compute the equations of motion for the position and momentum moments. Since this time the equations contain white noise, we should use Ito's lemma when finding the variance equations, eg.

$$dV_x = d\langle x^2\rangle - 2\langle x\rangle d\langle x\rangle - (d\langle x\rangle)^2. \tag{3.34}$$

By assuming a Gaussian state we can also re-express the expectation value of any arising higher order moments, in terms of the first and second order position and momentum. The resulting equations are,

$$d\langle x\rangle = \frac{1}{m}\langle p\rangle dt - 2\gamma_{th}\langle x\rangle dt + \sqrt{8\eta\kappa}V_x\,\mathrm{d}W\,, \tag{3.35}$$

$$d\langle p\rangle = -m\omega^2\langle x\rangle dt - 2\gamma_{th}\langle p\rangle dt + \sqrt{8\eta\kappa}C_{xp}\,\mathrm{d}W\,, \tag{3.36}$$

$$\frac{\mathrm{d}V_x}{\mathrm{d}t} = \frac{2}{m}C_{xp} - 4\gamma_{th}\left(V_x - \left(\bar{n}+\frac{1}{2}\right)\frac{\hbar}{m\omega}\right) - 8\eta\kappa V_x^2, \tag{3.37}$$

$$\frac{\mathrm{d}V_p}{\mathrm{d}t} = -2m\omega^2 C_{xp} - 4\gamma_{th}\left(V_p - \left(\bar{n}+\frac{1}{2}\right)\hbar m\omega\right) + 2\hbar^2\kappa - 8\eta\kappa C_{xp}^2, \tag{3.38}$$

$$\frac{\mathrm{d}C_{xp}}{\mathrm{d}t} = -\frac{2}{m}V_p + 2m\omega^2 V_x - 2\gamma_{th}C_{xp} - 8\eta\kappa V_x C_{xp}. \tag{3.39}$$

We can see from these equations that the measurement causes extra diffusion in the momentum variance. This is the back-action associated with the measurement interaction. We can argue that physically this diffusion should correspond to the total momentum recoil imparted by the field,

$$2\hbar^2\kappa = \gamma\hbar^2 k_L^2 \quad \rightarrow \quad \kappa = \frac{\gamma k_L^2}{2}, \tag{3.40}$$

where $k_L = 2\pi/\lambda$ is the optical wavenumber and we have considered diffusion only in one dimension. This agrees with our estimate for the measurement strength based on the ideal level of resolution. The information gained from the measurement manifests as damping of the position variance. In turn, the momentum variance is also damped proportional to the covaraince with the position. The expectation value of the first order position and momentum now have a stochastic drift induced by the continuous measurement collapse. This drift is conditioned on the specific realisation of the measurement record, and averag-

ing over these realisations is exactly enough to hide the reduction in the position variance. In which case this is equivalent to setting $\eta = 0$ and discarding any measurement information. This leaves only the dissipative affect on the momentum variance, as is the case when coupling to any environment we know nothing about.

In order to reach the quantum regime it will be necessary for environmental heating to be made negligibly small on the time-scales required to achieve measurement resolution. A reasonable goal in a magnetic trap would be to cool a particle in a time comparable to the oscillation period of a $\omega = 2\pi \times 100\text{Hz}$. In this case the phonon reheating rate would need to be reduced to around $\Gamma_{\text{th}} = k_B T \gamma_{th}/\hbar\omega \sim 1\text{Hz}$, where T represents the surrounding gas temperature and γ_{th} is the thermal damping rate. Current typical reheating values are around 100Hz, and below 10 mbar, thermal decoherence is expected to be linear in gas pressure and in the temperature of the environment. By better isolating the particle, or with the help of cryogenically cooling the trap chamber, reheating rates two orders of magnitude lower could feasibly be reached.

It is helpful to consider the necessary measurement strength to reach a desired position resolution in a given time. A simple estimate of the resolution achievable across an interval Δt, can be found be integrating the measurement record [72],

$$\Delta I = \int_t^{t+\Delta t} dI \approx \langle x \rangle \Delta t + \int_t^{t+\Delta t} \frac{dW}{\sqrt{8\eta\kappa}}. \tag{3.41}$$

In this expression we have assumed that the expected value of the position of the particle will not change much over the time interval. This is not a well justified assumption but will allow us to determine an upper bound for the resolution. The integrated measurement signal ΔI has a mean value of $\sqrt{8\eta\kappa}\langle x \rangle \Delta t$ that grows linearly in time, and its width grows as the square root, $\sigma = \sqrt{\Delta t}$. Continuous measurement over this interval could therefore resolve at best

$$\delta x \approx \frac{1}{\sqrt{8\Delta t\, \eta\kappa}}, \tag{3.42}$$

with a signal to noise ratio of one. We would like to achieve resolution comparable to the

size of the quantum ground state $x_0 = \sqrt{\hbar/2m\omega}$, in some time interval which for now we will consider to be on the order of a mechanical oscillation $\Delta t = 1/\omega$, to outpace a realistic thermal heating rate,

$$\delta x_\omega = \sqrt{\frac{\omega}{8\eta\kappa}} \equiv x_0. \tag{3.43}$$

From this, we can conclude in order to approach ground state cooling sufficiently quickly, it is necessary for $\kappa\, x_0^2 \sim \omega/8\eta$. This places a lower bound on the necessary measurement strength.

Attempting to cool on time-scales much shorter than the trap period has its own physical limitations. Earlier we quantitatively established that the measurement strength should be proportional to the scattering rate, which could always in principle be increased with stronger laser illumination. The trade-off for higher scattering rates, is greater back-action heating and stochastic drift. Even idealized measurements cause unavoidable heating through momentum diffusion, which in the best case manifests as squeezing of the state variances for any finite κ. Actively counteracting the disturbance caused by a probe light relies on efficiently detecting as much of the scattered light as possible. This along with the necessary resolution requirement, are the criteria for a suitable measurement. In the following section we use this criteria to asses several potential physical measurement schemes.

3.3 Methods for measuring levitated particles

We assessed the merits and shortcomings of various measurement techniques, and we outline the results of our investigation here. The most suitable method we found involves measuring the amplitude modulation of a standing wave due to a particle's motion in front of a single mirror. This technique has been successfully demonstrated with trapped ions[16, 36] and has the potential to be very effective for monitoring magnetically levitated nanoscopic particles, when combined with initial cooling of the oscillation amplitude to around a single optical wavelength. To provide context as to why this method was chosen

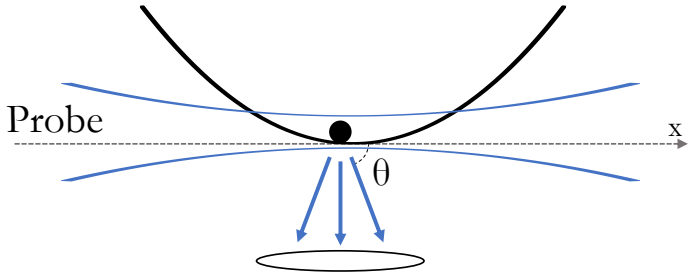

Figure 3.1: Sketch of a trapped particle, illuminated by a probe so that it can be imaged. The lens and detection system must be situated perpendicular to the axis of the particle's motion. Capturing light scattered at large angles θ translates to a poor quantum measurement efficiency.

we outline the benefits and limitations of some other well established methods.

3.3.1 Imaging

Camera-like imaging has been used in previous experiments with particles in low frequency traps. As sketched in Fig. 3.1, a camera follows a particle's position in a plane perpendicular to the direction of light being scattered from it. However, it is light scattered parallel to this plane that imparts the most recoil to the visible motion of the particle. We will see that this translates to a very low quantum efficiency.

We saw in the derivation of a stochastic Schrödinger equation that information in the environment can be measured to infer the state of a quantum system. If we include the spatial dependence of the field in the interaction Hamiltonian it is of the correct form to allow for a position measurement,

$$H_I = \hbar \sum_k \sqrt{\gamma}\big(b_k \exp(i\mathbf{k}.\mathbf{r}) + b_k^\dagger \exp(-i\mathbf{k}.\mathbf{r})\big), \tag{3.44}$$

where γ is the scattering rate into each mode of the optical electric field, $b_k(b_k^\dagger)$ is the

usual quantised field mode amplitude, with wavenumber and angular frequency of k, ω_k respectively. The momentum recoil due to the scattered photons is represented by $\mathbf{k}.\mathbf{r}$, where $\mathbf{r}$ is the particle's position. This Hamiltonian could for example model a particle interacting with an optical probe beam. Magnetic confinement provides large trapping potentials capable of holding very massive particles, with the potential to explore truly macroscopic quantum objects. We will however initially focus on smaller particles, tens of nanometers in size, for their simple light scattering properties. Nanoparticles can be treated as point dipoles and their motion is simpler to measure over distances shorter than the optical wavelength of a probe beam. We will treat the internal dynamics of the light scattering process adiabatically and model the particle as a point dipole in the Rayleigh regime. We saw in the Lindblad master equation for a 2-level system that the internal dynamics of a driven dipole are damped due to coupling with the environment. If this damping is much faster than the dynamics of the external particle motion, in the adiabatic limit the operators corresponding to the internal dipole transition can be replaced by their steady state values and absorbed into the scattering rate.

If there is a large detuning of the probe beam from any resonant frequency of the particle, then scattering would happen in the Rayleigh regime, where light scatters elastically at the same frequency as the incoming probe. In this case we can consider a single dominant frequency. If we write the joint state equation of the particle and field, as when we considered photo-detection of a two-level system (2.49), after a single time-step

$$|\psi\rangle = \int \mathrm{d}p\, \psi(p)\big(c_e\,|p,0\rangle + c_g\,|p-\hbar k,1\rangle\,\big), \tag{3.45}$$

where $\psi(p)$ is the momentum state of the particle and $|c_e|^2$, $|c_g|^2$, correspond to the probabilities of free system evolution with a vacuum field state, or a momentum kick after a photo-detection event. We can identify the corresponding jump operators for this interaction,

$$c(\theta,\phi) = \sqrt{f(\theta,\phi)}\, e^{i\mathbf{k}.\mathbf{r}}, \tag{3.46}$$

such that

$$\int d\Omega\, c^\dagger(\theta,\phi)c(\theta,\phi) = 1. \tag{3.47}$$

where we have explicitly included the angular dependence of the scattering, into the continuum of modes with wavevectors k. Detection in each mode tells us there has been a momentum kick in a given direction.

An imaging process transforms these operators, trading the directional information about the light for position information. A lens for example can effectively project the scattered light, and consequently the jump operators, onto a plane

$$c(x) = \sqrt{\frac{k}{4\pi^2}} \int_0^{2\pi} d\phi \int_0^{\pi} \sin\theta d\theta \sqrt{f(\theta,\phi)} e^{ik(x-x_0)\cos\theta}, \tag{3.48}$$

where x_0 is the atomic position and x is the coordinate for the plane being imaged. We have normalized the the operators in the same way so that when integrating over all modes

$$\int c^\dagger(x)c(x) = c^\dagger(\theta,\phi)c(\theta,\phi). \tag{3.49}$$

In the most simple case, we can consider isotropic scattering with $f(\theta,\phi) = 1/4\pi$. Carrying out the integration we obtain the operators

$$c(x) = \sqrt{\frac{k}{\pi}}\mathrm{sinc}(k(x-x_0)). \tag{3.50}$$

We can relate these to the Gaussian operators we considered earlier (3.31), if we approximate the function $\mathrm{sinc}(kx)$ as a Gaussian with width $\sigma \approx 3.8/k$. This corresponds to localising the particle within the order of an optical wavelength after each detection, as expected for an ideal measurement system. We will continue with a qualitative description of the imaging process, since we only wish to show why it is not best suited for highly efficient measurement.

The position operators we have derived correspond to an idealised case where all the

scattered light is collected and imaged. To calculate a more realistic collection efficiency, we can find out the fraction of light radiated from the atoms that overlaps with a lens,

$$\eta_\theta = \int \mathrm{d}\Omega\, f(\theta,\phi)T(\theta,\phi). \tag{3.51}$$

We have introduced the aperture function $T(\theta,\phi)$, which we will model as a mask, such that light is only collected over some small angle $\delta\theta$,

$$T(\theta) = \begin{cases} 0 & \text{if} \quad \left|\theta - \frac{\pi}{2}\right| > \delta\theta \\ 1 & \text{if} \quad \left|\theta - \frac{\pi}{2}\right| < \delta\theta \end{cases}. \tag{3.52}$$

The angles here are shifted by $\pi/2$ so that the lens collects light perpendicular to the particle's motion as is necessary to produce an image, illustrated in Figure 3.1.

If we consider isotropic scattering, $\eta_\theta \approx \delta\theta$. This however is not the collection efficiency that should be used in the measurement master equation (3.32). This is the collection efficiency of the scattered light, but it does not take into account that for each detection, only a fraction of the recoil operator acts in the x direction. Only this component of the scattered light carries information that is relevant to the particle's position along x. To account for this in the detection efficiency, we should let $\sqrt{f} \to \sqrt{f}\cos(\theta)$, which would appropriately weight the jump operator's contribution to recoil along the x-axis,

$$\eta = 2\pi \int_0^\pi \mathrm{d}\theta\, f(\theta)T(\theta)\cos^2(\theta) \approx \frac{\delta\theta^3}{3}. \tag{3.53}$$

The approximate value here, again corresponds to isotropic scattering, and qualitatively matches up with the result of more rigorous treatment[73].

This is a very poor quantum efficiency and reflects the fact that an imaging system necessarily collects light perpendicular to to the motion of the particle. The light scattered at these angles contributes very little recoil along the x direction and correspondingly carries very little information. This suggests that a method of measuring the light scattered

parallel to the particle's motion is necessary for an efficient position measurement. Even so, imaging is simple to implement and for the purpose of initially damping the position variance to around a fraction of a micron, low quantum efficiency will not be an issue. For comparison, a $0.1\mu m$ diameter diamond in a trap $\omega = 2\pi \times 100$Hz, will only be quantum limited when approaching the ground state variance of roughly $x_0 \approx 0.1nm$. Many high efficiency measurements, capable of resolving beyond optical-wavelength amplitude motion, require the particle to already be tightly confined. In a large trap this necessitates some initial cooling so that the particle does not move outside the range of these measurement techniques.

3.3.2 Cavity phase shifts

Introducing a cavity around the suspended particle is often a reliable way to improve light collection efficiency, and homodyning the light from a partially transparent mirror can be used to efficiently track the position of a particle. In order to explore this effect it is first useful to omit the particle, and briefly outline input-output theory for a cavity and a single optical mode, coupled to its environment through a lossy mirror. The relevant Hamiltonians for this system are,

$$H_C = \hbar\omega_0 a^\dagger a, \qquad H_E = \hbar \int_{-\infty}^{\infty} \mathrm{d}\omega\, \omega b^\dagger(\omega) b(\omega), \tag{3.54}$$

$$H_{int} = \frac{\hbar}{\sqrt{2\pi}} \int_{-\infty}^{\infty} \mathrm{d}\omega\, \sqrt{\Gamma}\big(a b^\dagger(\omega) + a^\dagger b(\omega)\big), \tag{3.55}$$

where a is the operator for the cavity mode, $b(\omega)$ are the environment modes, and we have already assumed a continuous and extended frequency range of the environment modes, with a constant coupling strength Γ. This relies on the Markov approximation, and the rotating wave approximation (without the RWA the fast oscillating terms, $e^{i(\omega-\omega')t}$, would be resonant at negative frequencies under the extended range, leading to nonphysical behaviour). The extended integral will allow for a much simpler treatment of the environ-

ment. Previously we have considered stochastic state evolution, here we will use quantum Langevin equations derived in the Heisenberg picture.

For an arbitrary operator, the Heisenberg equation of motion is $\dot{A} = -(i/\hbar)[A, H]$. For the cavity annihilation operator and the environment operator,

$$\dot{a} = \frac{i}{\hbar}[a, H_C] - \frac{i}{\hbar}[a, H_{int}] = -i\omega_0 a(t) - \frac{i}{\sqrt{2\pi}} \int_{-\infty}^{\infty} \mathrm{d}\omega \, \sqrt{\Gamma} b(\omega), \tag{3.56}$$

$$\dot{b}(\omega) = \frac{i}{\hbar}[b, H_E] - \frac{i}{\hbar}[b, H_{int}] = -i\omega b(\omega) - i\sqrt{\frac{\Gamma}{2\pi}} a(t). \tag{3.57}$$

To solve the evolution equation for the environment mode, it is helpful to transform into a rotating frame such that

$$\begin{aligned} \frac{\mathrm{d}}{\mathrm{d}t}\left[b(\omega)e^{i\omega t}\right] &= \left[\frac{\mathrm{d}}{\mathrm{d}t} b(\omega)\right] e^{i\omega t} + i\omega b(\omega) e^{i\omega t} \\ &= -i\sqrt{\frac{\Gamma}{2\pi}} a(t) e^{i\omega t}, \end{aligned} \tag{3.58}$$

where in the first line we have applied the phase shift operator and expanded using the product rule, and on the second line substituted in (3.57). We can try integrating this equation over some arbitrary time period. For now we consider integrating from some point in the past t_0 to t,

$$\begin{aligned} \int_{t_0}^{t} \frac{\mathrm{d}}{\mathrm{d}t}\left[b(\omega)e^{i\omega t}\right] \mathrm{d}t &= b(\omega)e^{i\omega t}|_{t=t} - b(\omega)e^{i\omega t}|_{t=t_0} \\ &= b(\omega)e^{i\omega t} - b_0(\omega)e^{i\omega t_0}, \end{aligned} \tag{3.59}$$

where we have defined $b_0(\omega)$ as the environment operator at $t = t_0$. We can re-write this equation as

$$b(\omega) = b_0(\omega)e^{-i\omega(t-t_0)} - i\sqrt{\frac{\Gamma}{2\pi}} \int_{t_0}^{t} a(t) e^{i\omega t} \, \mathrm{d}t \,, \tag{3.60}$$

and then finally substitute this expression back into the equation for the cavity operator,

$$\dot{a}(t) = -i\omega_0 a(t) - \frac{i}{\sqrt{2\pi}} \int_{-\infty}^{\infty} \mathrm{d}\omega \, \sqrt{\Gamma}\, b_0(\omega) e^{-i\omega(t-t_0)} - \frac{\Gamma}{2\pi} \int_{t_0}^{t} a(t') \int_{-\infty}^{\infty} \mathrm{d}\omega \, e^{i\omega(t-t')} \, \mathrm{d}t' \,. \tag{3.61}$$

After making some assumptions about the statistical properties of the environment, this can be interpreted as a quantum Langevin equation. In the last term of this expression we can identify the frequency integral as a delta function, which in turn lets us evaluate the integral over time. We can also define the input operator

$$a_{in}(t) = \frac{i}{\sqrt{2\pi}} \int_{-\infty}^{\infty} \mathrm{d}\omega \, b_0(\omega) e^{i\omega(t-t_0)}. \tag{3.62}$$

which we will argue represents noise introduced by the environment. With these adjustments we can write

$$\dot{a}(t) = -i\omega_0 a(t) - \frac{\Gamma}{2} a(t) - \sqrt{\Gamma}\, a_{in}(t). \tag{3.63}$$

This equation specifically describes the evolution of the cavity mode operator, however similar Langevin equations can be derived for any other system operator coupled to the cavity field.

We can interpret $a_{in}(t)$ as an input to the system, since it represents the influence of the external modes $b(\omega)$ at time in the past, on the present system operator $a(t)$. By integrating (3.60) over all frequencies we can find another useful expression for the input operator,

$$\int_{-\infty}^{\infty} \mathrm{d}\omega \, b(\omega) = -i\sqrt{2\pi} \left(\frac{\Gamma}{2} a(t) + \sqrt{\Gamma}\, a_{in}(t) \right). \tag{3.64}$$

We could have equally derived a similar expression, by choosing instead to integrate the evolution equation for $b(\omega)$ to some point in the future. This would have resulted in a reversed time equation, from which an output field operator can be defined. Using the corresponding result (3.64) for the output field, the key input-output relation can be found,

$$a_{out}(t) - a_{in}(t) = \sqrt{\Gamma} a(t) \tag{3.65}$$

Conversely to $a_{in}(t)$, the output operator $a_{out}(t)$ represents the coupling of the system to future environment modes, and we can interpret this to be the system output through the partially transparent cavity mirror. The operator a_{out} then represents the field that would be measured outside of the cavity, where as a_{in} represents the vacuum fluctuations in the environment that enter the system and mix with the cavity state. We can see that the input operator introduces noise by tracing out the environment degrees of freedom and considering the expectation values $\langle a_{in}^{\dagger}(t)\, a_{in}(t)\rangle$. If the environment is a vacuum state or an ensemble in which the number of excitations per unit bandwidth is constant, we can show in a similar way to treating the increment in homodyne detection, that $a_{in}(t)$ is well approximated by white noise. These assumptions about the environment are certainly an idealisation, but a useful one, and are what make the quantum Langevin equations stochastic.

The general methodology for using the input-output formalism is to first specify the input fields, solve the quantum Langevin equations for the operators of interest, and then use the relation (3.65) to compute the output field. A useful example case is a cavity with a resonant driving field specified by the Hamiltonian

$$H_D = \hbar E_0\big(a e^{i\omega t} + a^{\dagger} e^{-i\omega t}\big), \tag{3.66}$$

where E_0 is the amplitude of the driving field. The quantum Langevin for the cavity field is then

$$\dot{a}(t) = iE_0 - \frac{\Gamma}{2}a(t) - \sqrt{\Gamma}\, a_{in}(t). \tag{3.67}$$

If we consider an ensemble average over the noise, where $\langle a_{in}\rangle = 0$, the evolution of the expectation value of the cavity operator is the same as would be found using the Lindblad equation. In steady state we can define the coherent state amplitude of the cavity field,

$$\alpha \equiv \langle a(t\to\infty)\rangle = \frac{i2E_0}{\Gamma} \tag{3.68}$$

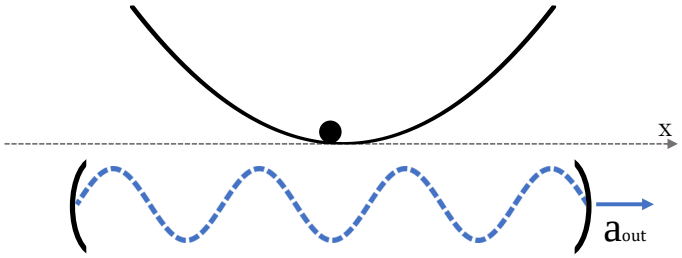

Figure 3.2: Sketch of a standing wave cavity containing a single particle. The particle could be suspended with an external field, or if the cavity field is strong enough, confinement is possible with the optical dipole force alone. In the dispersive regime the particle's motion causes phase shifts in the cavity and output field, which can be measured to infer information about the particle's position.

In this case, using (3.65), the output field would be

$$a_{out} = i\sqrt{\Gamma}\alpha + \xi(t), \tag{3.69}$$

where we have explicitly represented the input field with white noise $\xi(t)$. The output field as might be expected, is composed of a component of the classical driving field proportional to the cavity decay rate, with the addition of noise from the environmental vacuum fluctuations.

Returning to measurements of trapped particles, we can use the Jaynes-Cummings Hamiltonian to describe an atom coupled to a cavity mode,

$$H_{atom} = \frac{p^2}{2m} + \hbar\omega\sigma^\dagger\sigma, \tag{3.70}$$

$$H_{int} = \hbar g \cos(kx)\left(\sigma a^\dagger + \sigma^\dagger a\right), \tag{3.71}$$

where we are working in the interaction picture with the RWA. σ is the ladder operator for the atomic transition and Δ is the detuning from the cavity field frequency. The spatially

varying coupling strength is due to the standing wave field in the cavity, as illustrated in Figure 3.2. In the dispersive regime, the cavity output will contain useful position information, so we will consider the limit of large detuning. As with the imaging example, we can adiabatically eliminate the internal dynamics of the atom. We can trace out the internal degrees of freedom, and replace them with their steady state values,

$$\langle\sigma\rangle \approx \frac{g}{\Delta}\cos(kx)a(t). \tag{3.72}$$

The quantum Langevin equation for the the cavity operator in this case is

$$\dot{a} = -iE_0 - i\frac{g^2}{\Delta}\cos^2(kx)a(t) - \frac{\Gamma}{2}a(t) - \sqrt{\Gamma}a_{in}(t). \tag{3.73}$$

Assuming the cavity field amplitude also reaches steady state on the timescales of the particle motion, we can then approximate

$$\langle a\rangle \approx -i\alpha\big[1 - i\frac{2g^2}{\Gamma\Delta}\cos^2(kx)\big]. \tag{3.74}$$

And finally, using the input output relation

$$a_{out} = \sqrt{\Gamma}\langle a\rangle - a_{in} = \alpha\frac{2g^2}{\Delta\sqrt{\Gamma}}\cos^2(kx) + \xi(t), \tag{3.75}$$

where we have omitted the drive and the cavity field component independent of x, since these terms only contribute a constant shift in the output field. We can see that a homodyne measurement of the output would provide a continuous measurement of the cosine squared of the particle position. The input field noise unavoidably makes its way into this measurement record, producing exactly the same form of measurement as in the master equation for homodyne detection we derived in chapter 2.

In the dispersive regime the particle will see an effective potential due to the off-resonant

cavity field. Following the previous approximations (3.70) becomes

$$H_{atom} \approx \frac{p^2}{2m} - \hbar \frac{g^2\alpha^2}{\Delta} \cos^2(kx). \tag{3.76}$$

The cavity output field (3.75) reflects the particle's position in this potential. Over small distances the particle's position can be well approximated as either simply quadratic at a field anti-node, or even linear at a node. Suspending a particle at a node, however, would require additional tight confinement, which is not the scenario we are interested in when considering large magnetic traps. Sufficiently cooled, a particle would sit at an anti-node without need for further confinement but parametric damping with quadratic position information has its own associated challenges [43]. We were motivated initially to include a cavity around a magnetically suspended particle in an attempt to improve light collection efficiency. In the following sections we consider options which do this whilst providing measurements linear in position or momentum.

3.3.3 Velocity measurement via electromagnetically induced transparency

Direct measurements of a particle's velocity are difficult, since velocity does not usually play a strong role in the coupling strength to a light field. For example, the effects of small Doppler shifts due to a particle's motion are not usually detectable, especially when the aim is to cool the particle. One way to get around this is to use electromagnetically induced transparency (EIT) as a very sensitive probe to small shifts in frequency. A velocity measurement was proposed for ion cooling by exploiting EIT[74], to effectively amplify the very small refractive properties of a single particle. Applying this technique to a nano-particle is not straightforward since the interference effect needed for EIT cannot be seen in a classical dipole. However, nano-diamonds with nitrogen vacancy centres are of particular interest as nano-mechanical resonators specifically because they have a measurable internal quantum structure. We investigated the possibility of such a measurement for a levitated diamond in a travelling wave cavity.

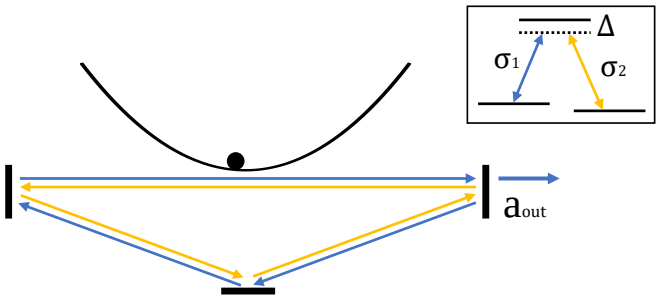

Figure 3.3: Sketch of travelling wave cavity configured to measure small changes in a particle's velocity. Two counter-propogating fields interact with two transitions in a lambda configuration 3-level system, as shown in the inset. A trapped particle suspended within the cavity mode will have a significantly increased refractive index in the regime of EIT. As a result, there are phase shifts in the output field that are highly sensitive to the Doppler shift in frequency caused by the particle's motion.

EIT relies on an internal 3-level Λ structure, and appropriate driving of the available transitions, as illustrated in Figure 3.3. For a particle in a travelling wave cavity, with two fields to drive both transitions, the relevant Hamiltonians are,

$$H = \hbar\Delta_1\sigma_1^\dagger\sigma_1 + \hbar\Delta_2\sigma_2^\dagger\sigma_2, \tag{3.77}$$

$$H_{int} = \hbar g\big(\sigma_1 a^\dagger + \sigma_1^\dagger a\big) + \frac{\hbar\Omega}{2}\big(\sigma_2 + \sigma_2^\dagger\big). \tag{3.78}$$

We have used the classical limit for the drive field Ω acting on the transition σ_2, where as the probe field a is still quantised and interacts with the transition σ_1, with coupling strength g. Δ_1 and Δ_2 are the detunings of the fields from the respective transitions. In the lambda configuration, if both fields are near resonant, and the probe only weakly excites the second transition $g\alpha \ll \Omega$, there will be electromagnetically induced transparency. In this limit, due to the usual damping via spontaneous emission, we can replace the probe

driven transition by its steady state value,

$$\langle \sigma_1 \rangle \approx 4g \frac{(\Delta_1 - \Delta_2)}{\Omega^2} a. \tag{3.79}$$

It is common to also account for the decoherence between the two ground states due to collisions with surrounding air molecules, for simplicity here we have assumed this effect to be negligible. When the drive and probe field are exactly resonant for a particle at rest, the only detuning is due to the Doppler shift in frequency caused by the particle's motion. If the drive and probe field counter-propagate $\Delta_1 - \Delta_2 = 2kv$, where v is the particle velocity and we have made the simplifying approximation that the drive and probe field have nearly the same wavenumber k. What is important, is that σ_1, and correspondingly the particle's refractive index are now linear in the velocity. The slope of the dispersion curve is incredibly steep and amplifies the probe's sensitivity to small changes in detuning, and hence velocity.

For a lossy cavity we know that the output field should obey the quantum Langevin equation

$$\dot{a} = -iE_0 - ig\langle \sigma_1 \rangle - \frac{\Gamma}{2} a - \sqrt{\Gamma} a_{in}. \tag{3.80}$$

And when the output field is approximately in steady state

$$a_{out} \approx \frac{4k\alpha g^2}{\sqrt{\Gamma}\, m\Omega^2} p + \xi(t), \qquad \text{if} \qquad \frac{4kg^2}{\Gamma m \Omega^2} p \ll 1, \tag{3.81}$$

where p is the particle momentum, and we have again dropped any constant terms in the output field. The expression for the output field is only accurate in the specified limit, where effectively the Doppler detuning must be small compared to the width of the transparency window. This is less restrictive for a massive particle since they will typically have a much lower velocity than individual trapped atoms. The restrictions for a strong pump however, severely limits the maximum value of the measurement strength. We can

express a homodyne measurement of (3.81),

$$dI = \langle p \rangle + \frac{dW}{\sqrt{8\eta\kappa_p}}, \qquad \kappa_p = \frac{k^2\alpha^2 g^2}{2\Gamma m^2 \Omega^4}. \tag{3.82}$$

Using similar arguments as for the necessary position resolution in section 3.2, we can see that the necessary measurement strength κ_p to damp on the timescales of a few oscillations $\kappa_p p_0^2/\omega \approx 1$. For generous estimates of the drive field and the coupling strength for a small cavity, with $\alpha g = \Omega/10$ the measurement strength is still several orders of magnitude less than unity for a nanoscopic particle. This is an unfortunate consequence of the measurement strength scaling inversely with the mass of the particle. Working in the limit of weak probe also prevents simply increasing the measurement strength. The limitation can be physically linked to the velocity information originating in the interference between the probe and the spontaneously emitted radiation from a necessarily weakly excited state. For single atoms, this is a feasible measurement to use for feedback cooling, but even then this would typically require damping over several thousand oscillations.

Our analysis of measurements via coupling to a cavity field concluded that these methods were not best suited to heavy particles in low frequency traps. Homodyning light from a standing wave cavity can be used to efficiently track the position of a particle, however the quadratic position measurement introduces further complications to cooling and does not work in conjunction with a large magnetic trap. Direct velocity measurements might be possible with a trapped nano-diamond, but the signal would be extremely weak and unable to suitably resolve the particle for damping on short time-scales. Sideband cooling with near resonance light within a cavity has also been proposed as a useful aid in nearing ground state cooling[75]. However, with high measurement efficiencies $\eta \sim 0.2$, cooling via active feedback can go beyond the limits of sideband cooling and it ceases to have additional benefits. This is a significantly higher quantum efficiency than has been previously been achieved in magnetic traps, but we propose that light collection with a single mirror can surpass this in future experiments.

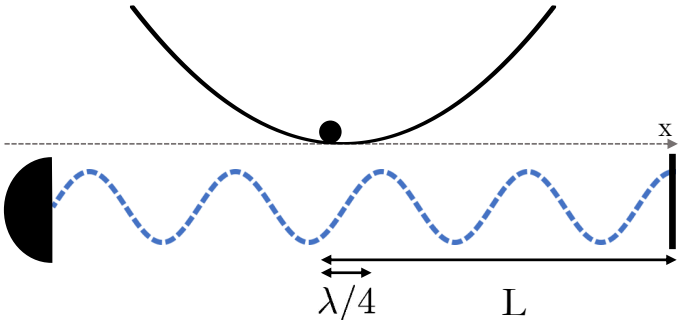

Figure 3.4: Sketch of apparatus for measuring the intensity of light scattered into the standing wave mode of a single mirror. The intensity is modulated by a particle's motion along its main trap axis x. The trap centre is marked a distance L from the mirror. The range of motion over which this measurement would be valid is restricted about a node of the standing light field, and has also been marked. A focused beam and a curved mirror that maximises coupling into the reflected mode could reasonably produce light collection efficiency $> 15\%$.

3.3.4 Single mirror

The dispersive measurement techniques we explored do not seem well suited for magnetically trapped particles, but on-axis light collection is important for high quantum efficiency. To this effect, measuring the modulation of light scattered into a standing wave mode has been shown to be effective with trapped ions[16, 36]. The set-up we consider uses a mirror to introduce a standing wave mode across the levitated particle, where some of the scattered light from the illumination probe will be collected, as shown schematically in Figure 3.4. The mirrors here can be quite large, capturing a significant fraction of the light scattered along the primary trap axis. The particle motion adds side-bands to the spectrum of light scattered in the mirror mode, positioned at $\pm\omega$ from the optical frequency. Continuous measurement of these side-bands can be used to infer the particle's current position after filtering out the elastically scattered signal. This is a non-intrusive set-up that could be implemented in magnetic traps to give a significant increase in measurement efficiency and resulting position resolution, over current imaging schemes.

Initially we will only consider emission into the standing wave mirror mode. In which case the interaction Hamiltonian is

$$H_{\mathrm{I}} = \hbar\gamma \sin(k_L(L+\hat{x}))\big(b + b^{\dagger}\big), \tag{3.83}$$

where γ is the scattering rate, k_L is the optical wavenumber and b are the field operators. If the position of the trap centre L is taken to be at a point where $k_L L = \pi/4$, we can define the jump operator

$$\hat{c} = \sin\big(k_L(L+\hat{x})\big) \approx \frac{1}{\sqrt{2}}\big(1 + k_L\hat{x})\big), \tag{3.84}$$

which corresponds to the field that would be measured by a photo-detector in line with the mirror mode. In the approximate form of this operator we have performed a Taylor expansion in the Lamb-Dicke regime. This expansion is possible when the typical length of the oscillation is small compared with the wavelength of incident light, $k_L x \ll 1$. The resulting operator has two separate components, one corresponding to the constant amplitude elastically scattered light and the other to the position-dependent modulated light. Some initial cooling would be required to reach this regime in a large trap, but this could be achieved using lower resolution imaging measurements. Current experiments have cooled a silicon micro-sphere in a magneto-gravitational trap to sub-mK temperatures[71]. Damping the position variance further, to within a micron, corresponds to a temperature of about a microKelvin and will require improved isolation from classical heating sources. Overcoming these classical noise challenges will bring experiments to the point where they could operate in this strong measurement regime.

Under the usual Born and Markov approximations, we can think of the operator $\hat{c}$ as being applied to the system after photo-detection in a stochastic Shrodinger evolution. As in

(2.67) we can define the stochastic increment

$$\begin{aligned} dN &= \gamma \hat{c}^\dagger \hat{c}\, \mathrm{d}t \\ &\approx \frac{\gamma}{2} dt + \gamma k_L x dt. \end{aligned} \tag{3.85}$$

In the Lamb-Dicke regime, the first term corresponding to elastically scattered light is comparatively large and can be treated like a local oscillator field in homodyne detection. In fact dN in this case has the same form as (2.69). If we identify $dX = \sqrt{2\gamma k_L^2}\, x\, \mathrm{d}t$, as a new stochastic increment, it has the appropriate properties to make the diffusion approximation, namely $dX^2 = dt$. The measured photo-current can be expressed as a renormalisation of the now continuous photon count, after subtracting the elastically scattered signal

$$dI = \langle x \rangle dt + \frac{1}{\sqrt{8\eta\kappa}} dW. \tag{3.86}$$

In this form $\kappa = \gamma k_L^2/4$ which is the same measurement strength we estimated for an idealised case in 1D (3.40) if we normalise the operators $\langle c^\dagger c \rangle = 1$, as we had for the free space modes. We have seen that the measurement strength reflects the rate of information gained about the system and the corresponding disturbance this necessarily causes. This exact expression for κ would be accurate if the scattering was exclusively along the x axis, the true value will be less in any other case where we should only count the momentum kicks projected along the x direction. κ otherwise scales with increasing scattering rate off the particle, and can be adjusted by increasing the laser power. The parameter η is the quantum efficiency, and accounts for the fraction of photons collected (after projection along the measurement axis) and any further loss that occurs in the detector. It has been suggested that light collection efficiency of $\eta \approx 0.15$ could be reasonably expected when monitoring an optically trapped ion in front of a mirror[36]. One of the significant advantages of magnetic levitation is that the probe light is independent of the trapping mechanism, which allows it to be shaped to optimize detection efficiency. This is of crucial importance when relying on active feedback cooling in order to counteract the random motion induced by the measurement itself. The shot-noise in optically trapped

nano-particle experiments currently poses a major obstacle to reaching the ground state, with typical collection efficiencies $\eta < 0.01$[65].

Having reviewed various measurement options we conclude that light collection with a single mirror has the advantages of simple implementation and high return on increased quantum efficiency. We will use $\eta = 0.15$ as a realistic baseline when evaluating various feedback strategies, whilst keeping in mind that this value could be made significantly higher with tailored directional scattering.

3.4 Feedback strategies

In chapter 2 we reviewed direct feedback of a general quantum measurement, following the methodology of Wiseman and Milburn. We have now established how we might obtain a suitably efficient measurement of a particle's position, and we can consider the specific form of the feedback Hamiltonian. We know that a classical oscillator will be damped by a force proportional to its current velocity. Although we have established that direct measurements of velocity are difficult, it will be enlightening to first consider a model where we assume this is possible. Following this we will explore methods for optimally using position information for cooling.

3.4.1 Velocity measurement and damping

We start by assuming we have access to a measurement record

$$I = \langle p \rangle + \frac{1}{\sqrt{8\eta\kappa_p}}\,\xi(t), \tag{3.87}$$

which has been scaled to be proportional to a particle's momentum. Following the procedure outlined in section 2.4 we should specify a feedback operation proportional to the

measurement record,

$$\mathcal{K}\rho = -\frac{i}{\hbar}G\big[x,\rho\big]. \tag{3.88}$$

This super-operator corresponds to simply introducing a linear position term into the Hamiltonian, which if proportional to the measurement record, equates to a standard damping force. Physically this could be achieved in many ways, either by adjusting the trapping potential or, for example, by applying a force via radiation pressure. We have also included a scaling factor G for the feedback strength, this gain parameter could be controlled independently of the measurement record. We can now use equation (2.107) to describe the average effects of the feedback,

$$\dot{\rho} = -i\omega\big[a^\dagger a,\rho\big] + 2\kappa_p\,\mathcal{D}[p]\rho - i\,\frac{G}{2\hbar}\big[x,p\rho+\rho p\big] + \frac{G^2}{8\,\eta\,\kappa_p\hbar^2}\mathcal{D}[x]\rho. \tag{3.89}$$

The term here proportional to G describes the damping effect of the feedback where as the term proportional to G^2 causes additional heating due to the fundamental noise in the measurement. We have ignored the effects of of environmental heating here. This will help simplify our analysis and is a valid approximation when operating in the back-action dominated regime $\bar{n}\gamma_{th} \ll p_0^2\kappa_p$. In this case the terms in equations (3.35-3.39) corresponding to the thermal coupling γ_{th}, produce negligible effects compared to the measurement localisation and back-action over short timescales $t \ll 1/(\bar{n}\gamma_{th})$.

Again making use of the fact that $d\langle A\rangle = Tr[A\,d\rho]$, we can see that the damping only directly affects the first order momentum,

$$\frac{\mathrm{d}\langle x\rangle}{\mathrm{d}t} = \frac{1}{m}\langle p\rangle, \qquad \frac{\mathrm{d}\langle p\rangle}{\mathrm{d}t} = m\omega^2\langle x\rangle - 2G\langle p\rangle. \tag{3.90}$$

Over several oscillations, both the mean position and momentum would damp to zero. The final energy of the state can be found by calculating the steady state variances,

$$\langle n\rangle_{t\to\infty} = \frac{1}{2}\left(\frac{\langle x^2\rangle}{2x_0^2} + \frac{\langle p^2\rangle}{2p_0^2} - 1\right) = \frac{1}{2}\left(\frac{G\,\tilde{\kappa_p}}{\omega^2} + \frac{2\tilde{\kappa_p}}{G} + \frac{G}{8\eta\tilde{\kappa_p}} - 1\right), \tag{3.91}$$

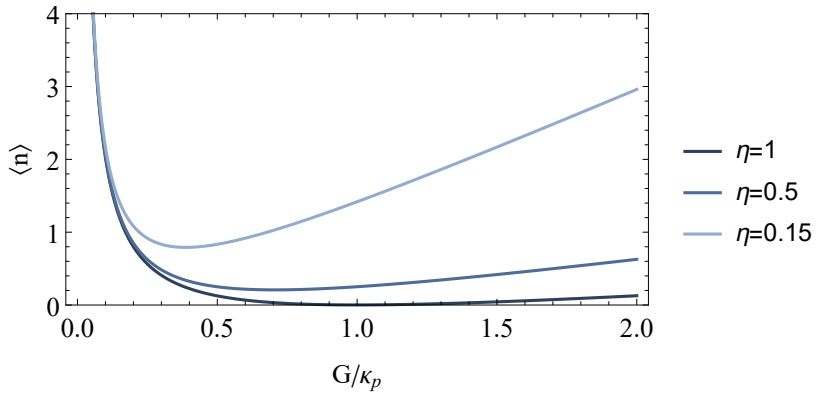

Figure 3.5: Steady state phonon occupation (3.91) after feedback cooling using a velocity measurement with $\tilde{\kappa_p} = \omega/100$, for varying measurement efficiency η. For an optimal choice of the gain parameter G, cooling with perfect efficiency approaches the quantum ground state.

where we have defined $\tilde{\kappa_p} = p_0^2 \kappa_p$. This is the steady state phonon occupancy for an ensemble average of damped particles. We can see that to minimise $\langle n \rangle$, there is a balance to strike between measurement and feedback strength, this is illustrated in Figure 3.5. The first term in this expression also shows that cooling works best when G and $\tilde{\kappa_p}$ are much smaller than the trap frequency ω. The physical reasoning for this is that only the momentum is being directly damped by the feedback loop, but if the position and momentum are rotating quickly they are both effectively cooled. When $\omega^2 \gg \tilde{\kappa_p} G$ the minimum achievable phonon number is

$$\langle n \rangle_{\min} \approx \frac{1}{\sqrt{4\eta}} - \frac{1}{2}. \tag{3.92}$$

With unit efficiency, the particle can effectively be cooled to its quantum ground state over many oscillation cycles.

3.4.2 Slowly varying quadrature measurement

The results for damping using a velocity measurement will serve as a useful guide. If we attempt to perform a similar damping procedure with a position measurement, we first have to manipulate the signal so that it suitable for feedback. As an initial approach we consider the case where $\omega \gg G, \kappa$. We have shown this is not the ideal regime for low frequency traps, as significant improvements would need to be made in thermal isolation to cool to the ground state over many oscillations. However, there is no fundamental limitation to reaching this regime and it is informative to explore the techniques used in this case. When there is a dominant oscillation frequency, greater than any thermal damping or back-action contributions, a signal proportional to the slowly varying momentum component can be obtained by demodulating the measured photo-current.

It will be helpful to define the slowly varying quadrature components,

$$X = \frac{(a^\dagger e^{i\omega t} + a\, e^{-i\omega t})}{\sqrt{2}}, \qquad P = i\frac{(a^\dagger\, e^{i\omega t} - a\, e^{-i\omega t})}{\sqrt{2}}. \tag{3.93}$$

It would often be natural in an experiment to demodulate the measurement signal and work with only these slowly varying quadratures. We know that X and P should slowly vary since the frequency spectrum of a high quality oscillator is sharply peaked about the resonance value ω, and this frequency component has been effectively been shifted to zero in their definition. The process of demodulation is analogous to the mathematical procedure of moving to an interaction picture, and making the rotating wave approximation.

We can expand the position operator in terms of the quadrature components,

$$x = x_0(a + a^\dagger) = x_0\big(\cos(\omega t)X + \sin(\omega t)P\big), \tag{3.94}$$

such that the measurement signal becomes

$$dI = x_0\big(\cos(\omega t)\langle X\rangle + \sin(\omega t)\langle P\rangle\big)dt + \frac{1}{\sqrt{8\eta\kappa}}\, dW. \tag{3.95}$$

If the measurement is mixed with a local oscillator, $\sqrt{2}\cos(\omega_0 t + \phi)$, it can be split into a combination of fast and slowly rotating terms. In the case where there is no detuning between the local oscillator and the trap frequency $\delta = \omega_0 - \omega = 0$ and $\phi = 0$,

$$\sqrt{2}\cos(\omega t)\, dI = x_0 \Big[\big(1 + \cos(2\omega t)\big)\langle X\rangle + \sin(2\omega t)\langle P\rangle \Big] dt + \frac{1}{\sqrt{4\eta\kappa}} \cos(\omega t)\, dW. \tag{3.96}$$

Demodulation is achieved by applying a high frequency filter. This can be interpreted as effectively averaging the signal over some time Δt that is long compared to $1/\omega$ but short compared to all other relevant timescales. The demodulated photo-current

$$\Delta I_X = \sqrt{2} \int_t^{t+\Delta t} \cos(\omega t)\, dI \approx x_0 \langle X\rangle dt + \frac{\Delta W_X}{\sqrt{8\eta\kappa}}, \tag{3.97}$$

where the newly defined stochastic increment

$$\Delta W_X = \sqrt{2} \int_t^{t+\Delta t} \cos(\omega t) dW. \tag{3.98}$$

Likewise for $\phi = \pi/2$,

$$\Delta I_P = \sqrt{2} \int_t^{t+\Delta t} \sin(\omega t)\, dI \approx x_0 \langle P\rangle dt + \frac{\Delta W_P}{\sqrt{8\eta\kappa}}. \tag{3.99}$$

These new noise increments usefully still obey Ito rules over timescales Δt, and are orthogonal to each other,

$$\begin{aligned} \Delta W_X^2 &= 2 \int_t^{t+\Delta t} \cos^2(\omega t') dt' \approx \Delta t, \\ \Delta W_X \Delta W_P &= 2 \int_t^{\Delta t} \sin\big(\omega t'\big) \cos\big(\omega t'\big) dt' = \int_t^{t+\Delta t} \sin(2\omega t) dt \approx 0. \end{aligned} \tag{3.100}$$

For $\phi = \pi/2$, the demodulated photo-current is proportional to the slowly varying momentum quadrature which is suitable for feedback cooling.

We can derive a measurement master equation of the usual form following a few approxi-

mations in the interaction picture,

$$U\mathcal{D}[x]\rho U^\dagger \approx x_0^2\Big(\mathcal{D}[a]+\mathcal{D}[a^\dagger]\Big)\tilde{\rho}, \tag{3.101}$$

$$U\mathcal{H}[x]\rho\,\mathrm{d}W\,U^\dagger \approx x_0\Big(\mathcal{H}[\tilde{X}]\,\mathrm{d}W_X+\mathcal{H}[\tilde{P}]\,\mathrm{d}W_P\Big)\tilde{\rho}. \tag{3.102}$$

After transforming into the rotating frame there are effectively two measurement channels corresponding to each quadrature $\tilde{X}=(a^\dagger+a)$ and $\tilde{P}=i(a^\dagger-a)$. By design the slowly varying quadratures lose their time dependence in the interaction picture. To achieve damping, the momentum quadrature $cos(\omega t)\Delta I_P$ can be fed back, where we have shifted the demodulated measurement signal to be in line with the system frequency again. If we re-scale gain parameter in (3.88), for momentum damping using the demodulated position measurement $G\rightarrow\tilde{G}=(p_0/x_0)G$, then the resulting feedback master equation is

$$\dot{\tilde{\rho}}=-i\delta\big[a^\dagger a,\tilde{\rho}\big]+2\kappa x_0^2(\mathcal{D}[a]+\mathcal{D}[a^\dagger])\tilde{\rho}-\frac{i}{\hbar}G\big[x,p\tilde{\rho}+\tilde{\rho}p\big]+\frac{G^2}{\eta\kappa\hbar^2}\left(\frac{p_0}{x_0}\right)^2\mathcal{D}[x]\tilde{\rho}. \tag{3.103}$$

From the master equation, the steady state phonon occupancy can be found,

$$\langle n\rangle=\frac{1}{2}\left(\frac{G\,\tilde{\kappa}}{2\delta^2}+\frac{2\tilde{\kappa}}{G}+\frac{G}{2\eta\tilde{\kappa}}-1\right), \tag{3.104}$$

where $\tilde{\kappa}=x_0^2\kappa$. This is a similar expression to that found when making a direct velocity measurement (3.91). The best cooling is achieved in the limit of high detuning δ so that both quadrature components are damped. However, in this feedback procedure, the information about the position quadrature is effectively discarded. As a result, even with perfect measurement efficiency, the minimum phonon occupancy never falls to zero,

$$\langle n\rangle_{\min}=\frac{1}{\sqrt{\eta}}-\frac{1}{2}. \tag{3.105}$$

3.4.3 Measurement post-processing

Demodulation was an example of signal post-processing, that thanks to certain approximations, allowed us to extract momentum information about the particle with the bonus of having an analytically tractable solution. The process relied on a large separation of timescales and threw away some measurement information, reducing the quantum efficiency. Rather than rely on a dominant frequency in the system, we could attempt to more directly take the derivative of the a position measurement to estimate the momentum. This requires smoothing out the noise in the signal, which can be achieved physically with a band pass filter. This was the technique used in[46], whilst operating in a classical cooling regime.

An RLC circuit consisting of a resistor, inductor and a capacitor, can be used to filter a driving signal,

$$I_{drive} = \frac{1}{C}Q + R\frac{dQ}{dt} + L\frac{d^2Q}{dt^2}. \tag{3.106}$$

where Q is the charge in the circuit and R, L and C are the resistance, inductance and capacitance of the circuit elements. The circuit functions as a damped harmonic oscillator where the rapid change of impedance near the resonant frequency can be used to block the high frequency noise components in the measurement signal. If we consider a single component of the drive signal $I_c = A_c\cos(\omega_c t)$, then below a cut-off range, the current in the circuit will be proportional to the derivative of the drive,

$$\begin{aligned}\frac{dQ}{dt} &= \frac{A_c}{\sqrt{(\omega_c^2-\omega_f^2)^2+\omega_c^2(R/L)^2}}\,\omega_c\cos(\omega_c t+\phi)\\ &\approx C\omega_c A_c\cos\Big(\omega_c t+\frac{\pi}{2}\Big),\end{aligned} \tag{3.107}$$

where $\omega_f = 1/LC$ is the circuit resonant frequency. For values of $\omega_c \ll \omega_f$ the current amplitude is roughly proportional to the original signal multiplied by its frequency, and its phase is shifted by around $\pi/2$. The filter can therefore be used to approximately take the derivative of signal components lower than the cut of frequency. For a critically damped

circuit, where $R = \sqrt{4L/C}$, if we use (3.86) as the drive signal, we can define a filtered measurement current which should approximate the momentum,

$$I_f = \frac{1}{C}\frac{dQ}{dt}. \tag{3.108}$$

Since the noise in the measurement has been filtered, there are no issues as to whether to use the Ito or Stratonovich interpretation when reintroducing the signal to influence the system evolution. We simulated feedback damping with a stochastic Schrödinger equation of the form (2.75), with the available energy levels in the system truncated to 100. We used the feedback Hamiltonian

$$H_{fb} = GI_f x, \tag{3.109}$$

where again G is used as a gain factor for the damping strength. In the parameter regime $\tilde{\kappa}, G < \omega$ we find similar cooling results to those with a demodulated position measurement. Figure 3.6 shows the average steady state phonon occupancy for a range of gain factors, with a best fit of a function following the form of (3.91,3.104),

$$\langle n \rangle_{fit} = a\left(\frac{\tilde{\kappa}}{G}\right) + b\left(\frac{G}{\eta\tilde{\kappa}}\right) - \frac{1}{2}, \tag{3.110}$$

where a and b were used as free variables. The fit indicates similar behaviour in response to damping. As in the case with a demodulated signal, ground state cooling is not achieved even with perfect quantum efficiency. The numerical results for larger $\tilde{\kappa}$ and G with respect to the trap frequency, also correspond to a rising minimum phonon number. This is in keeping with the idea that the position and momentum variances are not rotating quickly enough to be optimally cooled.

We have identified two difficulties in achieving ground state cooling using our proposed position measurement scheme. Damping solely using a force proportional to the particle's velocity, requires many oscillation cycles to reach the quantum ground state, and damping harder with the above methods is limited by reintroducing noise from the measurement

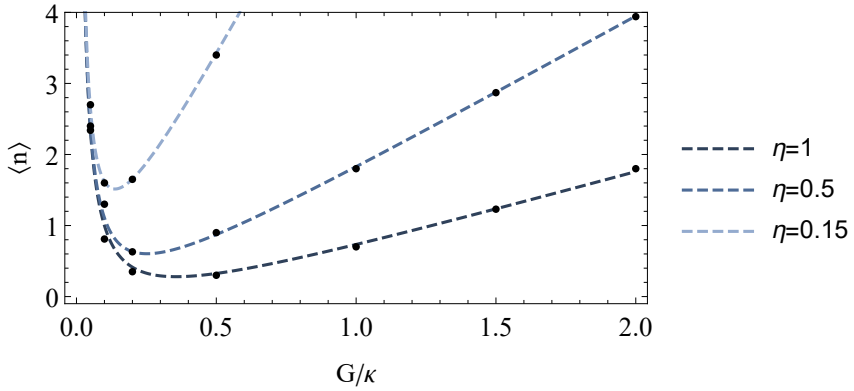

Figure 3.6: Steady state phonon occupation for numerically simulated feedback cooling, in the parameter regime $\tilde{\kappa} = \omega/100$. The state was simulated using a diffusive Schrödinger equation and the position measurement information was filtered using the equations for an RLC circuit (3.106). The time averaged steady state phonon occupancy, for single trajectories, was found for a range of gain values. A single set of fit parameters were obtained by fitting the function (3.110) to each set of points corresponding to different measurement efficiencies η.

signal. Estimating the velocity from a position measurement using the above techniques also effectively reduces the measurement efficiency. Damping directly with the position information is possible but more difficult to physically implement, as we will later discuss in detail. In this case there is still the problem of being reliant on cooling over timescales $t \gg 1/\omega$.

Both of these issues can be solved with a better approach to state estimation. The RLC filter that we examined successfully estimates the particle's momentum, but we did not optimise the circuit parameters. Rather than try to optimise the circuit however, we can use the equations of motion we already derived. Solving the master equation (3.32) with the measurement signal as an input should give a best estimate of the full state. Although solving the full master equation in real-time would be practically infeasible, using the equations for a Gaussian state would not. The Gaussian state equations mimic the effects of a band-pass filter for the measurement signal, but are already optimised to best estimate the position and momentum. This technique has been suggested for cavity

cooling [76], and variations of state estimation have been proposed for cooling different configurations of trapped particles. We find that this method of state estimation is very well suited to cooling in low frequency traps. The methodology can be exactly mapped onto control theory for classical particles, and shows that simultaneous damping of position and momentum can be used to achieve ground state cooling over short timescales. In the following chapter we outline this approach alongside numerical simulations. We then go on to consider alternative uses of state estimation in low frequency traps.

4 Preparing quantum states of motion

In this chapter an analysis for cooling magnetically confined particles is presented. A final model is shown together with measurement simulations and the outcomes of a proposed feedback procedure. The chapter concludes with discussion of an ongoing project to look for diffusion of a free particle's position that is expected in a continuous spontaneous localisation model. Predictions are made using the same models from the feedback analysis, that are applicable to proposed future experiments. The results for cooling magnetically trapped particles were published in Ref. [77].

4.1 Cooling in low frequency traps

In the previous chapter we outlined a quantum model for a levitated particle, and explored ways to effectively monitor its motion. The most suitable method we found involves measuring the amplitude modulation of a standing wave due to the particle's motion in front of a single mirror, Fig. 3.4. The Hamiltonians for the freely oscillating particle, H_{sys}, the optical field, H_F, and the interaction Hamiltonian, H_I, are given by

$$H_{\mathrm{sys}} = \frac{p^2}{2m} + \frac{m\omega^2 x^2}{2}, \tag{4.1}$$

$$H_{\mathrm{F}} = \sum_k \hbar\omega_k b_k^\dagger b_k, \tag{4.2}$$

$$H_{\mathrm{I}} = \sum_k \hbar\sqrt{\gamma}\big(b_k \exp(i\mathbf{k}.\mathbf{r}) + b_k^\dagger \exp(-i\mathbf{k}.\mathbf{r})\big), \tag{4.3}$$

where m is the particle mass, ω is the magnetic trap frequency, γ is the scattering rate into each mode of the optical electric field, $b_k(b_k^\dagger)$ is the usual quantised field mode amplitude, with wavenumber and angular frequency of k, ω_k respectively. The momentum recoil due to the scattered photons is represented by $\mathbf{k}.\mathbf{r}$, where $\mathbf{r}$ is the particle's position. It is

sufficient to model the motion of the particle in 1D, as although some cooling is often applied along each trap axis, the frequencies of each motional degree of freedom can be well separated and safely decoupled, as is done in current experiments [46].

If the particle is initially damped using classical cooling techniques so that its motion is confined to within a quarter of wavelength, then photo-detection of the standing wave mirror mode yields a signal proportional to the particle's position,

$$dI(t) = \langle x \rangle + \frac{dW}{\sqrt{8\eta\kappa}}. \tag{4.4}$$

The measurement strength κ scales proportionally with the scattering rate, which can be physically adjusted by varying the intensity of a probe beam. We established that to damp faster than the thermal heating rate, the measurement strength would have to be large enough such that $\eta\, x_0^2 \kappa \approx \Gamma_{th}$, where $\Gamma_{th} = (k_b T/\hbar\omega)\gamma_{th}$ is the phonon reheating rate due to the environment. In large magnetic traps this requires control of the system on a timescale comparable to the inverse of the trap frequency. This corresponds to over-damping the particle, which limits the effectiveness of techniques otherwise suitable for trapped ions and other nano-mechanical resonators. We find however, that these traps are an excellent platform for performing optimal feedback control via real-time state estimation, and we illustrate this in the following sections.

4.1.1 State estimation

The global positioning system (GPS) is a common example of classical state estimation. A network of satellites can periodically measure the position of a receiver on the Earth's surface to within a few metres, however, much greater accuracy can be achieved by combining these measurements with a physical model. Rather than take each measurement and its associated uncertainty as the new position estimate, the measurement is compared and averaged against the predictions of a physical model. The GPS estimate is likely to be noisy but remain within the same level of error, whilst a model of an object's velocity and

acceleration can predict a smooth evolution, but its accuracy will drift over time as small errors accumulate. In control theory, a Kalman filter is the name given to the operation of combining the two predictions, along with their associated variances, to best estimate the state of the system[78]. The Gaussian state equations we derived in chapter 3 do exactly this, and are an example of a continuous Kalman filter. Using these equations of motion, combined with a measurement record, the full system state can be continuously estimated. From an initial guess this type of information processing can quickly converge on both the mean position and momentum of the particle, whilst updating the expected error in the estimation.

We will consider the back-action dominated regime, where thermal heating due to the environment can be considered negligible. From the continuous measurement master equation (3.32),

$$d\langle x\rangle = \frac{1}{m}\langle p\rangle dt - 8\eta\kappa\, V_x \left(\langle x\rangle \,\mathrm{d}t + \mathrm{d}I\,(t)\right), \tag{4.5}$$

$$d\langle p\rangle = -m\omega^2\langle x\rangle dt - 8\eta\kappa\, V_x \left(\langle x\rangle \,\mathrm{d}t + \mathrm{d}I\,(t)\right), \tag{4.6}$$

$$\partial_t V_x = \frac{2}{m} C_{xp} - 8\eta\kappa\, V_x^2, \tag{4.7}$$

$$\partial_t V_p = -2m\omega^2 C_{xp} + 2\hbar^2\,\kappa - 8\eta\kappa\, C_{xp}^2, \tag{4.8}$$

$$\partial_t C_{xp} = \frac{1}{m}\, V_p - m\omega^2 V_x - 8\eta\kappa\, V_x\, C_{xp}. \tag{4.9}$$

where V_x and V_p are the position and momentum variances, and $C_{xp} = (1/2)\langle [x,p]_+\rangle - \langle x\rangle\langle p\rangle$ is the symmetrised covariance. We have written the stochastic increments dW in terms of the measurement record dI, and the equations can be solved to estimate the particle's full motional state. The integration would need to be carried out in real time with time-steps δt much shorter than the damping timescale e.g. $\delta t \ll 1/x_0^2\kappa$. In principle, the

state could be estimated by integrating the full SME using the measurement results, but in practice this is too complex to compute in real time. The particle's motion is expected to look thermal when cooling starts and this provides a good guess for the particle's initial state variances. The measurement process itself also drives any state towards looking Gaussian, ensuring the continued reliability of these state equations. These equations are also exactly equivalent to Kalman equations for a noisy classical system, which we could see by enforcing a diffusion term proportional to the rate of information gain in (3.5), to simulate quantum back-action.

The effectiveness of estimating the state of a levitated particle over a single oscillation cycle is illustrated in Fig. 4.1(a), for a general position measurement. The true state is numerically modelled using the Gaussian moment equations (4.5 - 4.9), with an initial temperature of $1\mu K$, which might be realistically achieved with classical feedback damping. The stochastic measurement record (4.4) is also numerically generated based on the the current true state. To simulate the evolution of a pure quantum state with an imperfect measurement, we split the measurement across two channels,

$$d\rho = 2\kappa\mathcal{D}[x]\rho\,\mathrm{d}t + \sqrt{2\kappa\eta}\,\mathcal{H}[x]\rho\,\mathrm{d}W_0 + \sqrt{2\kappa(1-\eta)}\,\mathcal{H}[x]\rho\,\mathrm{d}W_1\,, \tag{4.10}$$

where $\mathrm{d}W_0$ and $\mathrm{d}W_1$ are distinct Wiener increments. The simulated measurement record has access to only one channel,

$$dI = \langle x\rangle\,\mathrm{d}t + \frac{\mathrm{d}W_0}{\sqrt{8\eta\kappa}}. \tag{4.11}$$

This measurement record is then used to update a second set of the same Gaussian moment equations to simulate the state estimation procedure. The state estimate is initiated with thermal variances, where as the true state is modelled as a coherent state with thermal energy. The estimator quickly converges on the true state of the system, until reaching the resolution limit set by the measurement strength and quantum efficiency. This full state model confirms the rough resolution limit (3.42). Quantum efficiency $\eta = 0.02$ was chosen

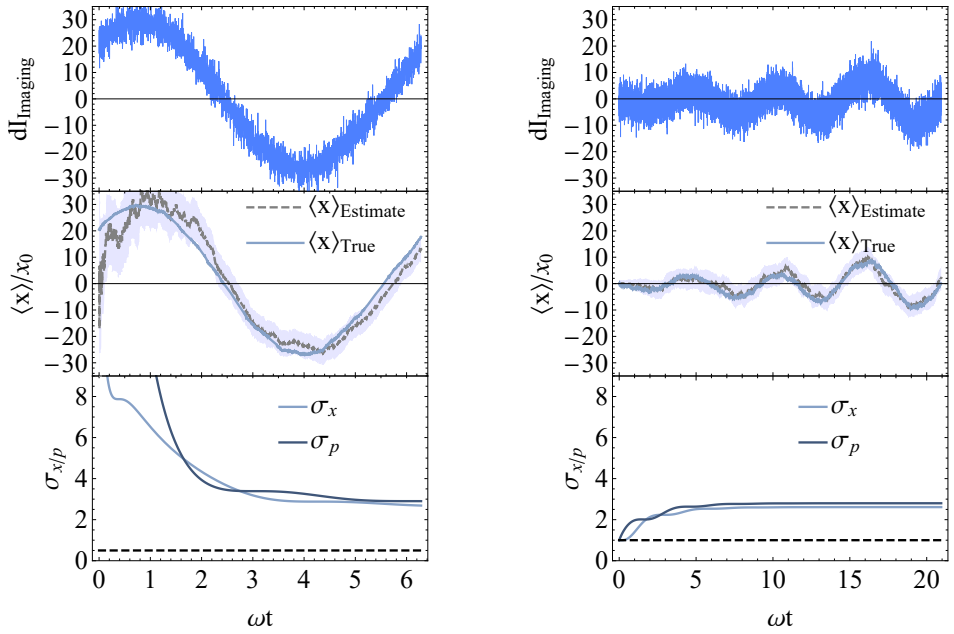

Figure 4.1: (a) Simulation of a trapped particle undergoing measurement, using (4.5-4.9). The normalised measurement strength, $\kappa x_0^2/\omega = 1$, with 2% quantum efficiency, and an initial particle energy corresponding to a temperature of $T = 1\mu K$. The top figure shows a numerically generated example of a position measurement and the middle figure shows the results of continuous state estimation using the same signal. The estimated mean position plotted beside the true value, and the shaded region covers 2 standard deviations in the estimate. The bottom figure shows the improvement in the standard deviation in both position (light line) and momentum (dark line) due to the measurement. The dashed line here indicates the width of the motional ground state.

(b) Simulation of particle heating due to measurement over several oscillation cycles, using (4.5-4.9). The normalised measurement strength, $\kappa x_0^2/\omega = 1$, with 2% quantum efficiency. The particle is initially in its ground state with temperature $T = 0K$.

for the figure to show more pronounced lag in the estimator following the true quantum state.

The Gaussian state equations can also be used to illustrate the heating effects due to the measurement itself Fig. 4.1(b). For the considered measurement strengths this is more easily visible with a state initially prepared at $T = 0K$. Without any other sources of environmental heating, the measurement will add energy into the system. The particle's temperature increases more quickly with more intense illumination, and presents a trade off when trying to achieve a better resolution.

Full state estimation could be implemented from room temperature but is not initially necessary. If the particle can be confined and stably cooled to micro-Kelvin temperatures it makes sense to switch to full state estimation when attempting to effectively over-damp the particle the rest of the way towards its quantum ground state. At higher temperatures damping using the effective derivative of the position measurement via a more simple band-pass filter should be sufficient.

4.1.2 Feedback damping

In chapter 2 we described two well established approaches to applying feedback that take into account the effects of quantum noise; direct feedback of a force proportional to the measurement signal[79], and feedback based on real time state estimation[76]. It is important to consider how the feedback is implemented in order to correctly account for how the noise in the measurement and in the system will be correlated. In the limit of instantaneous feedback, shot noise can be reintroduced from the measurement that directly correlates and interferes with the quantum noise driving the system evolution. Indirect feedback always filters out this noise in an intermediate step. In chapter 3 we considered possible direct feedback schemes, but found these techniques require cooling over at least hundreds of oscillation cycles, which is not feasible in low frequency traps. In contrast we find that with indirect feedback using a state estimate, the low trap frequencies will

in fact be beneficial. The optimal feedback strategy can be determined using classical control theory. In a classical system there would not be noise fundamentally linked to the measurement strength, but this can be artificially enforced. This is useful because it allows well developed control methods to be adapted for cooling[43, 44, 45]. Our sketch of the idea follows closely the work in Ref. [76].

For this system it turns out not to be optimal to include the estimated state variances in the feedback function. They will be necessary to continuously solve for the mean position and momentum but the feedback will not directly involve the variance values. The feedback Hamiltonian should simply be some linear function of the momentum and position operators scaled by functions of the estimated first order moments,

$$H_f = f(\langle x\rangle, \langle p\rangle)x + g(\langle x\rangle, \langle p\rangle)p. \tag{4.12}$$

To find the appropriate form of the functions f and g we can define a cost function for the parameter we want to minimise, in this case the energy,

$$C = \int_0^t \left[Tr(\mathbf{x}^T P \mathbf{x}\rho) + q^2 \mathbf{u}^T Q \mathbf{u}\right]. \tag{4.13}$$

Here $\mathbf{x} = \{x, p\}$ is the state vector, and $\mathbf{u} = -K\langle \mathbf{x}\rangle$ is the feedback vector we want to introduce in the dynamical equations for the mean moments (4.5,4.6); the optimal form of the matrix K is what needs to be determined. The matrices P and Q are chosen so that the cost function represents the system energy,

$$P = Q = \begin{pmatrix} m\omega^2 & 0 \\ 0 & 1/m \end{pmatrix}. \tag{4.14}$$

The matrix Q can be interpreted as accounting for an energy cost associated with the feedback. Including it in this way reflects a restriction on the magnitude of the feedback weighted by the parameter q, which will work out to be inversely proportional to the system damping rate.

Optimal feedback should attempt to localise both position and momentum simultaneously. To achieve this, the Hamiltonian should be of the form

$$H_f = \Gamma_0\big(\langle p\rangle x + \langle x\rangle p\big), \tag{4.15}$$

where we define $\Gamma_0 = 1/q$ to be the system damping rate, and the parameter q can be interpreted as a bound on the feedback response time. This accounts for the physical limitations of the feedback mechanism, and places an upper bound on the optimal damping rate. For an infinitely broadband signal $q \to 0$, and the damping rate could be arbitrarily high. With feedback, the new equations for the damped position and momentum are

$$d\langle x\rangle = \frac{1}{m}\langle p\rangle dt + \sqrt{8\eta\kappa}\, V_x\, dW - \Gamma_0\langle x\rangle, \tag{4.16}$$

$$d\langle p\rangle = -m\omega^2\langle x\rangle dt + \sqrt{8\eta\kappa}\, C_{xp}\, dW - \Gamma_0\langle p\rangle. \tag{4.17}$$

We have previously considered directly damping the particle's velocity, and know a position term in the Hamiltonian can be introduced simply by using an externally applied force. When damping over many oscillation cycles this also damps the position variance. To directly damp the position, however, requires a momentum term in the Hamiltonian.

One option to introduce this is with a time dependent shift in the origin of the position coordinates, which in the rest frame of the trap manifests itself as a shift to the canonical momentum. The harmonic trap could be displaced mechanically or by applying additional fields. If the trap origin is shifted at a rate v, such that the displacement of the trap $s(t) = \int v\, dt$, then

$$H' = \frac{m\dot{x}'^2}{2} + \frac{m\omega^2\big(x' + s(t)\big)^2}{2}, \tag{4.18}$$

where we have defined H' to be the Hamiltonian in the lab frame. If we instead shift coordinates to a frame of reference moving with the trap $x = x' - s(t)$, with the canonical momentum $p = m(\dot{x} + v)$, the displacement manifests as a momentum term in the

Hamiltonian,

$$H' \to H = \frac{p^2}{2m} + \frac{m\omega^2 x^2}{2} - vp. \tag{4.19}$$

Identifying $v = \Gamma_0\langle x\rangle$ produces the desired position damping. Momentum damping could then also then be implemented with respect to the trap frame coordinates,

$$H = \frac{p^2}{2m} + \frac{m\omega^2 x^2}{2} - \Gamma_0\langle x\rangle p - \Gamma_0\langle p\rangle x, \tag{4.20}$$

where the estimates of $\langle x\rangle$ and $\langle p\rangle$ are obtained by solving the state estimator equations (4.16,4.17) using the position measurement I shifted to the trap frame, eg. $I \to \big(I - s(t)\big) = \big(\langle x'\rangle - s(t)\big) + \xi(t)/\sqrt{8\kappa\eta}$.

This produces optimal damping in the rest frame of the trap. Transformed back to the lab frame, with the momentum defined as $p' = m\dot{x}'$, the Hamiltonian now reads

$$\begin{aligned} H' &= \frac{p'^2}{2m} + \frac{m\omega^2\big(x' - s(t)\big)^2}{2} - \Gamma_0\langle p\rangle\big(x' - s(t)\big) \\ &= \frac{p'^2}{2m} + \frac{m\omega^2 x'^2}{2} - m\omega^2 s(t)x' - \Gamma_0\langle p\rangle x'. \end{aligned} \tag{4.21}$$

The shifts made to the trap centre would have to be small, given the measurement's sensitivity to where the particle sits in the standing wave field, but a piezoelectric device could be used to shake the trap in a controlled manner to achieve damping.

In this system the introduction of linear feedback has no effect on the estimated variances conditioned on the measurement record. Their dynamics are governed by the measurement alone and we can therefore find the steady state values for our feedback controlled state from the original equations for the Gaussian moments (4.7,4.8,4.9),

$$\tilde{V}_x = \frac{2m\omega}{\hbar} V_x = \left(\frac{2}{\eta}\frac{1}{\xi^{1/2}+1}\right)^{1/2}, \tag{4.22}$$

$$\tilde{V}_p = \frac{2}{\hbar m\omega} V_p = \left(\frac{2}{\eta}\frac{\xi}{\xi^{1/2}+1}\right)^{1/2}, \tag{4.23}$$

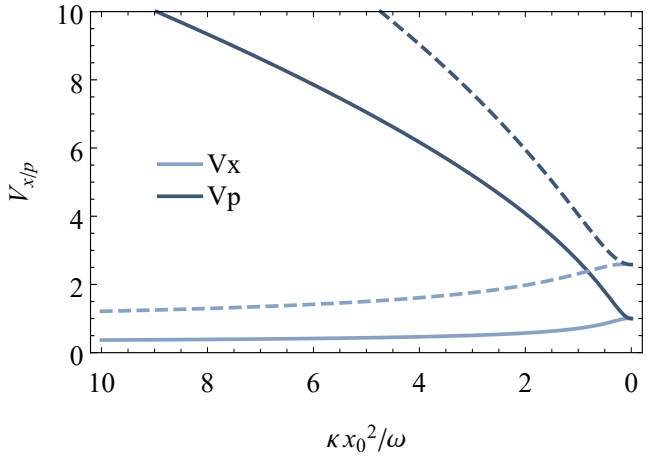

Figure 4.2: Final resolution of the normalised position (light line) and momentum (dark line) variances of trapped particle, from the steady state solutions of a Guassian estimator (4.22,4.23). Variance values less than 1 are squeezed compared to the harmonic oscillator ground state. The solid lines correspond to a measurement with perfect efficiency $\eta = 1$ and the dashed lines $\eta = 0.15$, these values and the measurement strength would vary depending on the nature of the measurement.

where $\xi = 1 + 16\eta\,(\kappa x_0^2/\omega)^2$. These normalised variances are equal to one for a minimum uncertainty state. This is the case for unit efficiency and when the parameter $\xi \to 1$, which in turn is the case when the measurement strength $\kappa \to 0$. Relative to the trap frequency in optical traps, κ is usually very small, but with a strong measurement $\kappa x_0^2 > \omega$, the steady state position variance is noticeably squeezed compared to the harmonic oscillator's natural ground state. Fig 4.2 shows how the conditional variances vary for the range of measurement strengths accessible in low frequency magnetic traps.

The estimated variances are the best that could be resolved with a given measurement. We can then average over the measurement record to account for the excess variance due to the particle's motion. The applied feedback should limit this as much as possible, keeping the mean position and momentum values centred on zero. Using the equations for the mean position and momentum (4.16,4.17), and following the rules of Ito calculus, we can

calculate the excess variances, which we have distinguished with a superscript 'E',

$$\partial_t \tilde{V}_x^E = -2\Gamma_0 \tilde{V}_x^E + 2\omega \tilde{C}_{xp}^E + \frac{2\omega}{\chi}\tilde{V}_x^2, \tag{4.24}$$

$$\partial_t \tilde{V}_p^E = -2\Gamma_0 \tilde{V}_p^E - 2\omega \tilde{C}_{xp}^E + \frac{2\omega}{\chi}\tilde{C}_{xp}^2, \tag{4.25}$$

$$\partial_t \tilde{C}_{xp}^E = -2\Gamma_0 \tilde{C}_{xp}^E - \omega\big(\tilde{V}_x^E - \tilde{V}_p^E\big) + \frac{2\omega}{\chi}\tilde{V}_x \tilde{C}_{xp}. \tag{4.26}$$

The final state is always improved with stronger damping which effectively counteracts the measurement shot noise, as well as removing the initial thermal energy. The return for increasing Γ_0 quickly drops off, and for moderate damping rates $\Gamma_0 > \omega$ the steady state variances approach the ideal limits given by the measurement resolution. This is reassuring since physically there would certainly be a bound to the feedback response time. Fig 4.3 shows a simulation of the feedback procedure for experimentally reasonable parameters $\eta = 0.15$, $\kappa x_0^2/\omega = 1$, $\Gamma_0/\omega = 10$, $T_{\text{initial}} = 1\mu K$. The state is again modelled as a coherent state with thermal energy and feedback is applied based on a numerically simulated state estimator. The particle's motion is almost completely damped after a single oscialltion cycle and the excess variance in the mean position is highlighted, $\tilde{V}_x^E \sim 0.1$. The remaining motion is small compared to the fundamental resolution limit due to the photon shot noise.

From the steady state expressions we can also find the purity of the final state[80],

$$Tr(\rho^2) = (\hbar/2)(V_x V_p - C_{xp}^2)^{-1/2}. \tag{4.27}$$

If the damping is strong, the steady state value is approximately that of a conditional state without any excess. With perfect detection the final measured state looks pure, and becomes increasingly mixed as the efficiency drops,

$$P_c = Tr(\rho_c^2) = \sqrt{\eta}. \tag{4.28}$$

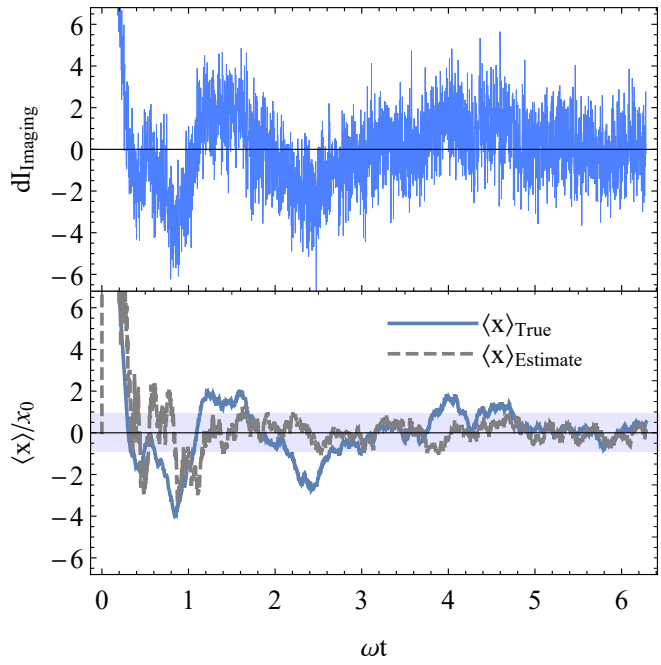

Figure 4.3: Simulation of a damped levitated particle, using (4.7,4.8,4.9,4.16,4.17). The normalised measurement strength, $\kappa x_0^2/\omega = 1$, with 15% quantum efficiency, and the initial particle energy corresponds to a temperature of $T = 1\mu K$. The top figure shows a numerically generated example of a position measurement. The bottom figure shows the evolution of the mean position of the true state alongside the estimated position from the measurement record. The estimated position is almost completely damped relative to the fundamental shot noise in the original measurement signal. The shaded region corresponds to the standard deviation of the true motion from $t = \pi/2 \to 2\pi$ and matches the estimated variance (4.22).

To reach the lowest temperatures, κ would ideally be kept as low as possible to avoid squeezing due to the measurement. There is a balance then between resolving the particle fast enough to outpace environmental heating, and wanting a weak probe to minimise squeezing. Notably however, state purity has no dependence on the measurement strength, suggesting that the squeezed states with higher energy could reasonably be expected to have quantum properties which are just as visible.

The final average phonon number can be calculated using the combined conditional vari-

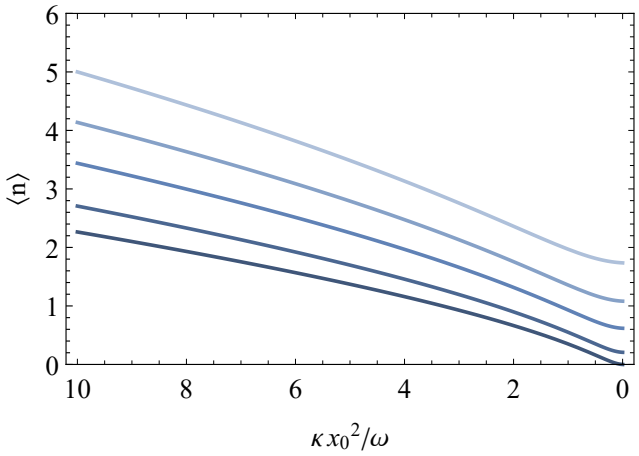

Figure 4.4: Average steady state phonon occupancy of a trapped nano-particle after undergoing active feedback, calculated using the equations for a damped Gaussian state with excess noise (4.29). The effective damping rate (feedback gain) was chosen to be $\Gamma_0/\omega = 10$, strong enough to remove almost all stochastic drift due to the measurement disturbance. The quantum efficiencies from the top line down are, $\eta = 0.05, 0.1, 0.2, 0.5, 1$. The final occupancies range from $\langle n \rangle < 3$, for currently feasible experimental parameters ($\eta = 0.15, \kappa x_0^2/\omega = 1$), and approach zero with perfect collection efficiency and a weaker measurement.

ances based on a particular measurement, and the excess variance seen when averaging over trajectories,

$$\langle n \rangle = \frac{\langle \tilde{x}^2 \rangle}{4} + \frac{\langle \tilde{p}^2 \rangle}{4} - \frac{1}{2}. \tag{4.29}$$

Steady state phonon occupancy, calculated with (4.29), is shown in Fig 4.4, for a range of measurement strengths and quantum efficiencies. These are the expected values that would be observed after damping, taking into account the estimated variance in the measurement signal (4.22,4.23), and the excess variance associated with the remaining particle motion (4.24-4.26).

4.1.3 Summary of proposed methods

We have analysed processes for state estimation and feedback cooling of a low-frequency, magnetically levitated nano-particle. Having considered several options for tracking a particle's position and momentum, we suggest making measurements in two steps. At first, scattered light from the particle can be imaged with a quadrant photo-diode, and an externally applied damping force can be used for cooling. After damping the particle's motion to sub-optical-wavelength amplitudes, significantly better resolution can be achieved by measuring how the particle scatters light into the mode of an adjacent single mirror. This should be relatively simple to integrate into current experiments, and would allow for a high degree of variation in the measurement strength which would be primarily dependent on the intensity of the probe beam. The need to damp both the particle momentum and position independently is likely to be the largest experimental difficulty after achieving sufficient isolation from environmental heating. The unique nature of the static magnets that make up these traps may make it possible to control the particle by dynamically shifting the trap centre, and alternate methods using a sequence of strong controlled laser pulses are also possible. With advances in isolation from environmental heating, and improvements in light collection efficiency, there are no fundamental limits to these techniques being used to reach the quantum motional ground state.

We suggest that measurement efficiency comparable to or greater than that achievable in ion traps, $\eta = 0.15$, could realistically be reached in an experiment. Optimal feedback via state estimation with this level of efficiency could produce states competitively near the quantum ground state with some additional degree of squeezing, $\langle n \rangle < 3$, with purity $P \approx 0.44$, in only a few oscillation periods. In current experiments there are many factors to consider in order to extend the system reheating time, which will be the main barrier to achieving lower temperatures as it prevents the use of a less disruptive measurement probe. As these values improve, and with the possibility of highly directional scattering for better collection efficiency, it may soon be feasible to reach below single phonon occu-

pancy using the methods we have outlined. Most related experiments have so far assessed success based on a temperature associated with the measured motional power spectrum. Alternatively, there are recent proposals for distinguishing quantum motion via dynamical model selection using solely position measurements[81]. They look to identify quantum statistics from a series of position measurements after introducing a small perturbation to the trapping potential. The distinguishability is closely related to state purity, which should be safely within reach of the proposed cooling methods.

All of the methods discussed are applicable to sub-micron sized Rayleigh scatterers that can be effectively treated as point dipoles. High quality nano-diamonds of this size have been produced for exactly the purpose of trapping and cooling[82]. These diamonds are of interest due to access to internal nitrogen-vacancies (NV). This second quantum handle on the particle is crucial for many proposed future experiments[58, 60] and may also provide a route to having fine control over micron, as opposed to nanometer, sized particles. The sub-wavelength measurements we have suggested could be applied to microscopic diamonds, by tracking the position of point-like NV impurities within them. Additionally, strong coupling between an NV spin and the mechanical oscillation of a nano-diamond can be engineered using a strong magnetic field gradient. There are proposals for generating low number Fock states and possible spatial superposition states, by manipulating a Jaynes-Cummings type interaction Hamiltonian, in states prepared near the quantum ground state[58].

In the following section we discuss other possible uses for cooled levitated particles. Rather than attempting to prepare the ground state of the harmonic potential, it may be feasible to produce minimum uncertainty position states effectively in free space. Our proposed cooling strategy aims to work in a regime where thermal reheating is comparable to low magnetic trap frequencies. Alternatively, these particles may be ideally suited to measure with a series of strong pulses, and then observe free evolution over timescales much shorter than the trap period. There are theories of measurement collapse that predict there should be visible diffusion in this regime beyond what would be expected simply due to the

standard quantum limit of measurement precision.

4.2 Tests of quantum collapse models

Due to the practical challenges of cooling, there has been interest in creating non-classical states of levitated nanoscopic particles without first preparing the harmonic ground state. Our proposed cooling methodology for low frequency traps looked to improve detection efficiency and damp a particle's motion on a timescale of less than an oscillation period. However, previously we limited ourselves to considering only moderately strong measurements since anything more powerful produced squeezed states further from the trap ground state. We now consider this regime, where it may be possible to observe quantum behaviour in what is essentially a quasi-free particle. What can be done with a free quantum particle is distinctly different to the possibilities with a cooled harmonic oscillator, but both systems have the potential to be used to probe exciting new physics.

The team of Dr. Brian D'Urso at the University of Montana have proposed using a sequence of pulsed measurements that reach the standard quantum limit (SQL) of precision. This is appealing since it relies on changing the measurement process rather than the trap itself and can be explored in tandem to improving cooling. Particles can already be trapped and isolated such that the reheating rate is much slower than the operational speed of the optics used for measurement. The fact that the optics are separate from the trapping potential, means that the duration and intensity of pulses can be freely varied, and the detection efficiency has the potential to be very high. Even if the motion of the particle is still classical over long timescales, sub-millisecond pulses could be used to observe quantum limited behaviour. Pulsed measurements schemes on timescales shorter than the mechanical period have been proposed for realising quantum state tomography and squeezing of massive mechanical oscillators[83]. With high measurement strengths we expect to produce squeezed states of the harmonic trap, which over short times can be considered free particles at the SQL. With the ability to prepare such states, there

are proposals for tests of wavefunction collapse models[84, 85, 86]. In particular, there is interest in using levitated particles to place limits on the parameters in these models[87].

Wavefucntion collapse models modify Schrödinger's equation so that superposition states naturally evolve towards being in one particular state over time. This modification is an attempt to resolve the measurement problem in quantum mechanics, where in the Copenhagen interpretation collapse is brought about by an ill-defined measurement event. Importantly for this proposal, collapse models have experimentally testable differences from standard quantum theory. Currently, the most well-developed of these models is Continuous Spontaneous Localization (CSL)[88, 89], which introduces a background fluctuating field that causes collapse through interacting with particles. Through this mechanism, wavefunction collapse effectively occurs randomly, and can happen at any time. In order to preserve the usual Heisenberg uncertainty limits, the field must also impart momentum to the particle. This is very similar to the back-action that arises in continuous measurement theory. Crucially CSL predicts diffusion of particle's motion without interaction with its environment. This effect is very small, but scales with the system size. Every individual quantum particle is proposed to interact with this new field, but wavefunction collapse due to the interaction is only expected over astronomical time periods. However, collapse of one particle in an ensemble, would result in the collapse of everything entangled with it. Only in huge ensembles of fundamental particles does collapse become likely over appreciable timescales. This mechanism aims to explain the discrepancy between classical and quantum physics. Experiments with massive levitated particles are ideally suited for testing this theory. Specifically, the extra diffusion predicted by CSL should visibly prevent measurements at the SQL.

4.2.1 Standard quantum limit

The standard quantum limit of measurement precision can be understood as a balance between achievable resolution and associated back-action. A simple and relevant example

is the case of 2 successive measurements of a free particle, where we try to minimise the final spread in the particle's position. We consider that after some initial measurement at $t = 0$ the particle's position and momentum are known to within some level of certainty,

$$x(0) \pm \Delta x(0) \quad , \quad p(0) \pm \Delta p(0), \tag{4.30}$$

where $\Delta x(0)$, $\Delta p(0)$ are the standard deviations in the position and momentum. In an ideal setup the particle will be in a minimum uncertainty state $\Delta x \Delta p = \hbar/2$. The second measurement takes place after some time τ, during which the particle undergoes free evolution. In this time, the initial uncertainty in the particle's state will propagate, and this will dictate the final state variance,

$$\Delta x(\tau)^2 = \Delta x(0)^2 + \Delta x_{add}(\tau)^2 + \Delta x_{measure}(\tau)^2. \tag{4.31}$$

We have expressed the uncertainty in the final state position as a sum of the squares of the contributing factors. The first term corresponds to the uncertainty in the initial state position, where as the second term corresponds to the additional propagation of the momentum uncertainty,

$$\Delta x_{add}(\tau) = \frac{\Delta p(0)\tau}{m} \geq \frac{\hbar\tau}{2m\Delta x(0)}. \tag{4.32}$$

The final term in (4.31) corresponds to the uncertainty in the second measurement. In considering the ideal limit of possible precision, we assume that this measurement has effectively no associated uncertainty $\Delta x_{measure}(\tau) = 0$. This is justifiable since the second measurement can be made arbitrarily strong, as it no longer matters if the momentum uncertainty is squeezed. In this case, we can see that the final state variance depends on the initial position resolution and the propagation error due to not knowing the particle's true velocity. To minimise $\Delta x(\tau)$ for a given τ, we can optimise $\Delta x(0)$,

$$\frac{\mathrm{d}(\Delta x(\tau)^2)}{\mathrm{d}(\Delta x(0)^2)} = 0 \quad \rightarrow \quad \Delta x(0) = \sqrt{\frac{\hbar\tau}{2m}}. \tag{4.33}$$

Substituting this into (4.31) gives

$$\Delta x(\tau)_{SQL} = \sqrt{\frac{\hbar\tau}{m}}. \tag{4.34}$$

This result shows the minimum possible deviation in a particle's expected position after a period of free evolution. The limit is rooted in the uncertainty relation, and can be physically interpreted using the state estimation equations (4.7 - 4.9). There is a compromise between position resolution, where measurement shot-noise is minimised with a high κ, and the associated back-action, where the momentum disturbance is minimised with a low κ. Notably, there is not an associated limitation with every state variable. In this example, if the momentum was measured with arbitrary precision at $t = 0$, it would still be known exactly at a later point τ, as it is uninfluenced by uncertainty in the particle's position. For a free particle, the momentum is known as a quantum non-demolition (QND) variable.

The growth of Δx_{SQL} is a special case for an optimal initial state, but in general the position variance (4.31) grows as τ^2, due the momentum uncertainty propagation. If we consider again the case of the state estimation equations (4.7 - 4.9), with zero detection efficiency $\eta = 0$,

$$\Delta x(\tau)^2 = \Delta x(0)^2 + \left(\frac{\Delta p(0)^2}{m^2}\right)\tau^2 + \left(\frac{\hbar^2\kappa}{3m^2}\right)\tau^3. \tag{4.35}$$

We can see that particle spread grows as τ^3, due to the continuous measurement back-action. This cubic growth term is the key to testing CSL. Diffusion processes usually have an associated damping term which leads to a linear growth in the position variance over long times, as would be the case for a Brownian particle (3.1). Cubic growth is a signature of diffusion due to a driving noise without damping. In deriving a diffusive state equation (2.75), we invoked projective measurements of an apparatus coupled to the system, which introduced noise proportional to the coupling strength. In the framework of CSL, the reason that the apparatus is repeatedly being projected onto a specific state, is due to

the intrinsic stochastic collapse of one of its constituent particles. The apparatus is a large ensemble of particles, and so undergoes collapse often, and in turn causes partial collapse of the coupled system. This gives rise to the same back-action term as in (4.35). In contrast however, the CSL theory also predicts that the same intrinsic collapse process happens in the system alone, which carries with it a similar diffusion term [87],

$$\Delta x(\tau)_{CSL} = \frac{\hbar}{m_N r_C}\sqrt{\frac{\lambda\tau^3}{6}}, \tag{4.36}$$

where m_N is the mass of an atomic nucleon, r_C is a correlation length for the noise field which causes collapse, and λ is the coupling rate between the system and the field. More specifically an isolated nucleon, in a superposition of two localized states separated by a distance greater than r_C, is expected to collapse to one of those states on a timescale of λ^{-1}. Since collapse narrows the wavefunction, the particle gains energy, and the CSL model predicts diffusion at a rate (4.36). This expression is true for particles with diameter $< r_C$, and we will consider a possible value of $r_C = 1\mu m$. There is a range of values for r_C and λ over which the theory might be viable. Past experiments have already been used to put bounds on these parameters [90], and the aim of this proposal is to test an extended range of values for the coupling strength. The unexplored CSL parameter regime is still large, and for $r_C = 1\mu m$, the possible values for the coupling rate span over several orders of magnitude. Free particle tests of CSL induced diffusion are of interest because of their long lifetime compared to other nano-mechanical systems. Since diffusion due to CSL grows faster than the bound of the SQL, over long periods of diffusion, free particle experiments have the potential to probe far deeper into the unexplored parameter regime. Figure 4.5 shows the point where diffusion due to continuous spontaneous localisation is predicted to be greater than what is visible due to the SQL. For the current upper bound $\lambda \approx 10^{-11}s^{-1}$, this cross over occurs $\tau \approx 3ms$ for a free particle with mass $m = 1.5pg$. If an experiment measures diffusion as predicted by standard quantum mechanics after this time, then the CSL parameters must be lower. It has been proposed that in vacuum at cryogenic temperatures, that massive levitated particles could test a large scope of the

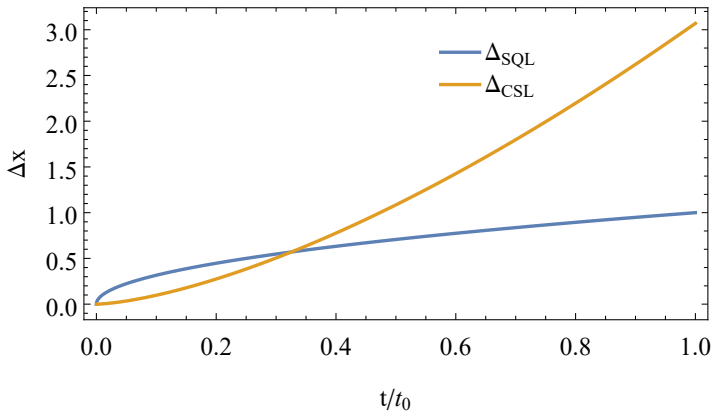

Figure 4.5: Expected diffusion of a free particle, due to measurements performed at the standard quantum limit, shown in blue, and due to continuous spontaneous localisation, shown in yellow. These curves correspond to values of $\lambda = 10^{-11}s^{-1}$, $r_C = 1\mu m$, and mass $m = 1.5pg$ using equations (4.34, 4.36). The x-axis shows time in units of $t_0 = 10^{-2}s$ and the y-axis shows the normalised position deviation in units $x_0 = \sqrt{\hbar t_0/m}$. A crossover occurs $t \approx 3ms$, at which point measuring diffusion at the SQL definitively reduces the possible value of the CSL coupling strength λ.

CSL model [86].

4.2.2 Simulating measurements of diffusion

The proposed experiment is simple in nature. Trapped particles are already accessible with long reheating times that could plausibly reach $1/\Gamma_{th} < \tau = 3ms$, which would give access to the regime needed to test for CSL diffusion. However, measurements at exactly the SQL are not possible without perfect measurement efficiency, and preparing idealised minimum uncertainty states is non-trivial using position measurements alone. As such, we use Guassian estimator equations to predict realistic measurable values, and at what point bounds could be placed on CSL parameters. Since we expect greater uncertainty in real measurements, we consider a time period $\tau = 30ms$, which would push particles in current magnetic traps $\omega = 2\pi \times 7Hz$, to the edge of the free-particle limit. In an initial model this can be circumvented by setting $\omega = 0$. More practically, the experiment lends

itself to a post-selection process, where particles seen to be at the edge of the trap or with high thermal velocities could be removed from the final data-sets. This is necessary since particle's that see significant influence of the trap potential would be expected to have suppressed diffusion.

As when modelling our proposed cooling procedure, we used the Gaussian estimator equations (4.5 - 4.9) to emulate a thermal state, this time of a free particle $\omega = 0$. Higher detection efficiency is expected in experiments by integrating light scattered from short pulses off the particle. We emulate this procedure by integrating the continuous measurement record (4.4) over a short pulse window δt_p,

$$x_{measure}(t) = \left(\int_{-\delta t_p/2}^{\delta t_p/2} dI(t) \right) \delta t_p^{-1}. \tag{4.37}$$

These numerically simulated values represent the experimentally accessible measurement. We simulate two initial short pulses to estimate the particle's starting position and momentum, and then allow for a period of free evolution before sampling the particle's final position. Over several trajectories we calculate the standard deviation in the particle's final position from its expected value, (4.31). This exactly mimics what could be measured in a physical experiment.

In more detail, we simulate the two initial position measurements at times t_A and t_B, which are then used to estimate the particle's momentum,

$$p(t_B) = m \frac{x(t_B) - x(t_A)}{\delta t_{AB}}, \tag{4.38}$$

where $\delta t_{AB} = t_B - t_A$. The values $\{x(t_B), p(t_B)\} \equiv \{x(0), p(0)\}$ are taken as the starting state values (4.30), which are in turn used to predict the final position,

$$x_{predict}(\tau) = x(0) + p(0)\tau. \tag{4.39}$$

These measurements have some level of associated uncertainty. With access to the full

measurement record and perfect detection efficiency $\eta = 1$, the uncertainty predicted would approach that of the true state $\Delta x_{true}(0), \Delta p_{true}(0)$. However, since we have simulated integrating the measurement signal with an efficiency $\eta < 1$, we can expect additional error in estimating the mean position,

$$\Delta x_{measure}(0) = |x_{true}(0) - x_{measure}(0)| > 0, \tag{4.40}$$

where x_{true} is the mean position of the simulated Guassian state. To minimise this difference and to prepare a range of starting states, we can vary the pulse power, duration δt_p, and spacing δt_{AB}. We can use our resolution estimate (3.42), to predict the necessary pulse duration and power to produce a state with a position variance (4.33),

$$\Delta x(0) \approx \sqrt{\frac{1}{8\delta_p \eta \kappa}} \equiv \sqrt{\frac{\hbar\tau}{2m}}. \tag{4.41}$$

Since there is a finite window for these measurements to take place, the pulse duration δ_p would ideally be short. It is expected to be reasonable to scatter μW of power off of a magnetically confined nano-particle without heating it out of the trap. The measurement strength can be related to this scattered power,

$$\kappa \approx \frac{P k_L^2}{\hbar \omega_L}, \tag{4.42}$$

where ω_L is the frequency of scattered light. Optimistically the measurement efficiency with directional scattering could reach $\eta \approx 0.3$. Using these values as guides, we choose $\delta_p = 0.5ms$. Likewise, the momentum uncertainty is expected to decrease with a larger interval δt_{AB} between the two pulses, which can be seen in the state estimation equations due to an increase in the position-momentum covariance. We find $\delta t_{AB} = 1ms$ is suitable to produce near minimum uncertainty states. We show the results of varying the measurement strength of the two pulses in Figure 4.6. We used the integrated measurement $x_{measure}(0)$, as an estimate of the particle's position at the middle of the second pulse. The standard deviation in the measurements from the true mean position, for each κ, was

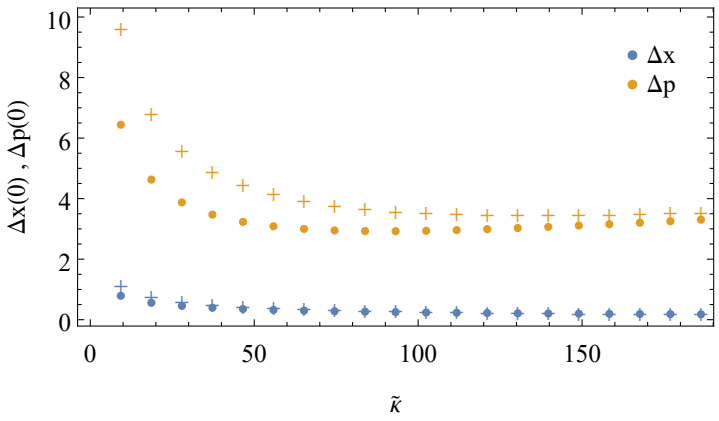

Figure 4.6: The uncertainty in a simulated measurement of position (blue) and momentum (yellow), of a free particle, is shown as a function of the normalised measurement strength $\tilde{\kappa} = \kappa x_0^2 t_0$. The measurement consists of two pulses, which directly measure the position and are used to estimate the momentum. The solid circles correspond to the 'true' or ideal quantum state uncertainty, where as the crosses include the uncertainty associated with imperfect measurement (4.40). The position and momentum uncertainty are shown in units $x_0 = (\hbar t_0/m)^{1/2}$, and $p_0 = (\hbar m/t_0)^{1/2}$ respectively.

calculated using 100 trajectories of a Gaussian state estimator. The range of κ corresponds to scattering powers from $0.01\mu W \rightarrow 0.2\mu W$. We find that increasing the pulse power, generally corresponds to producing a state with less total uncertainty. However, it is easier to look for an ideal measurement strength by considering the position variance in the final measurement. There is a small extra uncertainty due to estimating the particle's state at the centre of a pulse. The continued illumination means that during the second half of the pulse the particle experiences extra momentum diffusion, and this effect is worse for higher κ.

After the initial pulses, we simulate the free evolution of the particle with $\kappa = 0$. Initially we looked at the case where the particle freely evolves for the full remaining time, up to $t = 30ms$. As when we derived the standard quantum limit, we assume that the last measurement can be made with arbitrary precision by scattering large amounts of light $\kappa \rightarrow \infty$. In this case, the final measurement will deviate from the predicted value (4.39)

by

$$\begin{aligned}\Delta x(\tau)^2 &= \left\langle \left(x_{measure}(\tau) - x_{predict}(\tau)\right)^2 \right\rangle \\ &= \left\langle \left(x_{true}(\tau) - x_{predict}(\tau)\right)^2 \right\rangle + \Delta x_{true}(\tau)^2,\end{aligned} \tag{4.43}$$

where the angled brackets denote an ensemble average. The standard deviation in the final particle position can be found using many trajectories or experimental realisations. In our simulations, $\Delta x_{true}(\tau)$ is determined by the deterministic variance equations, equivalent to (4.31), and so doesn't vary over trajectories. The total deviation is the value needed for comparison against the diffusion predictions of CSL. Figure 4.7 shows how simulated diffusion measurements compare with what is predicted by (4.36), for the current highest possible value of $\lambda = 10^{-11}s^{-1}$, with $r_C = 1\mu m$. We find that after this period of free evolution, that an experiment should be able to measure diffusion less than that predicted by CSL. This would lower the possible bound on the coupling strength λ, since if CSL is true we would not expect to be able to make these measurements. We also find that for the specific pulse duration, the optimal scattered power corresponds to around $0.1\mu W$.

We can go on to use the optimal pulse power, found when allowing free evolution up to $t = 30ms$, and calculate $\Delta x(\tau)$ for shorter times τ. These results are shown in Figure 4.8. We can see that with the estimated efficiency of $\eta = 0.3$, improvements on the parameter bounds for CSL could be made with this setup after a free evolution of $\tau \approx 15ms$.

4.2.3 Outlook

In future iterations of this model it will be important to reintroduce the effect of the trapping potential. Over timescales comparable to the trap period, the diffusion in the particle's expected position due to initial measurement uncertainty or spontaneous collapse, would be suppressed compared to the free particle case presented. A more extensive analysis of the optimal pulse duration and generally the state preparation procedure, would also be useful. Although by design this experiment should operate in a regime where ther-

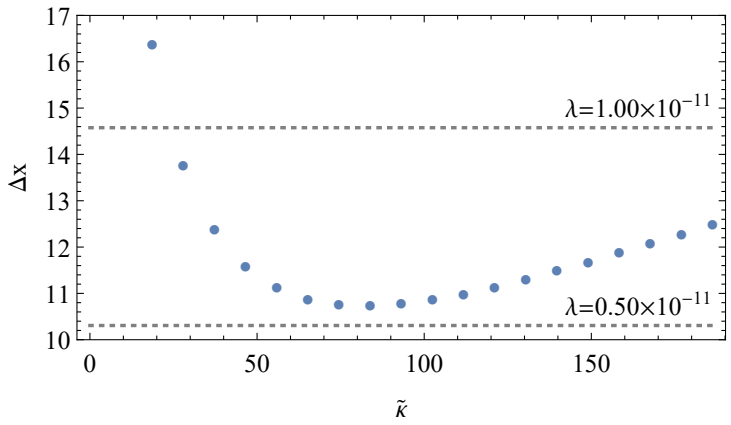

Figure 4.7: The average deviation of a simulated particle from its predicted trajectory after $\tau \approx 30ms$, shown as a function of the initial normalised measurement strength $\tilde{\kappa} = \kappa x_0^2 t_0$. An initial estimate of the state is made, and then the diffusion from a predicted trajectory was calculated over 100 trajectories. The plot markers correspond to the total average deviation of the particle, including its quantum state variance and measurement imprecision (4.43), in units of $x_0 = (\hbar t_0/m)^{1/2}$. The dashed lines correspond to the predicted diffusion by the CSL model (4.36) for the labeled coupling parameters λ.

mal heating is negligibly small, a more detailed calculation of exactly when this heating becomes an issue could be included. A quantum Brownian master equation[40] shares the same form as the ensemble averaged feedback damping equation (3.89). It could be used to account for the effects of weak thermal coupling which would adjust the observable limits on CSL.

To summarise the results presented in this section, we have explored the possibility of measuring the small amount of diffusion predicted by the continuous spontaneous localisation model. The uncertainty inherent in standard quantum mechanics predicts that this diffusion would be hidden by the standard quantum limit of measurement precision, but after a long enough period of free evolution, diffusion due to CSL is expected to become more prominent. Current experiments with magnetically levitated nanoparticles are already close to the regime where measurement precision could approach the SQL. With improvements in isolation and cryogenic cooling, it should then be feasible to wait long

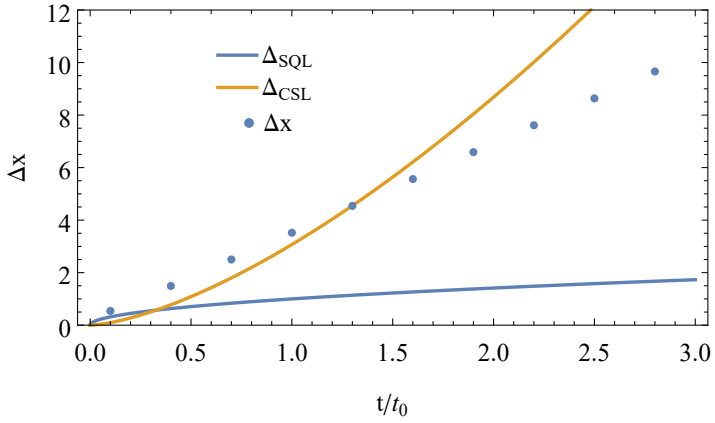

Figure 4.8: Expected diffusion of a free particle, due to the standard quantum limit (blue), and due to continuous spontaneous localisation (yellow), alongside simulated measurements of diffusion (blue markers). These curves correspond to values of $\lambda = 10^{-11}s^{-1}$, $r_C = 1\mu m$, and mass $m = 1.5pg$, using equations (4.34, 4.36). Time is shown in units of $t_0 = 10^{-2}s$ and the normalised position deviation in units $x_0 = \sqrt{\hbar t_0/m}$. The simulated diffusion measurements (4.43), fall below the predictions of the CSL model around $t = 15ms$.

enough to test for the diffusion predicted by CSL. We have modelled a realistic proposed measurement scheme and found in simulated results where bounds could be made on the CSL model parameters.

Overall, in this chapter we have looked at two ways of preparing quantum states of motion with magnetically levitated particles. We proposed a cooling procedure that could reach single phonon occupancy levels, with no fundamental limit to reaching the ground state. We also presented a detailed outline of how these systems might be prepared as free-particle minimum uncertainty states, useful for tests of quantum collapse models. Both of these procedures could be implemented in near-future experiments with improvements in isolation from classical heating sources. In the following chapter we continue to focus on methods of measurement and feedback in quantum systems, but applied to a many-body atomic ensemble.

5 Atomic spin ensembles

In this chapter the focus shifts to many-body systems, opening with an overview of spin squeezing in atomic ensembles. In a spin squeezed state many-body entanglement is engineered to reduce uncertainty in one component of the collective spin, allowing measurement precision beyond the so-called standard quantum limit. The research in this chapter is motivated by a proposed experiment that would have access to typically discarded measurement channels, when probing an atomic cloud in free space. An analysis of how these measurements can be used to stabilise noise to produce enhanced levels of spin squeezing is presented. The imaging system is modelled in detail and the effects of the proposed feedback procedure are also demonstrated in an analogous beam-splitter setup. The chapter ends with details of an ongoing investigation into techniques to produce a steady state of the feedback procedure that is useful for metrology.

5.1 Spin-squeezing in atomic ensembles

The previous chapters have focused on measurement and feedback with single particle systems. A similar treatment, using quantum trajectories and the quantum feedback formalism, can equally be applied to many-body systems[91], with the caveat that numerical simulations can quickly become resource-heavy as the number of particles increases. We will look at the preparation of spin-squeezed states in ensembles of atoms, a form of many-body entanglement[92].

In this context spin refers to the z-component of angular momentum of atoms, associated with two internal magnetic sub-levels. Such a two-level system, with density matrix elements $\rho_{ij} = |i\rangle\langle j| \ \ (i, j = 1, 2)$, can be treated as a pseudo spin one-half system where the spin operators are

$$j_x^{(n)} = \frac{1}{2}(\rho_{21}^{(n)} + \rho_{12}^{(n)}), \tag{5.1}$$

$$j_y^{(n)} = -\frac{i}{2}(\rho_{21}^{(n)} - \rho_{12}^{(n)}), \tag{5.2}$$

$$j_z^{(n)} = \frac{1}{2}(\rho_{22}^{(n)} - \rho_{11}^{(n)}), \tag{5.3}$$

and the superscript n labels each atom. The z-spin operator j_z measures the population difference of the atomic sub-levels, where as j_x and j_y provide information about the coherent superposition of the two states. The spin operators are also useful for visualising the state evolution using an enlarged Bloch sphere representation. The collective properties of the atoms can be described by a spin-J system[93], where $J = N/2$ in a system with N atoms. The collective spin operators are,

$$J_\alpha = \sum_{n=1}^{N} j_\alpha^{(n)}, \tag{5.4}$$

where $\alpha = x, y, z$. These operators obey the cyclic angular momentum algebra,

$$[J_x, J_y] = i\epsilon_{xyz} J_z, \tag{5.5}$$

where ϵ_{xys} is the Levi-Civita tensor.

In a coherent spin state (CSS), each individual spin system points in the same direction without any correlations between them. A CSS will have a minimum uncertainty relation. For example, if each spin is orientated along x, this is an eigenstate of the J_x operator with

$$(\Delta J_y)^2 (\Delta J_z)^2 = \frac{1}{4}|\langle J_x \rangle|^2, \tag{5.6}$$

where $(\Delta J_\alpha)^2 = \langle J_\alpha^2 \rangle - \langle J_\alpha \rangle^2$ is the standard deviation in the spin. A spin-squeezed state has a smaller uncertainty associated with one spin component than in a CSS. By engineering correlations between the atoms, fluctuations in one spin direction can be reduced at the expense of the other. There are different metrics that can be used to characterise

the degree of spin squeezing. Here we will use the parameter

$$\xi_z^2 = \frac{N(\Delta J_z)^2}{\langle J_x\rangle^2 + \langle J_y\rangle^2}, \tag{5.7}$$

which as written, measures squeezing in the z-spin component[94]. For a coherent spin state this squeezing parameter equals one, and if $\xi^2 < 1$ the state can be said to be spin squeezed. Theoretically, the lower bound on ξ^2 is of the order $1/N$, however current experiments are far from realising such maximally squeezed states. This parameter is designed to be used with Gaussian states. Later in this chapter we will also consider the Quantum Fisher Information as a useful metric for non-Gaussian squeezing.

There are applications for spin squeezing in quantum information[95] and in metrology[96]. In general, spin squeezed systems can outperform coherent states in the same manner as squeezed optical fields. For example, high precision timekeeping with atomic clocks relies on measuring the absorption frequency of an atomic transition to use as a frequency reference. This can be achieved using Ramsey spectroscopy[97], which relies on making measurements of the population difference J_z in an atomic ensemble after a period of free evolution. The precision of this measurement can be improved by initially preparing a spin squeezed state. There are several methods for producing squeezing, including engineering controlled collisions in a BEC via non-linear spin interactions[98], transferring non-classical light states onto atoms[99], and creating conditional squeezing by making QND measurements[100, 101]. We will be interested in the latter, where a suitably polarised probe beam can be used to make dispersive measurements of J_z whilst preserving the total atomic population[102].

5.2 Dispersive measurement model

We first outline a simple model of a dispersive measurement of the atomic population difference, including the imaging process and the effects of decoherence due to scattering light into different measurement channels. Following this, we will examine feedback of the

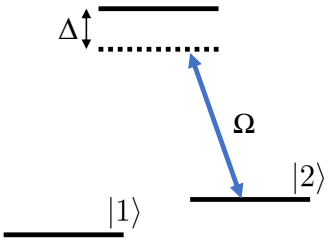

Figure 5.1: Sub-level diagram for a single atom. A far detuned probe field Ω measures the collective population in $|2\rangle$, and can be used to infer J_z.

measurement to stabilise drift in the mean spin direction so as to produce unconditional squeezing. We start by considering the dynamics of an ensemble of two-level atoms which we will assume can be prepared in an equal superposition of the two internal states. For consistency we will always assume the atoms are initially prepared in a CSS orientated along x, unless stated otherwise. Light with the appropriate polarization and frequency can then be used to probe a transition to an auxiliary level in these systems, effectively making a non-destructive measurement of the two-level state.

We can model the interaction with a far-detuned probe using the standard form of the optical Bloch equations. In the case where the probe interacts with the internal atomic level $|2\rangle$ and an auxiliary level which we will label $|3\rangle$ (illustrated in Fig. 5.1), the Hamiltonians for the atom and atom-field coupling in the rotating wave approximation are

$$H_A = \hbar\Delta \left|3\right\rangle\!\left\langle 3\right|, \tag{5.8}$$

$$H_{AF} = \frac{\hbar\Omega}{2}(\sigma^\dagger + \sigma), \tag{5.9}$$

where $\sigma = |2\rangle\langle 3|$. The master equation for this system, including a Lindblad term for

spontaneous emission into the electromagnetic vacuum at a rate Γ, is

$$\dot{\rho} = -\frac{i}{\hbar}\big[H_A + H_{AF}, \rho\big] + \Gamma\mathcal{D}[\sigma]\rho. \tag{5.10}$$

Written explicitly, the equations for the level occupancy and corresponding coherence terms are

$$\dot{\rho_{22}} = -\frac{i}{2}\Omega(\tilde{\rho_{32}} - \tilde{\rho_{23}}) + \Gamma\rho_{33}, \tag{5.11}$$

$$\dot{\rho_{33}} = \frac{i}{2}\Omega(\tilde{\rho_{32}} - \tilde{\rho_{23}}) - \Gamma\rho_{33}, \tag{5.12}$$

$$\dot{\rho_{23}} = -(\frac{\Gamma}{2} + i\Delta)\tilde{\rho_{23}} - \frac{i}{2}\Omega(\rho_{33} - \rho_{22}), \tag{5.13}$$

$$\dot{\rho_{32}} = -(\frac{\Gamma}{2} - i\Delta)\tilde{\rho_{32}} - \frac{i}{2}\Omega(\rho_{22} - \rho_{33}). \tag{5.14}$$

The steady state of ρ_{33} will be small in the case where the detuning is large, on the order of $(\Omega/\Delta)^2$ as opposed to (Ω/Δ) for the coherence terms ρ_{23} and ρ_{32}. We can therefore find approximate steady state solutions by neglecting terms proportional to ρ_{33}.

$$\lim_{t\to\infty}\rho_{23} \approx \frac{i}{2}\frac{\Omega\rho_{22}}{\Gamma/2 + i\Delta} \approx \frac{\Omega}{2\Delta}\rho_{22}. \tag{5.15}$$

If we assume that in this limit the atomic population is effectively split between the first two levels, $\rho_{11} + \rho_{22} = 1$, then using the definition (5.3) we can approximate

$$\sigma = \rho_{23} \approx \frac{\Omega}{2\Delta}(j_z + \frac{1}{2}). \tag{5.16}$$

We can now trace out the auxiliary level and write a master equation solely for the first and second atomic levels,

$$\dot{\rho} = \gamma\mathcal{D}[j_z]\rho. \tag{5.17}$$

where we have defined $\gamma = \Gamma\Omega^2/4\Delta^2$. In this limit we can also see by substituting (5.16)

into (5.11) that we recover the general form of the interaction for a single atom in the presence of a far detuned probe $\dot{\rho} = (-i/\hbar)[V, \rho]$ with the potential

$$V = \frac{\hbar\Omega^2}{4\Delta}(j_z - \frac{1}{2}). \tag{5.18}$$

If we want to include the spatial dependence of the field modes we can let $j_z \to j_z e^{-i\mathbf{k}.\mathbf{r}}$, where $\mathbf{k}$ is the scattered wave-vector and $\mathbf{r}$ is the fixed atomic position. For a single atom this extra phase does not affect the dynamics, but if we have many atoms the relative phases do matter. We can define a continuum of operators $b(\theta, \phi)$, that describe the combined field from N atoms,

$$b(\theta, \phi) = \sqrt{\gamma} \sum_{n=0}^{N-1} j_z^{(n)} e^{-i\mathbf{k}.\mathbf{r^{(n)}}}, \tag{5.19}$$

where $r^{(n)}$ is the position of the atom labelled n. In the master equation we can then include an integral over the continuum of angle-dependent modes,

$$\dot{\rho} = \int d\Omega\, f(\theta, \phi)\mathcal{D}[b(\theta, \phi)]\rho, \tag{5.20}$$

where we have introduced a normalized angular distribution function $f(\theta, \phi)$. In the limit that the spacing between the atoms relative to the optical wavelength tends to zero, all the phases match and the jump operator simplifies to the collective z-spin operator $b(\theta, \phi) = \sqrt{\gamma}\, J_z$.

We can numerically simulate the master equation at this stage by considering spontaneous emission into discrete bins. The integral of a general function can be approximated with a sum

$$\int_{x_a}^{x_b} dx\, f(x) \approx \sum_{m}^{M} f(m\Delta x)\Delta x, \tag{5.21}$$

where $\Delta x = (x_b - x_a)/M$. For (5.20) this translates to

$$\begin{aligned}\dot{\rho} &= \int_0^{2\pi} d\phi \int_0^{\pi} d\theta \sin\theta \, f(\theta,\phi)\mathcal{D}[b(\theta,\phi)]\rho, \\ &\approx \sum_{\alpha=1}^{A} \Delta\phi \sum_{\beta=1}^{B} \Delta\theta \sin(\theta_\beta) \, f(\theta_\beta,\phi_\alpha)\mathcal{D}[b(\theta_\beta,\phi_\alpha)]\rho.\end{aligned} \tag{5.22}$$

In the first line we have explicitly written out the integral over the solid angle, and in the second line we defined $\phi_\alpha = \alpha\Delta\phi$, $\theta_\beta = \beta\Delta\theta$, where $\Delta\phi = 2\pi/A$, $\Delta\theta = \pi/B$ and A, B are the number of discrete bins in the approximation. Equivalently we can define a discrete set of jump operators $b(\theta,\phi) \to b_{\alpha,\beta}$, where

$$b_{\alpha,\beta} = \sqrt{\Delta\phi\Delta\theta \sin(\theta_\beta) f(\theta_\beta,\phi_\alpha)} \, b(\theta_\beta,\phi_\alpha), \tag{5.23}$$

$$\dot{\rho} \approx \sum_{\alpha=1}^{A}\sum_{\beta=1}^{B} \mathcal{D}[b_{\alpha,\beta}]\rho. \tag{5.24}$$

We can see from the form of the jump operator (5.19) that when the atoms are close together the scattered light carries away information predominantly about the collective spin J_z. As the spacing increases, local information about the atoms can be measured. If the spacing is greater than an optical wavelength, then in principle each individual atom is resolvable. Numerical simulation of a small number of atoms (N=8) with uniform spacing between them, shows faster decoherence as the spacing is increased. This effect can be seen in the rate of decay of the total state purity of a coherent spin state, illustrated in Fig. 5.2. The spacing, labelled a, is expressed in units of the optical wavelength λ used for the scattered wave-vector.

5.2.1 Imaging

Using a Fourier transform we can relate the angle-dependent operators (5.19), to spatial operators, which is the appropriate form for an imaging measurement. Since this is a

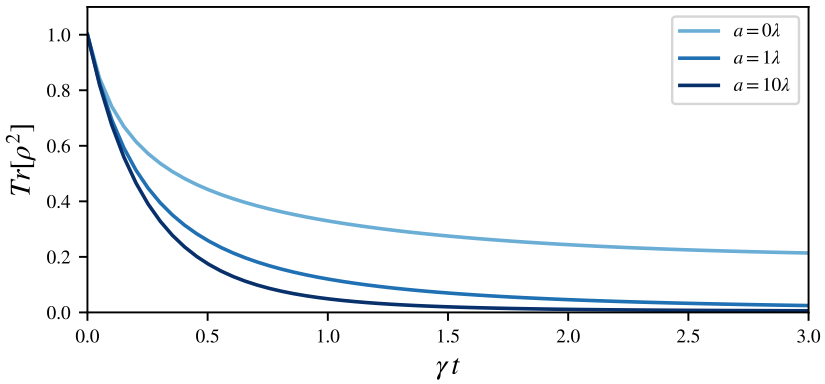

Figure 5.2: State purity calculated via numerical integration of the master equation (5.24), for a 1D chain of 8 atoms with equal spacing $a = (0, 1, 10)\lambda$.

unitary transformation it will intrinsically preserve normalization, and as we are taking the Fourier transform over the bounded domain of θ and ϕ, we will obtain a discrete set of operators. The transformed operators for a single atom confined to the x-axis are

$$b^{(n)}_{\alpha,\beta} = \sqrt{\frac{\gamma}{4\pi}} \int_0^{2\pi} d\phi \int_0^{\pi} d\theta \sin\theta \sqrt{f(\theta,\phi)}\, e^{ikx_0 \cos\theta} e^{-i\alpha\pi\cos\theta} e^{i\beta\phi}\, j_z^{(n)}. \tag{5.25}$$

If we assume isotropic scattering, $f(\theta, \phi) = 1/4\pi$, we can eliminate the β dependence. Making the substitution $u = \cos\theta$ we find

$$\begin{aligned} b^{(n)}_{\alpha} &= \sqrt{\gamma\,\pi} \int_{-1}^{1} du\, \frac{1}{\sqrt{4\pi}}\, e^{ikxu} e^{-i\alpha\pi u}\, j_z^{(n)} \\ &= \sqrt{\gamma}\,\mathrm{sinc}\left(k\left(\frac{\alpha\lambda}{2} - x^{(n)}\right)\right) j_z^{(n)}. \end{aligned} \tag{5.26}$$

In practice the discrete spacing of the operators due to the bounded θ and ϕ domains would not be resolvable in any individual measurement, and we can express the operators in the continuum limit. In this case the combined field from each atom,

$$b(x) = \sum_{n=0}^{N-1} \sqrt{\frac{\gamma k}{\pi}}\,\mathrm{sinc}\left(k(x - x^{(n)})\right) j_z^{(n)}. \tag{5.27}$$

These operators can be interpreted as the atomic field projected onto the x-axis, and are of the same form as the imaging operators we derived in chapter 3. The exact profile is dependent on the true scattering function $f(\theta, \phi)$ but in general will be peaked with a width on the order of an optical wavelength.

Knowing the field in the plane of the atoms, we can consider how it propagates and how it can be imaged. To do this we can use the framework of Fourier optics. For single wavelength light we can use the Helmholtz equation,

$$\nabla^2 U(\mathbf{r}) + k^2 U(\mathbf{r}) = 0, \tag{5.28}$$

where $U(\mathbf{r})$ is a complex field amplitude, and k is the associated wave number. In rectangular coordinates the solution to the Helmholtz equation can be expressed as a weighted superposition of plane waves,

$$U(x, y, z) = \int\int_{-\infty}^{\infty} dk_x dk_y \, K(k_x, k_y) \, e^{i(k_x x + k_y y)} \, e^{iz\sqrt{k^2 - k_x^2 - k_y^2}}, \tag{5.29}$$

with the separation condition $k_x^2 + k_y^2 + k_z^2 = k^2$. The coefficients of the exponential terms are a function of the spatial wave numbers, and at $z = 0$, $K(k_x, k_y)$ can be seen to be the spatial Fourier transform of the field $U(x, y, 0)$,

$$\begin{aligned} U(x, y, 0) &= \int\int_{-\infty}^{\infty} dk_x dk_y \, K(k_x, k_y) \, e^{i(k_x x + k_y y)} \\ &= \mathcal{F}^{-1}(K(k_x, k_y)). \end{aligned} \tag{5.30}$$

The full solution to the Helmholtz equation describes the field at any point. However, this is a complicated integral to compute and can be greatly simplified with the paraxial approximation,

$$k_x^2 + k_y^2 \ll k_z^2. \tag{5.31}$$

In this limit we only consider components of the field with small angles from the optical

axis (z), and can arrive at a simpler expression for the field in a plane away from the source. This is the Fresnel diffraction pattern

$$U(x_0, y_0) = \int\int_{-\infty}^{\infty} dxdy\, h(x_0 - x, y_0 - y)\, U(x, y)\big|_{z=0}, \tag{5.32}$$

where,

$$h(x_0, y_0) = \frac{-e^{-ikz}}{i\lambda z}\, e^{-\frac{ik}{2z}(x_0^2 + y_0^2)}, \tag{5.33}$$

and (x_0, y_0) are the coordinates in the new plane at some fixed distance z. The equation for the Fresnel diffraction pattern has a convolution structure and is still somewhat difficult to evaluate. Under certain conditions it simplifies further.

The effect of a lens on a propagating monochromatic field can be described with a phase transformation. If $U_l(x, y)$ is the field incident on a lens, then the field directly after the lens can be expressed as,

$$U_l'(x, y) = t_l(x, y)\, U_l(x, y), \tag{5.34}$$

For a thin lens, under the paraxial approximation

$$t_l(x, y) = e^{ikn\Delta_0} e^{\frac{ik}{2f}(x^2 + y^2)}, \tag{5.35}$$

where n is the refractive index of the lens, Δ_0 is its width and f is the focal length. Knowing this, the field equations simplify greatly in the special case when propagating from an initial plane one focal length before the lens, to a detection plane one focal length ahead of the lens. In this case, the quadratic phase introduced by the lens cancels out the quadratic phase when propagating the field using the Fresnel equation. As a result the field in the detection plane is proportional to the Fourier transform of the field in the initial plane,

$$U(x_0, y_0) = -\frac{1}{i\lambda f} \int\int_{-\infty}^{\infty} dxdy\, e^{i\frac{2\pi}{\lambda f}(x_0 x + y_0 y)}\, U(x, y). \tag{5.36}$$

This is the form of a normalised Fourier transform, and so Parseval's theorem ensures that the field intensity is conserved and that transformed operators will remain consistently

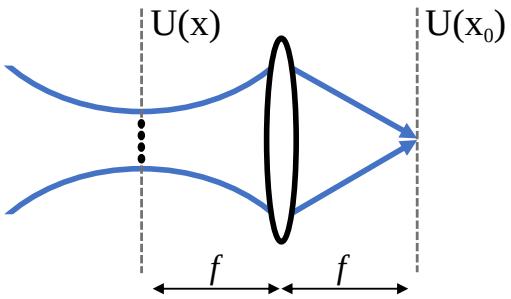

Figure 5.3: Sketch of optics for a imaging a 1D string of atoms. A probe illuminates the atoms and the field $U(x)$ propagates according to the Fresnel equation (5.32) through a lens to the focal plane, where the Fourier transform of the field is formed $U(x_0)$.

normalised,

$$\int dx_0 dy_0 \, |U(x_0, y_0)|^2 = \int dx dy \, |U(x, y)|^2. \tag{5.37}$$

As illustrated in Fig. 5.3, we can now propagate the atomic field (5.27) to the imaging plane using (5.36). Identifying $U(x) = b(x)$,

$$U(x_0) = \sqrt{\frac{1}{\lambda f}} \int_{\infty}^{\infty} dx \, e^{i\frac{2\pi}{\lambda f} x x_0} b(x), \tag{5.38}$$

where we have dropped the global phase and considered only the field along the x-axis. Relabelling the field in the image plane, $U(x_0) = \tilde{b}(x)$ and evaluating the integral,

$$\tilde{b}(x) = \sum_{n=0}^{N-1} \sqrt{\frac{\gamma}{2f}} \, rect\left(\frac{x}{2f}\right) e^{i x^{(n)} \frac{2\pi x}{\lambda f}} \, j_z^{(n)}. \tag{5.39}$$

Here the $rect(x)$ function forms a window, outside of which the field is zero,

$$rect(x) = \begin{cases} 0 & \text{if} \quad |x| > 1/2 \\ 1 & \text{if} \quad |x| \leq 1/2 \end{cases}. \tag{5.40}$$

The optical wavelength effectively determines how quickly the phase of the individual atomic contributions varies, and the focal length acts as a scaling factor for the whole

image. The imaged field will not always have hard boundaries. The rectangular window here is a reflection of the particular choice of $f(\theta, \phi)$, but in general the imaged field will be windowed by a smoothly decaying function. Although these measurement operators are a normalized set, they will not accurately represent the field outside of the range of the paraxial approximation.

5.2.2 Discrete mode operators

If we define an equal spacing between the atoms $x^{(n)} = an$, we can consider the limit of a dense cloud $aN/\lambda \ll 1$. In this limit the complex exponential in the operators (5.39) is approximately constant over the width of the window function, effectively eliminating the spatial dependence and reducing the collapse operators to $\tilde{b}(x) = \sqrt{\gamma}\, J_z$. This is the same limit we found with the angle-dependent operators (5.19).

We can also consider measuring the field across a discrete set of pixels, such as on a charge-coupled device (CCD) imaging system. We can define a pixel size Δx, and make the transformation to a discrete set of operators that approximates the field at each pixel. Returning first to the field in the plane of the atoms, with reasonably large spacing $a = \lambda/2$, there is almost no overlap between the spatial modes (5.27). If we approximate this field with a discrete set of modes $b_n = \sqrt{\Delta x}\, b(n\Delta x)$, where $\Delta x = a$, then

$$\begin{aligned} b_n &= \sqrt{\gamma} \sum_m^N \operatorname{sinc}\big(\pi(n-m)\big)\, j_z^{(m)} \\ &= \sqrt{\gamma}\, j_z^{(n)}. \end{aligned} \tag{5.41}$$

Each mode corresponds to the spin state of an individual atom. In this discrete operator description the field in the Fourier plane can likewise be expressed as $\tilde{b}_k = \sqrt{\Delta\tilde{x}}\, \tilde{b}(k\Delta\tilde{x})$. Here, and from now on, we will switch to using k as a mode index as opposed to a wavenumber. k takes on integer values and corresponds to the spatial frequency components in the

plane of the atoms. If we choose the pixel size in the Fourier plane $\Delta\tilde{x} = \lambda f/Na$,

$$\tilde{b}_k = \sqrt{\frac{1}{N}} \sum_{n=0}^{N-1} e^{-i\frac{2\pi}{N}nk} b_n. \tag{5.42}$$

These operators correspond to the discrete Fourier coefficients of the atomic field. In the continuous case the corresponding operators would exist at integer multiples of the position $\Delta\tilde{x}$, and as the atomic spacing is increased more of these Fourier coefficients become visible. For a large number of atoms these modes are relatively well resolved, and for the spacing $a = \lambda/2$, one Fourier mode is visible for each atom. This discrete mode approximation helps to simplify the model and we will use it throughout the rest of the chapter.

5.2.3 Spin squeezing via measurement and feedback

A uniform probe field across the atoms will largely be focused at the centre of the Fourier plane. This acts like the reference field in a homodyne measurement for the atomic signal, and measuring the phase shift to the probe tells us about the symmetric total z-spin component of the atomic ensemble. We can also mix a reference field with the rest of the scattered light before it reaches the Fourier plane, effectively performing a homodyne measurement at each pixel. We can model this by transforming the jump operators for pixels in the Fourier plane,

$$\tilde{b}_k \to \tilde{b}_k + \alpha_{l.o.}, \tag{5.43}$$

where we have defined $\alpha_{l.o.} = |\alpha|e^{i\phi}$ as the classical reference field, including the probe contribution. In this form, following the procedure in section 2.3, we can describe the measurement process with a diffusive measurement master equation,

$$d\rho = \sum_k^N \left(\mathcal{D}[\tilde{b}_k]\rho\, dt + \sqrt{\eta_k}\, \mathcal{H}[\tilde{b}_k]\rho\, dW \right). \tag{5.44}$$

Here we have introduced the measurement efficiency η_k for each mode.

As discussed previously, when exclusively measuring light imaged at the centre of the plane $\tilde{b}_{k=0}$, or in the limit of a dense cloud, the measurement operators approximate J_z. Initially we will explore the effects of solely this measurement channel

$$d\rho = \gamma \mathcal{D}[J_z]\rho \, dt + \sqrt{\gamma} \, \mathcal{H}[J_z]\rho \, dW, \tag{5.45}$$

with the measurement record defined as

$$dI(t) = \sqrt{4\gamma} \, \langle J_z \rangle dt + dW. \tag{5.46}$$

Measurement causes the desired conditional squeezing of the total z-spin variance in a single trajectory, but is washed out in an average ensemble by the stochastic drift of the mean z-spin component. We can model the evolution of an operator using the master equation $d\langle c \rangle = Tr[c \, d\rho]$. The drift in J_z caused by the measurement is described by the stochastic equation

$$d\langle J_z \rangle = 2\sqrt{\gamma}(\Delta J_z)^2 \, \mathrm{d}W \, . \tag{5.47}$$

This is analogous to that which we studied in the position of a nano-mechanical oscillator (3.35), where the mean position also drifted at a rate proportional to its variance. In fact, if we have a large number of atoms and the mean spin predominantly points along x, it can be useful to introduce new canonical position and momentum operators,

$$X_{spin} = \frac{J_y}{\sqrt{\langle J_x \rangle}}, \qquad P_{spin} = \frac{J_z}{\sqrt{\langle J_x \rangle}}. \tag{5.48}$$

When the mean x-spin is large and only weakly perturbed, we can approximate $J_x \approx \langle J_x \rangle$[103]. In this case the y and z spin components obey the usual position momentum commutation relation $[X_{spin}, P_{spin}] = i$. Similarly to drift in mechanical momentum, the drift in the z-spin can be counteracted by feedback of the measurement record proportional to the orthogonal y-spin operator. Fig. 5.4 illustrates the conditional squeezing and drift

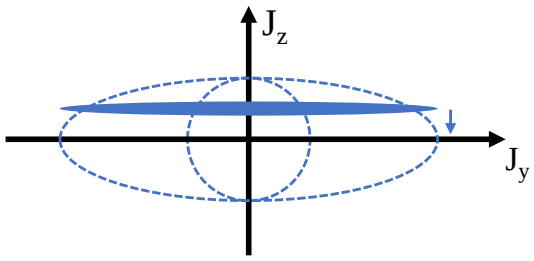

Figure 5.4: Projection of the y and z quasi-probability distributions for the collective spin state of an atomic ensemble. The central circle represents a CSS orientated along x with diameter $\sqrt{J/2}$ satisfying the minimum uncertainty relation (5.6). The shaded oval represents a squeezed state conditioned on measurement of J_z, where as the larger oval represents an ensemble average where the visible squeezing is washed out by the drift in the conditioned state.

induced by measurement.

Feedback can be applied using the averaged measurement signal after a short pulse, to realign the mean spin allowing for non-conditional spin squeezed states useful for Ramsey spectroscopy[104, 105]. This requires a simple form of state estimation. The system is also well suited for control via direct continuous feedback [106, 15]. Both approaches rely on the same principles, however, we will focus on the case of continuous feedback as it provides a useful framework for analytical analysis and numerical simulation. Following the details of the feedback procedure discussed in section 2.4, the feedback term that we will add to the master equation should be of the form

$$d\rho_f = -i\, dI(t)\big[F, \rho\big], \tag{5.49}$$

where F is an arbitrary operator corresponding to a physical shift to the system proportional to the measurement record $I(t)$. As previously discussed, correlations between the measurement and system noise give rise to additional terms in the dynamics. If we write the full master equation split into a deterministic and diffusive parts,

$$d\rho = \rho_A\, dt + \rho_B\, dW, \tag{5.50}$$

then,

$$\begin{aligned}\rho_A &= -i\big[H,\rho\big] - i\big[F, c\rho + \rho c^\dagger\big] + \mathcal{D}[c]\rho + \frac{1}{\eta}\mathcal{D}[F]\rho \\ &= -i\big[H + \frac{1}{2}(c^\dagger F + Fc), \rho\big] + \mathcal{D}[c - iF]\rho + \frac{1-\eta}{\eta}\mathcal{D}[F]\rho,\end{aligned} \tag{5.51}$$

$$\rho_B = \sqrt{\eta}\mathcal{H}[c]\rho - \frac{i}{\sqrt{\eta}}\big[F,\rho\big]. \tag{5.52}$$

In the second line of (5.51) we have expressed the deterministic evolution in Lindblad form. Following closely the analogy of damping a mechanical system, feedback can be used to counteract the drift induced by measurement. The additional Ito term that arose due to the noise introduces further heating, in this case causing diffusion of the y-spin component.

To cancel the stochastic drift (5.47) requires a rotation of the mean spin about the y-axis, which is achieved with a Hamiltonian of the form

$$H_f = \lambda(t) I(t) J_y / \sqrt{\gamma}, \tag{5.53}$$

where $\lambda(t)$ is a time dependent scaling factor. This can be implemented within the feedback master equation by identifying $c = \sqrt{\gamma} J_z$ and $F = (\lambda(t)/\sqrt{\gamma}) J_y$. We can then average over the noise to obtain a non-conditional feedback master equation,

$$\dot{\rho} = \gamma\mathcal{D}[J_z]\rho - i\lambda(t)\big[J_y, J_z\rho + \rho J_z\big] + \frac{\lambda(t)^2}{\gamma}\mathcal{D}[J_y]\rho. \tag{5.54}$$

We can see from the Lindblad form of (5.54) that along with heating terms, feedback produces the effective Hamiltonian

$$H_{\text{eff}} = \frac{1}{2}\big(c^\dagger F + Fc\big) = \frac{\lambda(t)}{2}\big(J_z J_y + J_y J_z\big), \tag{5.55}$$

which is known to generate transient spin squeezing [92]. Under the influence of this Hamiltonian the squeezing parameter ξ^2 will decrease to a minimum value, and then

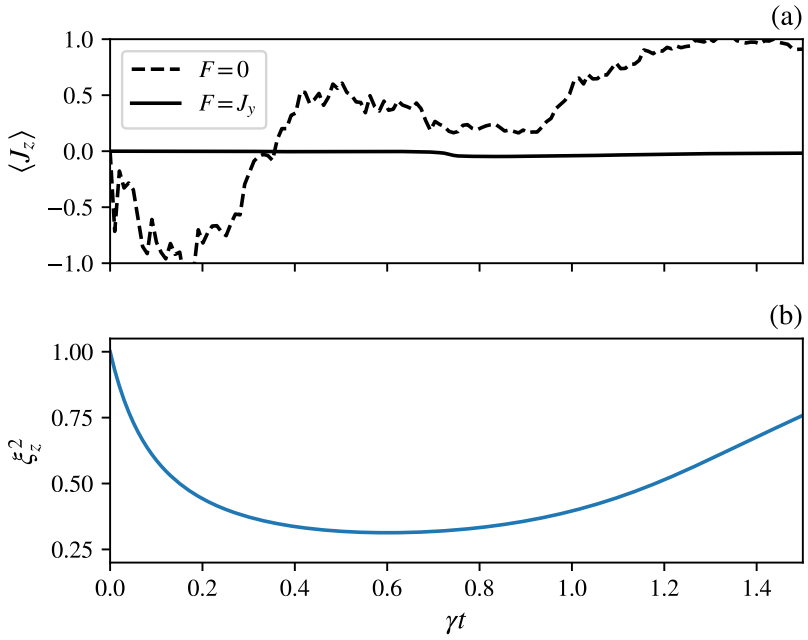

Figure 5.5: Sub-plot a) shows a single trajectory of 8 spins undergoing continuous measurement of the collective spin component J_z. The dashed line shows the stochastic drift of the mean z-spin without feedback ($F = 0$), whilst the solid line shows stable behaviour with feedback turned on ($F = J_y$). Sub-plot b) shows the unconditional evolution of the spin squeezing parameter ξ_z^2 with feedback.

begin to increase again. The time dependent coefficient $\lambda(t)$ can be chosen to optimise this transient squeezing by considering the affect of the feedback on the evolution of J_z,

$$\begin{aligned} d\langle J_z \rangle_f &= -\frac{\lambda(t)}{\sqrt{\gamma}} \langle J_x \rangle \, \mathrm{d}W - \left(\frac{\lambda(t)^2}{2\gamma} \langle J_z \rangle + \lambda(t) \langle J_x J_z + J_z J_x \rangle \right) \mathrm{d}t \\ &\approx -\frac{\lambda(t)}{\sqrt{\gamma}} \langle J_x \rangle \, \mathrm{d}W \, . \end{aligned} \tag{5.56}$$

In the second line we drop the correlation term between J_x and J_z, as it is initially zero due to the symmetry of the CSS and the feedback procedure does not change this. We also assume that $\langle J_z \rangle = 0$, which is true for the initial state and should be maintained by successful feedback. The drift of $\langle J_z \rangle$ caused by the measurement (5.47) can be cancelled

by (5.56), by choosing

$$\lambda(t) = 2\gamma\langle J_z^2\rangle/\langle J_x\rangle. \tag{5.57}$$

This idealised feedback strength is a time dependent function depending on conditional averages of the spin system parameters. This choice of feedback stabilises the orientation of the mean spin whilst the measurement reduces the z-spin variance, initially resulting in unconditional squeezing. However, as the state continues to evolve it becomes distorted and the variance in J_z eventually increases again, destroying the squeezed state. A substantial benefit of engineering squeezing through measurement and feedback is that it can be turned off after reaching the desired value, although later we will explore the possibility of producing steady state squeezing. Under ideal conditions, in a large system, the minimum value of ξ^2 scales inversely with the system size N [15]. Fig. 5.5 (a) shows numerical simulation of the conditional evolution (5.50) of 8 atoms with and without feedback to stabilise $\langle J_z\rangle$. Sub-plot (b) shows the spin squeezing parameter fall to its optimal value before increasing again in the unconditional evolution of an ensemble average of states using the feedback equation (5.54).

5.3 Feedback of higher order modes

Having looked at the effects of measuring the collective spin J_z we can go back and add in the effect of the other measurement channels. We saw when modelling the radiation profile of the atoms, that when the spacing between them is small compared to the probe wavelength, each atom is almost indistinguishable. As a result of this, most of the scattered light contains only information about the collective spin. In the previous section we showed that measuring J_z creates correlations between the atoms and produces squeezing. When the atoms are spaced far apart the scattered light starts to carry away local information about each individual atomic states. Measuring this local information will not correlate the atoms and, in fact, will in time destroy any correlations that exist [107]. We saw a manifestation of this in the increased rate of decoherence of a CSS as a function of

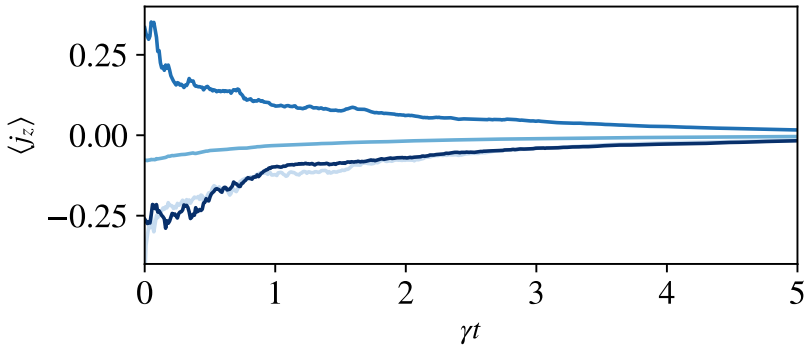

Figure 5.6: Evolution of the z-spin components j_z of 4 randomly orientated atoms across a single trajectory, undergoing continuous measurement and feedback to align them along x. Feedback was performed using information from the discrete measurement modes (5.42), and each line corresponds to a single atomic spin.

atomic spacing. In this section we outline a combination of measurement and feedback to counteract this effect.

If N modes are visible in the Fourier plane, measuring each of them can reveal the local state of each atom. Measuring the Fourier modes (5.42) it is possible to reconstruct each local spin $j_z^{(n)}$, by effectively performing the inverse Fourier transform. Fig. 5.6 shows a numerical simulation of measuring the Fourier modes and using the information to align each spin individually along x, in the same fashion as when rotating the collective spin J_z. The collective z-spin variance in this case is not squeezed as correlations never accumulate between the atoms. It is however possible to alter these measurements so as not to obtain any local information.

Previously, when examining damping of the motion of an oscillator, or stabilising the drift in a spin vector, we have seen that feedback can be used to counteract the effect of measurement noise. In these cases a system observable is also measured, and in turn the system is driven towards an eigenstate of the measured operator. This latter effect is undesirable in the case of measuring the higher order modes of scattered light (5.42). This can be circumvented using a homodyne measurement, where it is possible to choose

the reference phase such that no information is gained about the state of the system. For example, for an arbitrary Hermitian operator $c = c^\dagger$ with a homodyne reference phase $\phi = \pi/2$, the measurement record (2.74) as defined in chapter 2, would be

$$\begin{aligned} dI(t) &= \sqrt{\gamma}\langle c\, e^{i\phi} + c^\dagger e^{-i\phi}\rangle \,\mathrm{d}t + \mathrm{d}W \\ &= i\sqrt{\gamma}\langle c - c^\dagger\rangle \,\mathrm{d}t + \mathrm{d}W \\ &= \mathrm{d}W\,. \end{aligned} \tag{5.58}$$

This specific choice of homodyne phase is such that measuring the scattered light reveals no information about the value of the system observable c, and only provides a record of the noise. Feeding back the measurement signal can perfectly cancel the effect of this noise, which in this special case eliminates any effect of the measurement channel. This can be seen in the feedback master equation (5.51) if we choose the feedback operator $F = c$,

$$\begin{aligned} d\rho &= -i[F, ic\rho - i\rho c]dt + \mathcal{D}[F]\rho\,\mathrm{d}t + \mathcal{D}[c]\rho\,\mathrm{d}t \\ &= -2\mathcal{D}[c]\rho\,\mathrm{d}t + 2\mathcal{D}[c]\rho\,\mathrm{d}t = 0. \end{aligned} \tag{5.59}$$

We can see an illustrative example of this type of feedback in a beam splitter model. If we imagine two fields b_0, b_1 originating from two atoms as the inputs to a 50/50 beam splitter, we can treat the output fields as analogous to the Fourier transformed fields in the optics setup,

$$\tilde{b}_0 = \frac{1}{\sqrt{2}}\big(b_0 + b_1\big), \qquad \tilde{b}_1 = \frac{1}{\sqrt{2}}\big(b_0 - b_1\big). \tag{5.60}$$

This is sketched in Fig. 5.7. We can again imagine making homodyne measurements of each of the output modes. With the homodyne reference phase $\phi = 0$, measurement of the mode $\tilde{b}_0$ is equivalent to measuring the total spin $J_z/\sqrt{N}$. This will produce conditional squeezing as desired. However, this measurement combined with that of $\tilde{b}_1$ would reveal the local state of the atoms, destroying the entanglement between them. Instead, measuring the second mode $\tilde{b}_1$ with a reference phase $\phi = \pi/2$, reveals no information about the

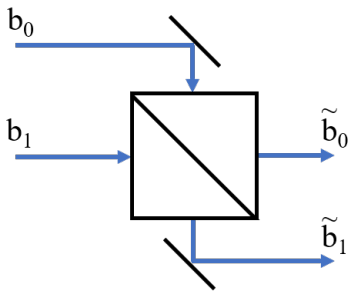

Figure 5.7: Sketch of a beam splitter configuration that mimics the effect of Fourier imaging light from two discrete atomic sources. The inputs b_0, b_1 reflect the state of the individual atoms where as the outputs contain collective information about the two states.

atomic states,

$$\begin{aligned} dI_1 &= \sqrt{\gamma}\langle \tilde{b}_1\, e^{i\phi} + \tilde{b}_1^\dagger e^{-i\phi}\rangle\, \mathrm{d}t + \mathrm{d}W \\ &= \mathrm{d}W\,. \end{aligned} \tag{5.61}$$

Following the feedback procedure (5.59) the effect of the noise induced by this measurement channel can be cancelled using the feedback operator $F_1 = \tilde{b}_1$. The resulting state evolution is exactly equivalent to having only measured the uniform spin channel $\tilde{b}_0$.

The beam splitter configuration outlined above has two key properties that allow it to work. First, combining the individual atomic fields at the beam splitter is necessary to measure the collective spin state $\tilde{b}_0$. Secondly, there exists a choice of reference phase such that the other output channel can be measured without gaining further information about the spin states. This second quality is not generally true for the higher modes $\tilde{b}_k$ in the optics setup. The complex phase differences between the individual atom contributions in the Fourier coefficients mean that the operators are no longer Hermitian, and no choice of reference phase can ensure $dI_k = \mathrm{d}W$. This can be rectified by undoing the optical Fourier transform with a second lens. We have seen that the individual atomic fields will impart a phase shift to a probe beam proportional to $j_z^{(n)}$. Since this a Hermitian observable, with the appropriate reference phase as discussed above, a homodyne measurement can be made blind to this. The optics setup sketched in Fig. 5.8 takes advantage of this fact

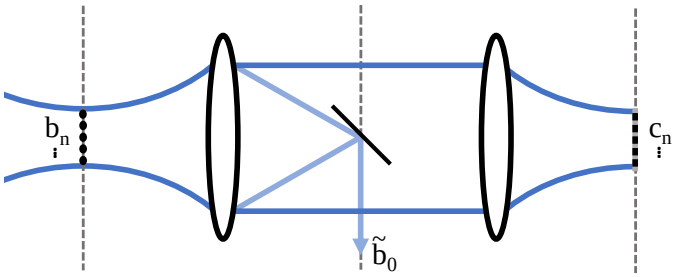

Figure 5.8: Sketch of modified optics for imaging a 1D string of atoms, with an isolated measurement of the uniform Fourier component $\tilde{b}_0$. A probe illuminates the atoms and the input field $b(x)$ propagates according to the Fresnel equation (5.32). The field at $\tilde{b}(x)$ is the optical Fourier transform of $b(x)$, and the output field $c(x)$ is the inverted image of $b(x)$.

after measuring the uniform collective spin mode $\tilde{b}_{k=0}$. As before, the field from the atoms propagates to the Fourier plane, and in this setup the $k = 0$ mode is isolated and measured separately. The rest of the field continues to propagate, passing through a second lens and is finally imaged onto a CCD. Once again, we consider mixing the light in the output field with a reference field so as to perform an effective homodyne measurement at each pixel.

In this setup the field operators undergo the following transformations. Initially each mode $b_n = \sqrt{\gamma}\, j_z^{(n)}$ carries information about the individual spin states. In the Fourier plane the central mode is isolated, and carries information about the collective spin $\tilde{b}_0 = \sqrt{\gamma/N}\, J_z$. Propagation through the second lens performs another optical Fourier transform, producing an inverted image of the original field. The measurement operators in this output plane are

$$\begin{aligned} c_n &= \frac{1}{\sqrt{N}} \left(\sum_{k=0}^{N-1} e^{-i\frac{2\pi}{N}nk} \tilde{b}_k - \tilde{b}_0 \right) \\ &= b_{-n} - \frac{1}{N} \sum_{m=0}^{N-1} b_m. \end{aligned} \tag{5.62}$$

In the first line here we have explicitly written out the transformation for the operators $\tilde{b}_k$, with the information from the $\tilde{b}_0$ mode removed. In the second line we carry out

the transformation, which leaves an inverted copy of the original atomic field operators, minus the contribution of the uniform collective spin component. The operators $\tilde{b}_0$ and c_n can then independently be measured. As in the beam splitter model the collective spin measurement produces squeezing and the other modes can be measured with a reference phase $\phi = \pi/2$ so as to extract no information. For the collective spin channel the corresponding feedback operator should be

$$F_{k=0} = \frac{\lambda(t)}{\sqrt{\kappa}} J_y, \tag{5.63}$$

where we have defined the measurement strength for this mode $\kappa = \gamma/N$, and the feedback strength,

$$\lambda(t) = 2\eta\kappa\langle J_z^2\rangle/\langle J_x\rangle. \tag{5.64}$$

We have also explicitly included that the feedback operators should be re-scaled to reflect the measurement efficiency η. For every other mode in the output plane there should be a corresponding feedback operator,

$$F_n = \eta c_n = \eta\sqrt{N\kappa}\left(j_z^{(-n)} - \frac{1}{N}J_z\right). \tag{5.65}$$

where we can see that implementing feedback would involve rotations of individual spins. The corresponding master equation in this case would be

$$\dot{\rho} = \kappa\mathcal{D}[J_z]\rho - i\lambda(t)\big[J_y, J_z\rho + \rho J_z\big] + \frac{\lambda(t)^2}{\eta\kappa}\mathcal{D}[J_y]\rho + \sum_{n=0}^{N-1}(1-\eta)\mathcal{D}[c_n]\rho. \tag{5.66}$$

With perfect detection efficiency $\eta = 1$, the last term in this equation vanishes as the feedback perfectly cancels out the dissipation caused by the measurement channels c_n. Under ideal conditions, this combination of measurement and feedback is equivalent to the best case squeezing from section 5.2.3, where only the J_z measurement channel was considered. Perfect measurement efficiency across every mode is, of course, not a realistic scenario. CCD pixels have operating noise and not all the scattered light will be collected

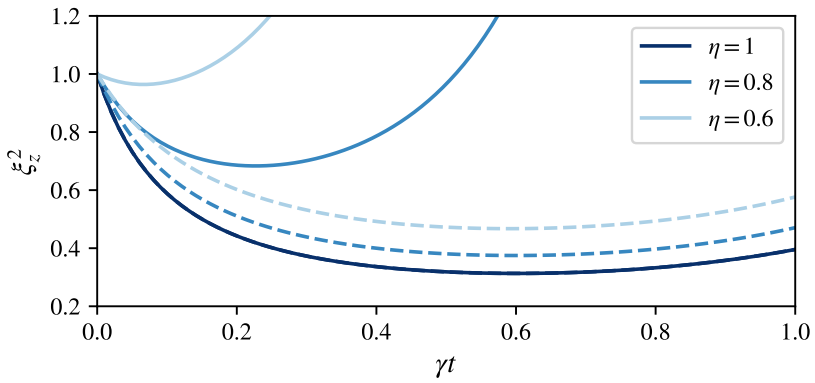

Figure 5.9: Simulation of the average evolution of the spin squeezing parameter (5.7), in a string of $N = 8$ atoms. The system evolution is driven by many mode feedback (5.66), for a range of quantum measurement efficiencies η. The solid lines correspond to a system with N measurement channels c_n (5.62), as well as the collective spin channel J_z, whereas the dashed lines show the evolution of a system with only the collective spin channel.

by the optics setup. Fig. 5.9 shows a simulation of the average squeezing that would be produced in a string of 8 discrete atoms, for various η. The evolution of the squeezing parameter ξ^2 was simulated using (5.66) with a uniform detection efficiency η across all modes. For comparison, the system evolution where only the J_z channel exists is included to illustrate that the presence of the higher order modes makes the system more sensitive to detection efficiency. This can be clearly seen in (5.66), where the last term, corresponding to the additional measurement channels, only serves to cause extra dissipation when $\eta < 1$.

So far we have examined two limiting cases, one in which each atom is initially connected to its own spatial mode, and another where every atom is connected to a single mode. The intermediate regime will more closely approximate a real free space measurement of an atomic cloud. We can model this by increasing the number of spins in each discrete mode, effectively increasing the cloud density as opposed to worrying about varying the spacing in the continuous mode description. If we allow each initial spatial mode to contain N_m atoms, the individual spin measurements can be replaced with measurements of the

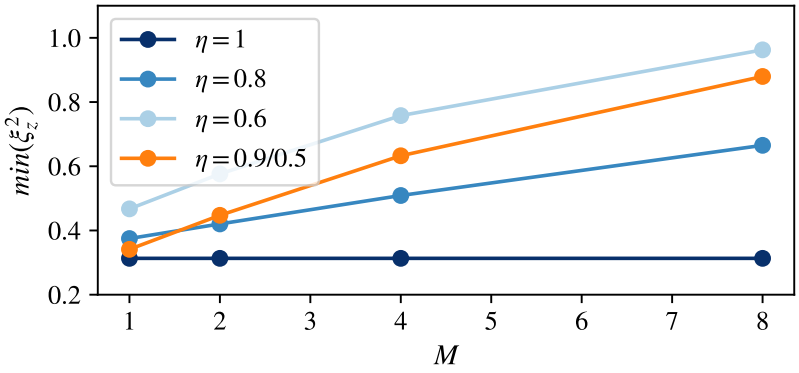

Figure 5.10: Minimum ξ^2 reached in a system of $N = 8$ atoms coupled to M spatial modes, using a combination measurement and feedback. The different lines correspond to different uniform detection efficiencies across each measurement channel. The yellow line shows a special case where the detection efficiency is higher for the measurement of the collective spin J_z, and lower for the other modes imaged onto the CCD.

collective sub-systems,

$$\begin{aligned} & b_n = \sqrt{\gamma}\, j_z^{(n)} \\ \rightarrow \quad & b_m = \sqrt{\gamma}\, J_z^{(m)} = \sqrt{\gamma} \sum_n^{N_m} j_z^{(n)}, \end{aligned} \tag{5.67}$$

where m is the mode index. The collective z-spin component of the full system is now

$$J_z = \sum_m^M J_z^{(m)}, \tag{5.68}$$

where M is the total number of input modes, and the total number of atoms in the system is $N = N_m \times M$. The other spin operators can be transformed accordingly, and otherwise the model remains unchanged. As in the case with a single input mode, in this idealised setup the total spin of each sub-system is conserved since there are no operations involving the individual atoms. This comes with the numerical advantage of good system size scaling, as each sub-system can be represented by a Dicke states [93] (eigenstates of $J_z^{(m)}$), which have dimension $N_m + 1$ as opposed to 2^{N_m}.

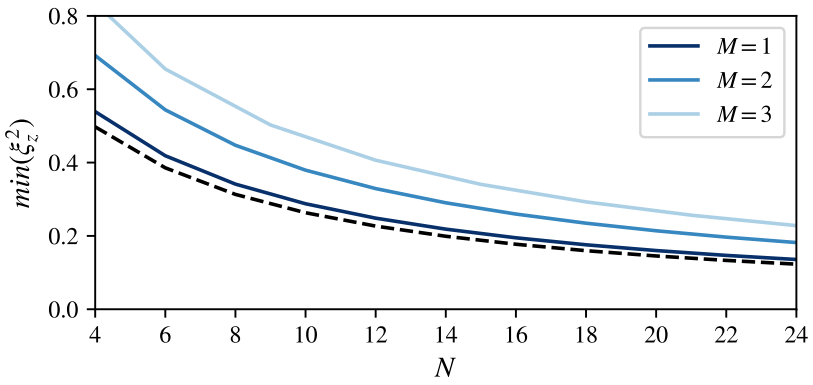

Figure 5.11: Minimum ξ^2 reached in a system of N atoms coupled to M spatial modes, using a combination measurement and feedback. The different lines correspond to an increasing number of modes M. The detection efficiency was kept constant at $\eta = 0.9$ for the central measurement mode, and $\eta = 0.5$ for the modes imaged onto the CCD. The dashed line shows a single example of how ξ^2 scales with perfect detection efficiency, which is independent of the number of modes M.

Figures 5.10 and 5.11 show how the maximum squeezing, using the outlined feedback scheme, scales with the number of modes M and the total number of atoms N. The point of maximum squeezing was taken to be the minimum values of ξ_z^2 in the time evolution of a state starting as a coherent spin state, like those shown in Figure 5.9. Figure 5.10 shows how the squeezing scales in a system of $N = 8$ atoms that are spread over an increasing number of modes M. This leads to an increased sensitivity to detection efficiency, which comes from the dependency on feedback to cancel out the noise from the additional measurement channels. Physically this corresponds to making measurement of an atomic cloud with a decreasing density. In this figure the detection efficiency was varied uniformly alongside an example of a more realistic efficiency split. If the central mode $\tilde{b}_0$ is separated in the Fourier plane and measured with a photodiode, the detection efficiency could be very high $\eta \approx 0.9$. The other modes imaged onto a CCD would have a significantly lower detection efficiency $\eta \approx 0.5$. These slightly more realistic values were also used in Figure 5.11. In this figure the total number of atoms is varied with the detection efficiency held constant. As before, for the same detection efficiency, the

achievable squeezing is less if the atoms are spread across more input modes. However, in each case the maximum squeezing still scales with the total number of atoms, suggesting this feedback scheme would continue to work well for large systems.

5.4 Steady state squeezing

So far, we have expanded upon a scheme for continuous measurement and feedback to produce spin squeezing, that makes use of information scattered outside of the uniform collective spin mode. An appropriate choice of feedback can be used to cancel out the noise otherwise induced by these additional measurement channels. As previously mentioned, this method of producing unconditional spin squeezing is transient, in the sense that a maximally squeezed state is achieved and if the measurement continues, the squeezing is undone. One solution to this issue is to simply stop the measurement, in practice however this is often not a convenient solution. Having a squeezed state as the steady state of the measurement procedure would be a much more useful resource. This would in principle be more robust against noise and could be prepared and held without worrying about the timing necessary to finish the measurement procedure at the point of maximum squeezing.

With the goal of producing steady state squeezing, we can initially try setting the feedback strength $\lambda(t)$ constant in the current model. In this case we can find the steady state solution to the equations for J_x, J_y and J_z using the master equation (5.66). This in turn can be used to find an expression for the steady state of the squeezing parameter ξ_z^2,

$$\begin{aligned} \lim_{t\to\infty} \xi_z^2 &= N\left(\frac{\kappa+\lambda^2/\kappa}{4\lambda}\right)\frac{1}{\langle J_x\rangle} \\ &= \frac{N}{2}\frac{1}{\langle J_x\rangle}. \end{aligned} \tag{5.69}$$

In the second line we have minimised the term in parenthesis which occurs when the measurement strength equals the feedback strength $\kappa = \lambda$. This does not necessarily maximise the value of $\langle J_x\rangle$, but we know that its theoretical maximum is $N/2$, which implies

in steady state that $\xi_z^2 \geq 1$. There are many ways to alter aspects of the measurement or feedback procedure that might improve upon this result. Before exploring this however, we will introduce another metric that might better quantify the usefulness of the final state, the Quantum Fisher Information (F_Q).

The main goal of the feedback procedure is to produce a state useful for metrology. There is a special class of entangled states that can provide sensitivity beyond the standard quantum limit of measurement precision. Squeezed states are among these, but the full class of states is identified by the Quantum Fisher Information [108]. For this reason we look at calculating this property in states produced by our model. Classically, Fisher Information is a measure of the information that some observable X carries about some unknown parameter θ, upon which the probability of X depends. Formally it is defined

$$F(\theta) = \sum_x \frac{1}{P(x|\theta)} \left(\frac{\mathrm{d}P(x|\theta)}{\mathrm{d}\theta} \right)^2, \tag{5.70}$$

where the sum covers over all possible results x of measuring X. $P(x|\theta)$ is a likelihood function, which gives the conditional probability of seeing a particular result x, given a value of θ. Good measurement observables are highly sensitive to changes in θ, and can be used to accurately determine its value. Correspondingly these observables have a high associated Fisher Information. The Quantum Fisher Information of a state ρ is defined as the maximum value of (5.70) considering all possible measurements.

In the spin system we are concerned with, X would be an observable property of the quantum state, and θ could be any phase shift arising from a unitary transformation $e^{-i\theta G}\rho\, e^{i\theta G}$, generated by some Hermitian operator G. For example, in Ramsey spectroscopy an initial state is effectively rotated by some angle which cannot be measured directly but needs to be estimated. Figure 5.12 shows a spin state rotated around the y axis, where the rotation is described by the transformation $e^{-i\theta J_y}\rho\, e^{i\theta J_y}$. The angle of this rotation can be estimated by measuring the observable J_z, and the Quantum Fisher Information quantifies how useful the initial state is for this. In this case a squeezed state would have a higher

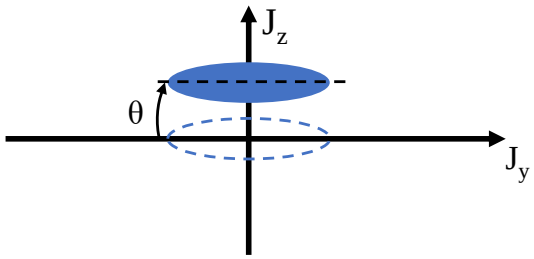

Figure 5.12: Projection of the y and z quasi-probability distributions for the collective spin state of an atomic ensemble. In a Ramsey spectroscopy process, an initial state, represented by the dotted line, is rotated after a sequence of optical pulses and free evolution, by some angle θ around the y axis. The variance of the final state dictates how well the angle θ can be estimated by making measurements of J_z.

value of F_Q because measurements of J_z would provide greater certainty as to the value of θ.

For phase shifts arising from a unitary transformation, the Quantum Fisher Information can be expressed as,

$$F_Q(\rho, G) = 2 \sum_{k,k'} \frac{(\alpha_k - \alpha_{k'})^2}{\alpha_k + \alpha_{k'}} \left| \langle k | G | k' \rangle \right|^2, \tag{5.71}$$

where $|k\rangle$ are the eigenstates in the spectral decomposition $\rho = \sum_k \alpha_k |k\rangle\langle k|$, and the sum only covers terms where $\alpha_k + \alpha_{k'} > 0$. In the example of Ramsey spectroscopy, with a state initially orientated along the x-axis, $G = J_y$ was a meaningful generating operator. With some manipulation it can be seen that for a pure state (5.71) is equivalent to measuring the variance of the generating operator $F_Q = 4(\Delta G)^2$. The squeezed states that we have been considering have a large variance in J_y to accommodate a reduced variance in J_z, and for pure states this has a clear correspondence with a high Quantum Fisher Information. For a coherent spin state $F_Q = N$, and in general a signature of states with enhanced usefulness for metrology is that F_Q increases better than linearly with system size, up to $F_Q \approx N^2$ at the so-called Heisenberg limit.

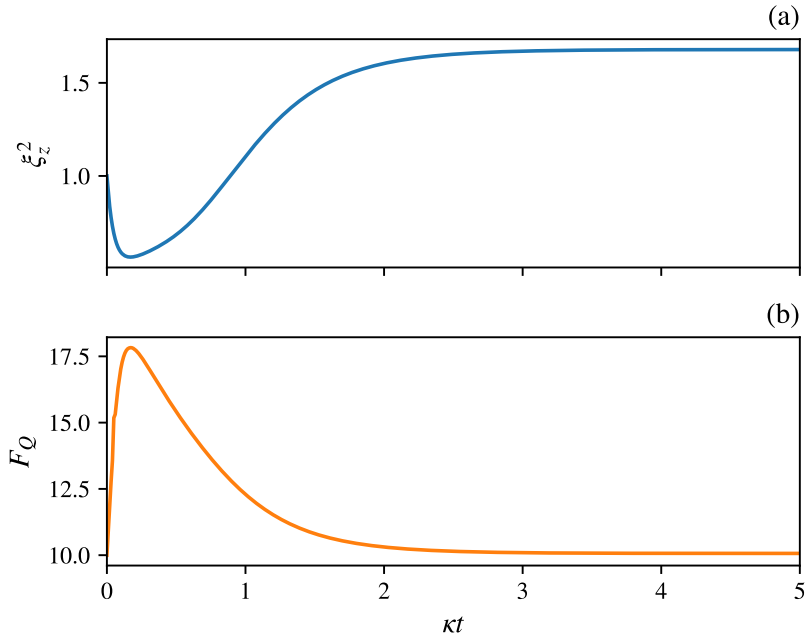

Figure 5.13: Time evolution of an ensemble average of $N = 10$ atoms, calculated using the feedback master equation (5.66), with a constant feedback strength λ. Sub-figure (a) shows the evolution of the squeezing parameter ξ_z^2, and sub-figure (b) shows the Quantum Fisher Information F_Q.

Figure 5.13 shows the time evolution of the squeezing paramater ξ_z^2 alongside F_Q in an ensemble average of $N = 10$ atoms, simulated using (5.66) with a constant feedback strength and perfect detection efficiency. Initially $F_Q = N$ as expected for a CSS, it increases as squeezing is established before dropping off again. This reflects the transient squeezing. Figure 5.14 shows how the steady state F_Q scales with system size, alongside the maximum value F_Q reaches in the earlier stages of the time evolution. The steady state value scales linearly with system size, again indicating that the steady state has no useful enhancement for metrology. By comparison the maximum Fisher information reached in the time evolution, exhibits quadratic growth with system size.

We can look at single trajectories to gain insight into why the steady state does not exhibit squeezing or a high Quantum Fisher Information. One visible factor in single trajectories is

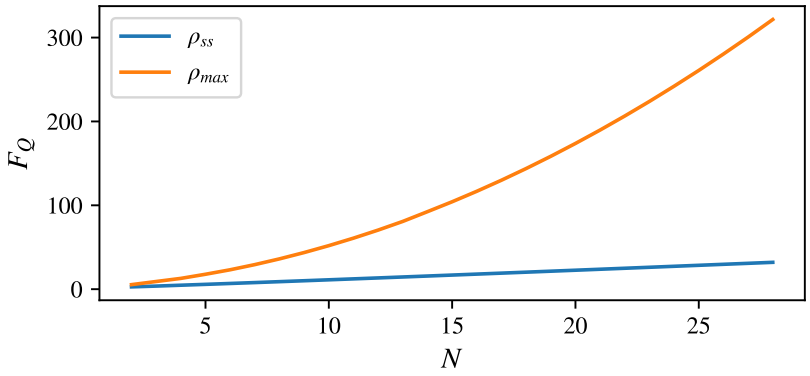

Figure 5.14: Scaling of the Quantum Fisher Information F_Q with system size N in an ensemble average of atoms undergoing measurement and feedback. The blue line ρ_{ss} was calculated from the steady state of the feedback procedure, whereas the orange line ρ_{max} corresponds to the highest point of F_Q in time evolution simulations of the system.

that the mean value of $\langle J_z \rangle$ has significant noisy oscillations around zero. This reduces the purity of the ensemble averaged state. This noisy drift might be alleviated by filtering the measurement record to remove high frequency noise. An error signal $\epsilon(t)$ can be derived from a temporal low-pass filter,

$$\tau \dot{\epsilon}(t) + \epsilon(t) = I(t), \tag{5.72}$$

where $I(t)$ is the measurement record (5.46). The measurement record drives the error signal, but $\epsilon(t)$ is damped and only ends up retaining the low frequency $< 1/\tau$ components. The high frequency components are dominated by the measurement noise, and removing them should lead to less noise being reintroduced to the system via feedback. The error signal can be used in place of $I(t)$ in the feedback term of the master equation,

$$\dot{\rho}_{fb} = -i\epsilon(t)[F, \rho]. \tag{5.73}$$

Since the error signal is no longer described by a Wiener process, (5.73) can be added to the measurement master equation (5.45) without an Ito correction term. The result-

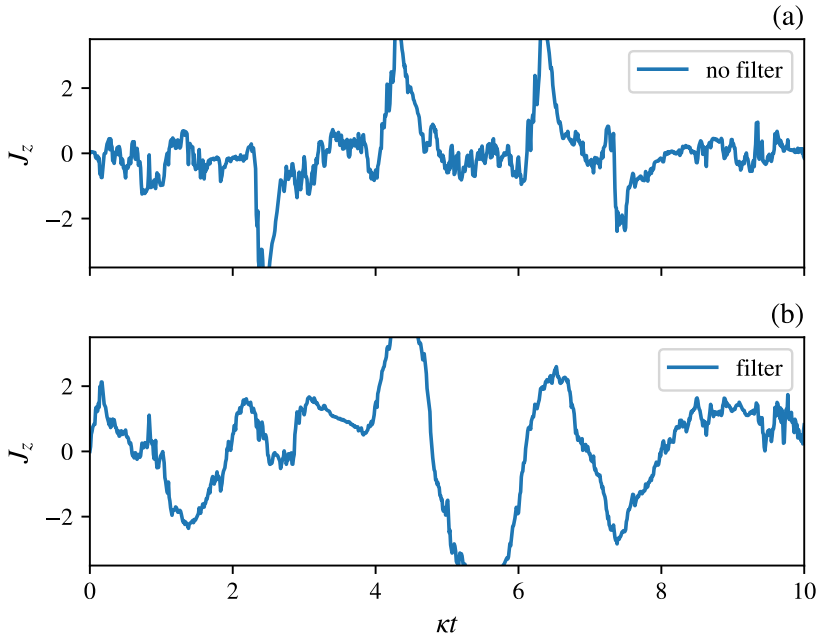

Figure 5.15: Single trajectories from a system undergoing continuous measurement, with feedback to try and stabilise the mean spin component J_z. The trajectories were simulated using a stochastic master equation, where in sub-figure (a) the measurement of J_z is directly reintroduced to the system via feedback. In figure (b) the measurement signal is first put through a low-pass filter and then used for feedback.

ing master equation is difficult to work with analytically but single trajectories can be simulated numerically. Figure 5.15 shows two trajectories following $\langle J_z \rangle$, using the direct measurement signal for feedback, and the other using the filtered signal. There is visibly less high frequency noise when using the filtered signal, however the mean spin still drifts significantly. A small sampling of possible measurement strengths λ, and filter time constants τ, suggest that a low-pass filter alone is not enough to successfully damp J_z.

Future work will be required, and is ongoing, to produce a stable steady state. In the limit of large N semi-classical equations of motion can be used to describe the spin system, which may give further insight into how to better damp J_z. It is also possible that the information scattered into other measurement channels could be useful to this end.

5.4.1 Outlook

In this chapter we have presented a free-space dispersive measurement model for a cloud of atoms. We outlined an approach to spin squeezing using measurement and feedback of the collective spin mode J_z, as well as examining the detrimental effects of scattering into other modes. With the measurement model we showed how increasing the atomic spacing created distinct modes where eventually local information about each atom could be obtained. Through detailed examples we showed how measurements of scattered light could be constructed so as to provide no information about the current state other than the noise from that mode driving it. In the idealised case of perfect measurement and direct feedback, the effect of this noise could be entirely negated. We illustrated how such measurements could be engineered in an optical setup, where information from the collective spin mode is extracted and measured independently. This makes non-conditional squeezing viable in the case where the atoms are spread across several spatial modes, and even when each individual atom is connected to its own spatial mode.

Following this, we looked at the steady state of the feedback procedure, motivated by finding a more practical and stable resource for metrology. To better analyse the final state we introduced the Quantum Fisher Information as a metric of useful entanglement. Currently the steady state of the feedback procedure is not useful for metrology, however we have begun exploring ways to improve this.

6 Conclusions

We have shown examples of where measurement and feedback can be used to produce non-classical states in nano-mechanical systems, and in an atomic spin ensemble. Measurement is an important aspect of all real experiments, and a continuous description of measurement can be used to construct powerful theoretical models, as well as practically provide a means to drive and prepare quantum states. Combined with feedback, these tools have broad application in both single-body and many-body systems, and this has been the foundation of the research in this thesis. Below we summarise the key results from previous chapters and discuss possible directions for future work.

In chapters 3 and 4, we focused on a single-body nano-mechanical resonator. Using a combination of state estimation and feedback we demonstrated a route to ground state cooling with a magnetically levitated particle. With measurement alone, we showed that a near minimum uncertainty state of a free particle could be produced, suitable for tests of a mechanism for wave-function collapse. The results presented offer plentiful scope for further work. Both state preparation procedures are limited by quantum measurement efficiency and we extensively explored methods for improving this. Physical implementation will rely on current experiments improving isolation from classical heating sources, and steady progress is being made in this direction[46, 71]. With no fundamental limit to reaching below single phonon-occupancy in these systems, theoretical models can prepare for when they are experimentally realised. A ground state system on its own does not exhibit novel quantum behaviour beyond achieving the minimum bound of the quantum uncertainty limit. Assuming ground state cooling can be successfully implemented, one way to observe quantum mechanical effects in the motion is to perturb the trapping potential[81]. The states predicted by the feedback models presented, could be used in further simulations of such a perturbation, to assess the visibility of quantum features as a function of phonon occupancy, state purity and squeezing. It would also be interesting to explore how the presence of a second quantum handle, such as the internal state of

a nitrogen vacancy centre, could be used to engineer novel states such as macroscopic superposition[58]. In the case of preparing a minimum uncertainty free particle state, there are clear directions for how to develop the current model, in order to bring it closer still to experiments. The purpose of this model was to find the practical limits of an experimental realisation, and to provide guidance as to the optimal measurement sequence. Including the effects of the weak trapping potential and classical heating sources would provide further insight into these questions.

In chapter 5 we explored measurement and feedback in a many-body context. We looked at preparing a form of many-body entanglement, a spin squeezed state of an atomic ensemble. These systems have been studied extensively and have applications in quantum information[95] and in metrology[96]. We examined how the detrimental effects of certain light scattering, which destroys quantum correlations by revealing local information about the atoms, can be suppressed with feedback. We showed that by careful choice of measurement, decoherence due to coupling to the environment could be completely undone under ideal conditions. The work presented initially considered the case of light scattering from the atoms into a single collective mode, and then the transition to where each atom is effectively coupled to completely separate modes. In the latter case, a free-space measurement of the atomic cloud is not expected to produce squeezing[107], however, this is rectified by the proposed feedback procedure. The possibility of steady state squeezing was then investigated, and there is ongoing work to this end. More generally, it would also be interesting to apply this method of cancelling noise from undesirable measurement channels, in other quantum systems.

In summary, the combination of measurement and feedback offers incredible flexibility in application to both theorists and experimentalists. As well as naturally being useful for gaining information and providing stabilisation, both measurement and feedback can be applied locally or globally, allowing for effective long-range couplings. State engineering via non-coherent processes is of growing interest[109], as control over quantum systems continuous to improve. These tools are likely to play a key part in future experiments and

in the next generation of quantum technologies.

References

[1] R. P. Feynman. “Quantum mechanical computers”. *Foundations of Physics* 16 (1986), pp. 507–531.

[2] I. Bloch, J. Dalibard, and S. Nascimbène. “Quantum simulations with ultracold quantum gases”. *Nature Physics* 8 (2012), pp. 267–276.

[3] L. Essen and J. V. Parry. “An atomic standard of frequency and time interval: A cæsium resonator”. *Nature* 176 (1955), pp. 280–282.

[4] B. P. Abbott et al. “Observation of gravitational waves from a binary black hole merger”. *Physical Review Letters* 116 (2016), p. 061102.

[5] I. Bloch, J. Dalibard, and W. Zwerger. “Many-body physics with ultracold gases”. *Reviews of Modern Physics* 80 (2008), pp. 885–964.

[6] J. Q. You and F. Nori. “Atomic physics and quantum optics using superconducting circuits”. *Nature* 474 (2011), pp. 589–597.

[7] W. P. Bowen and G. J. Milburn. *Quantum optomechanics*. CRC Press, 2016.

[8] J. M. Geremia, J. K. Stockton, and H. Mabuchi. “Suppression of spin projection noise in broadband atomic magnetometry”. *Physical Review Letters* 94 (2005), p. 203002.

[9] C. Ahn, A. C. Doherty, and A. J. Landahl. “Continuous quantum error correction via quantum feedback control”. *Physical Review A* 65 (2002), p. 10.

[10] D. W. Berry and H. M. Wiseman. “Adaptive quantum measurements of a continuously varying phase”. *Physical Review A* 65 (2002), pp. 438031–438034.

[11] M. Sarovar et al. “Practical scheme for error control using feedback”. *Physical Review A* 69 (2004), p. 052324.

[12] T. Bhattacharya, S. Habib, and K. Jacobs. “Continuous quantum measurement and the emergence of classical chaos”. *Physical Review Letters* 85 (2000), pp. 4852–4855.

[13] C. H. Ren, Y. M. Lai, and T. Q. Song. "Decoherence of an open system under continuous quantum measurement of energy". *International Journal of Theoretical Physics* 48 (2009), pp. 2081–2087.

[14] C. K. Andersen et al. "Entanglement stabilization using ancilla-based parity detection and real-time feedback in superconducting circuits". *npj Quantum Information* 5 (2019), pp. 1–7.

[15] L. K. Thomsen, S. Mancini, and H. M. Wiseman. "Continuous quantum nondemolition feedback and unconditional atomic spin squeezing". *Journal of Physics B: Atomic, Molecular and Optical Physics* 35 (2002), pp. 4937–4952.

[16] V. Steixner, P. Rabl, and P. Zoller. "Quantum feedback cooling of a single trapped ion in front of a mirror". *Physical Review A* 72 (2005), pp. 1–13.

[17] M. Müller et al. "Engineered Open Systems and Quantum Simulations with Atoms and Ions". *Advances in Atomic, Molecular and Optical Physics*. Vol. 61. Academic Press Inc., 2012, pp. 1–80.

[18] K. B. Davis et al. "Bose-Einstein condensation in a gas of sodium atoms". *Physical Review Letters* 75 (1995), pp. 3969–3973.

[19] C. C. Bradley et al. "Evidence of Bose-Einstein condensation in an atomic gas with attractive interactions". *Physical Review Letters* 75 (1995), pp. 1687–1690.

[20] M. H. Anderson et al. "Observation of Bose-Einstein condensation in a dilute atomic vapor". *Science* 269 (1995), pp. 198–201.

[21] B. DeMarco and D. S. Jin. "Onset of Fermi degeneracy in a trapped atomic gas". *Science* 285 (1999), pp. 1703–1706.

[22] A. G. Truscott et al. "Observation of fermi pressure in a gas of trapped atoms". *Science* 291 (2001), pp. 2570–2572.

[23] A. D. O'Connell et al. "Quantum ground state and single-phonon control of a mechanical resonator". *Nature* 464 (2010), pp. 697–703.

[24] K. H. Lee et al. “Cooling and control of a cavity optoelectromechanical system”. *Physical Review Letters* 104 (2010), p. 123604.

[25] M. Poggio et al. “Feedback cooling of a cantilever’s fundamental mode below 5 mK”. *Physical Review Letters* 99 (2007), p. 017201.

[26] P. F. Cohadon, A. Heidmann, and M. Pinard. “Cooling of a mirror by radiation pressure”. *Physical Review Letters* 83 (1999), pp. 3174–3177.

[27] T. Sauter et al. “Observation of quantum jumps”. *Physical Review Letters* 57 (1986), pp. 1696–1698.

[28] J. C. Bergquist et al. “Observation of quantum jumps in a single atom”. *Physical Review Letters* 57 (1986), pp. 1699–1702.

[29] W. Nagourney, J. Sandberg, and H. Dehmelt. “Shelved optical electron amplifier: Observation of quantum jumps”. *Physical Review Letters* 56 (1986), pp. 2797–2799.

[30] H. Carmichael. *An open systems approach to quantum optics: lectures presented at the Université Libre de Bruxelles, October 28 to November 4, 1991*. Vol. 18. Springer, 1993.

[31] P. Zoller, M. Marte, and D. F. Walls. “Quantum jumps in atomic systems”. *Physical Review A* 35 (1987), pp. 198–207.

[32] J. Dalibard, Y. Castin, and K. Mølmer. “Wave-function approach to dissipative processes in quantum optics”. *Physical Review Letters* 68 (1992), pp. 580–583.

[33] R. E. Slusher et al. “Observation of squeezed states generated by four-wave mixing in an optical cavity”. *Physical Review Letters* 55 (1985), pp. 2409–2412.

[34] L. A. Wu et al. “Generation of squeezed states by parametric down conversion”. *Physical Review Letters* 57 (1986), pp. 2520–2523.

[35] H. M. Wiseman and G. J. Milburn. “Quantum theory of optical feedback via homodyne detection”. *Physical Review Letters* 70 (1993), pp. 548–551.

[36] P. Bushev et al. “Feedback cooling of a single trapped ion”. *Physical Review Letters* 96 (2006), pp. 1–4.

[37] V. P. Belavkin. "Measurement, filtering and control in quantum open dynamical systems". *Reports on Mathematical Physics* 7 (1999), pp. 405–425.

[38] R. Dum, P. Zoller, and H. Ritsch. "Monte Carlo simulation of the atomic master equation for spontaneous emission". *Physical Review A* 45 (1992), pp. 4879–4887.

[39] M. B. Plenio and P. L. Knight. "The quantum-jump approach to dissipative dynamics in quantum optics". *Reviews of Modern Physics* 70 (1998), pp. 101–144.

[40] C. Gardiner and P. Zoller. *Quantum noise: a handbook of Markovian and non-Markovian quantum stochastic methods with applications to quantum optics*. Vol. 56. Springer, 2004.

[41] U. Leonhardt. *Essential quantum optics: from quantum measurements to black holes*. Cambridge University Press, 2010.

[42] C. W. Gardiner. *Stochastic methods*. Springer, 1985.

[43] D. A. Steck et al. "Feedback cooling of atomic motion in cavity QED". *Physical Review A* 74 (2006), pp. 1–21.

[44] D. A. Steck et al. "Quantum feedback control of atomic motion in an optical cavity". *Physical Review Letters* 92 (2004), pp. 1–4.

[45] A. C. Doherty et al. "Motional states of atoms in cavity QED". *Physical Review A* 57 (1998), pp. 4804–4817.

[46] J.-F. Hsu et al. "Cooling the Motion of Diamond Nanocrystals in a Magneto-Gravitational Trap in High Vacuum". *Scientific Reports* 6 (2016), pp. 1–10.

[47] J. M. Martinis, M. H. Devoret, and J. Clarke. "Experimental tests for the quantum behavior of a macroscopic degree of freedom: The phase difference across a Josephson junction". *Physical Review B* 35 (1987), pp. 4682–4698.

[48] H. E. Hall and W. F. Vinen. "The rotation of liquid helium II II. The theory of mutual friction in uniformly rotating helium II". *Proceedings of the Royal Society of London. Series A. Mathematical and Physical Sciences* 238 (1956), pp. 215–234.

[49] J. Chan et al. “Laser cooling of a nanomechanical oscillator into its quantum ground state”. *Nature* 478 (2011), pp. 89–92.

[50] E. Verhagen et al. “Quantum-coherent coupling of a mechanical oscillator to an optical cavity mode”. *Nature* 482 (2012), pp. 63–67.

[51] J. Millen et al. “Optomechanics with levitated particles”. *Reports on Progress in Physics* 83 (2020), p. 026401.

[52] A. Ashkin. “Acceleration and Trapping of Particles by Radiation Pressure”. *Physical Review Letters* 24 (1970), pp. 156–159.

[53] D. Leibfried and C. Monroe. “Quantum dynamics of single trapped ions”. *Reviews of Modern Physics* 75 (2003), pp. 281–324.

[54] F. Diedrich et al. “Laser Cooling to the Zero-Point Energy of Motion”. *Physical Review Letters* 62 (1989), pp. 403–406.

[55] C. Monroe et al. “A ”Schrödinger cat” superposition state of an atom”. *Science* 272 (1996), pp. 1131–1136.

[56] D. M. Meekhof et al. “Generation of nonclassical motional states of a trapped atom”. *Physical Review Letters* 76 (1996), pp. 1796–1799.

[57] I. M. Georgescu, S. Ashhab, and F. Nori. “Quantum simulation”. *Reviews of Modern Physics* 86 (2014), p. 153.

[58] Z. Q. Yin et al. “Large quantum superpositions of a levitated nanodiamond through spin-optomechanical coupling”. *Physical Review A* 88 (2013), pp. 1–6.

[59] I. Pikovski et al. “Probing planck-scale physics with quantum optics”. *Nature Physics* 8 (2012), pp. 393–397.

[60] A. Albrecht, A. Retzker, and M. B. Plenio. “Testing quantum gravity by nanodiamond interferometry with nitrogen-vacancy centers”. *Physical Review A* 90 (2014), pp. 1–19.

[61] A. A. Geraci, S. B. Papp, and J. Kitching. "Short-range force detection using optically cooled levitated microspheres". *Physical Review Letters* 105 (2010), pp. 3–6.

[62] A. Arvanitaki and A. A. Geraci. "Detecting high-frequency gravitational waves with optically levitated sensors". *Physical Review Letters* 110 (2013), p. 071105.

[63] I. Alda et al. "Trapping and manipulation of individual nanoparticles in a planar Paul trap". *Applied Physics Letters* 109 (2016).

[64] D. Goldwater et al. "Levitated electromechanics: All-electrical cooling of charged nano- and micro-particles". *Quantum Science and Technology* 4 (2019).

[65] V. Jain et al. "Direct Measurement of Photon Recoil from a Levitated Nanoparticle". *Physical Review Letters* 116 (2016), pp. 1–7.

[66] J. Gieseler, L. Novotny, and R. Quidant. "Thermal nonlinearities in a nanomechanical oscillator". *Nature Physics* 9 (2013), pp. 806–810.

[67] G. Ranjit et al. "Attonewton force detection using microspheres in a dual-beam optical trap in high vacuum". *Physical Review A* 91 (2015), p. 051805.

[68] U. Delić et al. "Cavity Cooling of a Levitated Nanosphere by Coherent Scattering". *Physical Review Letters* 122 (2019), p. 123602.

[69] M. C. O'Brien et al. "Magneto-mechanical trapping of micro-diamonds at low pressures". *Applied Physics Letters* 114 (2019), p. 053103.

[70] A. T. M. A. Rahman et al. "Burning and graphitization of optically levitated nanodiamonds in vacuum". *Nature Publishing Group* 6 (2016), pp. 1–7.

[71] B. R. Slezak et al. "Cooling the motion of a silica microsphere in a magneto-gravitational trap in ultra-high vacuum". *New Journal of Physics* 20 (2018).

[72] A. C. Doherty et al. "The quantum trajectory approach to quantum feedback control of an oscillator revisited". *Philosophical Transactions of the Royal Society A: Mathematical, Physical and Engineering Sciences* 370 (2012), pp. 5338–5353.

[73] K. Jacobs and D. A. Steck. "A straightforward introduction to continuous quantum measurement". *Contemporary Physics* 47 (2006), pp. 279–303.

[74] P. Rabl, V. Steixner, and P. Zoller. "Quantum-limited velocity readout and quantum feedback cooling of a trapped ion via electromagnetically induced transparency". *Physical Review A* 72 (2005), pp. 1–13.

[75] M. G. Genoni et al. "Quantum cooling and squeezing of a levitating nanosphere via time-continuous measurements". *New Journal of Physics* 17 (2015).

[76] A. C. Doherty and K. Jacobs. "Feedback control of quantum systems using continuous state estimation". *Physical Review Letters* 60 (1999).

[77] L. S. Walker, G. R. Robb, and A. J. Daley. "Measurement and feedback for cooling heavy levitated particles in low-frequency traps". *Physical Review A* 100 (2019), p. 063819.

[78] O. L. R. Jacobs. *Introduction to Control Theory*. Oxford University Press, 1993.

[79] H. M. Wiseman and G. J. Milburn. "Squeezing via feedback". *Physical Review A* 49 (1994), pp. 1350–1366.

[80] W. H. Zurek, S. Habib, and J. P. Paz. "Coherent states via decoherence". *Physical Review Letters* 70 (1993), pp. 1187–1190.

[81] J. F. Ralph et al. "Dynamical model selection near the quantum-classical boundary". *Physical Review A* 98 (2018), p. 010102.

[82] A. C. Frangeskou et al. "Pure nanodiamonds for levitated optomechanics in vacuum". *New Journal of Physics* 20 (2018), p. 043016.

[83] M. R. Vanner et al. "Pulsed quantum optomechanics". *Proceedings of the National Academy of Sciences of the United States of America* 108 (2011), pp. 16182–16187.

[84] S. L. Adler and A. Bassi. "Collapse models with non-white noises". *Journal of Physics A: Mathematical and Theoretical* 40 (2007), p. 15083.

[85] D. J. Bedingham and H. Ulbricht. "Correlated random walks caused by dynamical wavefunction collapse". *Scientific Reports* 5 (2015), p. 13380.

[86] S. Bera et al. “A proposal for the experimental detection of CSL induced random walk”. *Scientific Reports* 5 (2015), p. 7664.

[87] B. Collett and P. Pearle. “Wavefunction Collapse and Random Walk”. *Foundations of Physics* 33 (2003), pp. 1495–1541.

[88] G. C. Ghirardi, P. Pearle, and A. Rimini. “Markov processes in Hilbert space and continuous spontaneous localization of systems of identical particles”. *Physical Review A* 42 (1990), pp. 78–89.

[89] P. Pearle. “Combining stochastic dynamical state-vector reduction with spontaneous localization”. *Physical Review A* 39 (1989), pp. 2277–2289.

[90] A. Motazedifard, F. Bemani, and M. H. Naderi. “Non-interferometric test of the continuous spontaneous localization model based on rotational optomechanics”. *New Journal of Physics* 20 (2018), p. 083022.

[91] A. J. Daley. “Quantum trajectories and open many-body quantum systems”. *Advances in Physics* 63 (2014), pp. 77–149.

[92] M. Kitagawa and M. Ueda. “Squeezed spin states”. *Physical Review A* 47 (1993), pp. 5138–5143.

[93] R. H. Dicke. “Coherence in spontaneous radiation processes”. *Physical Review* 93 (1954), pp. 99–110.

[94] X. Wang. “Spin squeezing in nonlinear spin-coherent states”. *Journal of Optics B: Quantum and Semiclassical Optics* 3 (2001), p. 93.

[95] B. Julsgaard, A. Kozhekin, and E. S. Polzik. “Experimental long-lived entanglement of two macroscopic objects”. *Nature* 413 (2001), pp. 400–403.

[96] D. J. Wineland et al. “Spin squeezing and reduced quantum noise in spectroscopy”. *Physical Review A* 46 (1992), R6797.

[97] N. F. Ramsey. “A molecular beam resonance method with separated oscillating fields”. *Physical Review* 78 (1950), pp. 695–699.

[98] A. Sorensen et al. “Many-particle entanglement with Bose–Einstein condensates”. *Nature* 409 (2000), pp. 63–66.

[99] A. Kozhekin, K. Mølmer, and E. Polzik. “Quantum memory for light”. *Physical Review A* 62 (2000), pp. 1–5.

[100] A. Kuzmich, N. P. Bigelow, and L. Mandel. “Atomic quantum non-demolition measurements and squeezing”. *Europhysics Letters* 42 (1998), pp. 481–486.

[101] A. Kuzmich, L. Mandel, and N. P. Bigelow. “Generation of spin squeezing via continuous quantum nondemolition measurement”. *Physical Review Letters* 85 (2000), pp. 1594–1597.

[102] M. R. Andrews et al. “Direct, nondestructive observation of a Bose condensate”. *Science* 273 (1996), pp. 84–87.

[103] K. Hammerer, A. S. Sørensen, and E. S. Polzik. “Quantum interface between light and atomic ensembles”. *Reviews of Modern Physics* 82 (2010), pp. 1041–1093.

[104] D. Oblak et al. “Quantum-noise-limited interferometric measurement of atomic noise: Towards spin squeezing on the Cs clock transition”. *Physical Review A* 71 (2005).

[105] J. Appel et al. “Mesoscopic atomic entanglement for precision measurements beyond the standard quantum limit”. *Proceedings of the National Academy of Sciences of the United States of America* 106 (2009), pp. 10960–10965.

[106] L. K. Thomsen, S. Mancini, and H. M. Wiseman. “Spin squeezing via quantum feedback”. *Physical Review A* 65 (2002), p. 061801.

[107] I. Bouchoule and K. Mølmer. “Preparation of spin-squeezed atomic states by optical-phase-shift measurement”. *Physical Review A* 66 (2002), p. 11.

[108] L. Pezzè et al. “Quantum metrology with nonclassical states of atomic ensembles”. *Reviews of Modern Physics* 90 (2018), p. 035005.

[109] F. Verstraete, M. M. Wolf, and J. Ignacio Cirac. “Quantum computation and quantum-state engineering driven by dissipation”. *Nature Physics* 5 (2009), pp. 633–636.